Università degli Studi di Firenze

DOTTORATO DI RICERCA IN

CHIMICA E TECNOLOGIA DEL FARMACO

CICLO XXV

COORDINATORE Prof. Elisabetta Teodori

"Development and optimization of nanocarriers for delivery of natural and semi-synthetic compounds in cancer therapy"

Settore Scientifico Disciplinare CHIM/09

Dottoranda

Dott.ssa Chiara Righeschi

Tutor

Prof. Anna Rita Bilia

SUMMARY

ABSTRACT

ABSTRACT

The main objective of this thesis has been the design and the evaluation of nanocarriers for the delivery of natural and semi-synthetic anticancer compounds.

The limitations of conventional therapies have resulted in a great interest for the use of nanocarriers for anticancer drug delivery. Nanomedicine is an innovative field with immense potential for improving the efficacy of cancer therapeutics. Numerous natural products have been studied to determine the molecular pathways for cancer prevention and treatment. Though it has been proven that many natural products have a strong therapeutic value, their poor solubility and bioavailability have severely limited their use. The use of nanocarriers enable us to overcome many of the inherent problems (stability, solubility, toxicity) associated with natural products, and also provide a platform for targeted delivery to tumor sites.

The aim of the work has been the development and characterization of three different nanocarriers: solid lipid nanoparticles, polymeric nanocapsules and liposomes.

The feasibility of the inclusion of the water-insoluble drug curcumin in solid lipid nanoparticles for oral delivery has been investigated. In fact despite multiple medicinal benefits its therapeutical utility is strongly limited by its poor aqueous solubility and low oral bioavailability.

Polymeric nanocapsules were selected for their positive features for drug delivery in anticancer therapy: the oily core of polymeric nanocapsules is an ideal environment to encapsulate most antitumor drugs at high payloads, with good encapsulation efficacies and in a stable environment; on the other hand, the polymeric shell can be chosen to improve the biodistribution and the pharmacokinetic profile of the nanocarrier and to increase the intracellular penetration. Taking this information in account, we evaluated the potential of innovative nanocapsules as vehicles for docetaxel as model drug.

Conventional and stealth liposomes were designed for the delivery of dihydroartemisinin, a semi-synthetic derivative of artemisinin. This compound, well know as a treatment for malaria, also has a cytotoxic effect on cancer cells but it is characterized by poor water-solubility and low bioavailability.

Formulations developed were fully characterized in terms of size, zeta potential, encapsulation efficiency and morphological analysis. Stability was evaluated during time and different *in vitro* studies were carried out.

CHAPTER 1

Introduction

1.1 Nanocarriers and cancer therapy

Cancer remains one of the world's most devastating diseases, reaching 7.6 million deaths (13% of all deaths) in 2008. Moreover, deaths from cancer worldwide are projected to continue rising to over 11 million in 2030 (World Health Organization, 2011).

Cancer is a lethal disorder characterised by the development of abnormalities in cells causing uncontrollable and fast growth and division due to a combination of mutagenic stages. As a consequence of these mutations, cancer cells obtain a battery of specific properties such as limitless proliferation potential, self-sufficiency in growth signals and resistance to growth inhibitory signals, as well as evasion from apoptotic cues, which would, in a normal situation, contain their growth (Luo, 2009). Besides, tumours have developed diverse methods to attain further support through interactions with surrounding stromal cells, promoting their angiogenesis, tissue invasion and metastasis to distant organs, along with evasion from immune detection (Hanahan, 2000).

Current cancer treatments include surgical intervention, radiation and chemotherapeutic drugs, which often also kill healthy cells and cause toxicity to the patient. Frequent challenges encountered by current cancer therapies include non specific systemic distribution of antitumor agents, inadequate drug concentrations reaching the tumor site, intolerable cytotoxicity, limited ability to monitor therapeutic responses and development of multiple drug resistance (Das, 2009; Parven, 2006; Parven, 2008). For this reason, important progress has been achieved in the field of nanotechnology to solve these problems and offer a promising and effective alternative for cancer treatment. Recent years have witnessed unprecedented use of nanocarriers (particularly in the size range from 10 nm to 100 nm) as an emerging class of therapeutics for cancer treatment. To address the challenges of targeting tumours with nanotechnology, it is necessary to combine the rational design of nanocarriers (Table 1) with the fundamental understanding of tumour biology.

Rational design of nanocarriers for cancer therapy	
Nanocarriers can offer many advantages over free drugs. They:	**For rapid and effective clinical translation, the nanocarrier should:**
• protect the drug from premature degradation • prevent drugs from prematurely interacting with the biological environment • enhance absorption of the drugs into a selected tissue (for example, solid tumour) • control the pharmacokinetic and drug tissue distribution profile • improve intracellular penetration	• be made from a material that is biocompatible, well characterized, and easily functionalized • exhibit high differential uptake efficiency in the target cells over normal cells (or tissue) • be either soluble or colloidal under aqueous conditions for increased effectiveness • have an extended circulating half-life, a low rate of aggregation, and a long shelf life

Table 1: *Rational design of nanocarriers for cancer therapy (Peer, 2007).*

1.2 Physiopathological characteristics of tumour tissues

The potential of nanotechnology is to overcome the shortcomings of conventional anticancer therapy. To achieve this goal is important to know the specific features of tumour cells.

1.2.1 Leaky vasculature

Angiogenesis is a crucial step for cell function and survival, involving the creation of new blood vessels, from pre-existing ones, to provide oxygen and essential nutrients to the newly forming tissue. In this way, tumours are able to obtain their own blood supply. Tumour cells divide at a rapid and uncontrollable rate, notably faster than other cells. This excessive growth soon leads to hypoxic conditions, due to restrictions of oxygen and nutrients on the tumour environment.
Consequently, a sequence of steps for the formation of the capillary tube takes place, in order to produce new vessels. This process is mediated by the effect of proangiogenic growth factors overexpressed at the tumour site (Kohandel, 2007) i.e., vascular endothelial growth factor (VEGF), basic fibroblast growth factor (bFGF), bradykinins, nitric oxide, prostaglandins and so on (Maeda, 2000). The abnormal proliferation of endothelial cells has some consequences for the newly formed microvascular network, giving rise to a defective architecture in these novel vessels, in contrast to the neovasculature in normal tissues. Thus, the new tumour blood vessels present a disorganised and tortuous structure, with large spaces between the endothelial cells, creating a leaky and porous vasculature, resulting in an increased vascular permeability to macromolecules (Jain, 2010).

1.2.2 Impaired lymphatic drainage

In addition to the previous alteration, proliferating cancer cells are capable of collapsing intratumour lymphatic vessels by compression, limiting functional lymphatic vessels to the outlying tumour (Padera, 2002). Furthermore, the active lymphatic vessels manage tumour metastasis through the lymphatic system. This impaired lymphatic drainage, together with the chaotic leakiness of the newly formed tumour blood vessels, is recognised as a phenomenon denominated enhanced permeability and retention (EPR) effect (Maeda, 2001). The EPR effect is one of the most important mechanisms whereby nanoparticles and other macromolecules over 50 KDa can be accumulated within the tumour interstitium (Cho, 2008).

1.2.3 Acidic tumour microenvironment

Besides the EPR effect, highly proliferative cancer cells exhibit an increased metabolic rate. To support their needs and, as the supply of oxygen and nutrients is never enough, tumour cells must obtain additional energy by glycolysis, producing an acidic environment (Pelicano, 2006).

1.3 Drug targeting

Ideally, for anticancer drugs to be effective in cancer treatment, they should first be able to reach the desired tumor tissues through the penetration of barriers in the body with minimal loss of volume or activity in the blood circulation. Second, after reaching the tumor tissue, drugs should have the ability to selectively kill tumor cells without affecting normal cells with a controlled release mechanism of the active form. These two basic strategies are also associated with improvements in patient survival and quality of life, by simultaneously increasing the intracellular concentration of drugs and reducing dose-limiting toxicities. To efficiently achieve these goals, three mechanisms of drug targeting to tumours have been described and are detailed below.

1.3.1 Passive Targeting

General features of tumours include leaky blood vessels and poor lymphatic drainage such as previously explained. Whereas free drugs may diffuse non specifically, a nanocarrier can extravasate (escape) into the tumour tissues via the leaky vessels by the EPR effect (Enhanced permeability and retention effect) (Matsumura, 1986; Figure 1). The increased permeability and the dysfunctional lymphatic drainage in tumours retains the accumulated nanocarriers and allows them to release drugs into the vicinity of the tumour cells. Very high local concentrations of drug-loaded nanocarriers can be achieved at the tumor site, for instance 10–50-fold higher than in normal tissue within 1–2 days (Iyer, 2006). Some properties of nanocarriers are particularly important:
(i) The ideal nanocarrier size should be somewhere between 10 and 100 nm. Indeed, for efficient extravasation from the fenestrations in leaky vasculature, nanocarriers should be much less than 400 nm. On the other hand, to avoid the filtration by the kidneys, nanocarriers need to be larger than 10 nm; and to avoid the aspecific capture by the liver, nanocarriers need to be smaller than 100 nm.
(ii) The charge of the particles should be neutral or anionic for efficient evasion of the renal elimination.
(iii) The nanocarriers must be hidden from the reticulo–endothelial system, which destroys any foreign material through opsonization followed by phagocytosis (Malam, 2009; Gullotti, 2009).
Neverthless, to reach passively the tumor, some limitation exist. Certain tumours do not exhibit the EPR effect, and the permeability of vessels may not be the same throughout a single tumour (Jain, 1994). In addition targeting cells within a tumour is not always feasible because some drugs cannot diffuse efficiently and the random nature of the approach makes it difficult to control the process. This lack of control may induce multi-drug resistance (MDR) that occurs because transporter proteins that expel drugs from cells are overexpressed on the surface of cancer cells (Ferrari, 2005; Gottesman, 2002; Peer, 2006).

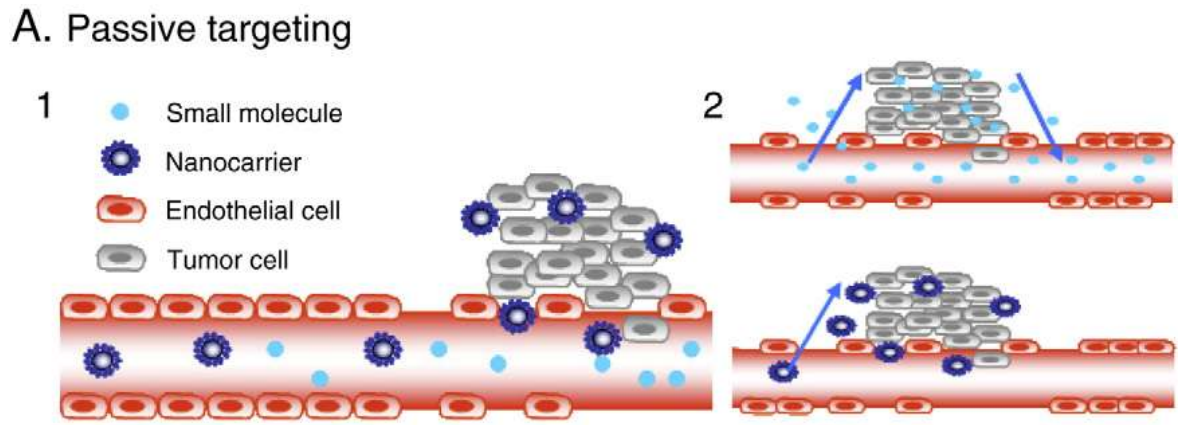

***Figure 1**: Passive targeting of nanocarriers. **(1)** Nanocarriers reach tumors selectively through the leaky vasculature surrounding the tumors. **(2)** Schematic representation of the influence of the size for retention in the tumor tissue. Drugs alone diffuse freely in and out the tumor blood vessels because of their small size and thus their effective concentrations in the tumor decrease rapidly. By contrast, drug-loaded nanocarriers cannot diffuse back into the blood stream because of their large size, resulting in progressive accumulation: the EPR effect.*

1.3.2 Active targeting

One way to overcome limitations of passive targeting is to programme the nanocarriers so they actively bind to specific cells after extravasation (Figure 2). This binding may be achieved by attaching targeting agents such as ligands-molecules, that bind to specific receptors on the cell surface, to the surface of the nanocarrier by a variety of conjugation chemistries (Torchilin, 2005). Nanocarriers will recognize and bind to target cells through ligand-receptor interactions, and bound carriers are internalized before the drug is released inside the cell. In general, when using a targeting agent to deliver nanocarriers to cancer cells, it is imperative that the agent binds with high selectivity to molecules that are uniquely expressed on the cell surface. To maximize specificity, a surface marker (antigen or receptor) should be overexpressed on target cells relative to normal cells. The binding of certain ligands to their receptors may cause receptor-mediated internalization, which is often necessary if nanocarriers are to release drugs inside the cell (Allen, 2002; Peer, 2007). In contrast, targeting nanocarriers to non-internalizing receptors may sometimes be advantageous in solid tumours owing to the bystander effect, where cells lacking the target receptor can be killed through drug release at the surface of the neighbouring cells, where carriers can bind (Allen, 1994).
Targeting agents can be broadly classified as proteins (mainly antibodies and their fragments), nucleic acids (aptamers), or other receptor ligands (peptides, vitamins, and carbohydrates).
Growth factor or vitamin interactions with cancer cells represent a commonly used targeting strategy, as cancer cells often overexpress the receptors for nutrition to maintain their fast-growing metabolism. Epidermal growth factor (EGF) has been shown to block and reduce tumour expression of the EGF receptor, which is overexpressed in a variety of tumour cells such as breast and tongue

cancer (Sanfilippo, 1996). Additionally, based on the same idea, the vitamin folic acid (folate) has also been used for cancer targeting because folate receptors (FRs) are frequently overexpressed in a range of tumour cells including ovarian, endometrial and kidney cancer (Antony, 1992). Transferrin (Tf) interacts with Tf receptors (TfRs), which are overexpressed on a variety of tumour cells (including pancreatic, colon, lung, and bladder cancer) owing to increased metabolic rates (Prost, 1998). Direct coupling of these targeting agents to nanocarriers containing chemotherapies such as drugs has improved intracellular delivery and therapeutic out come in animal tumour models (Kukowska-Latallo, 2005; Ishida, 2001).

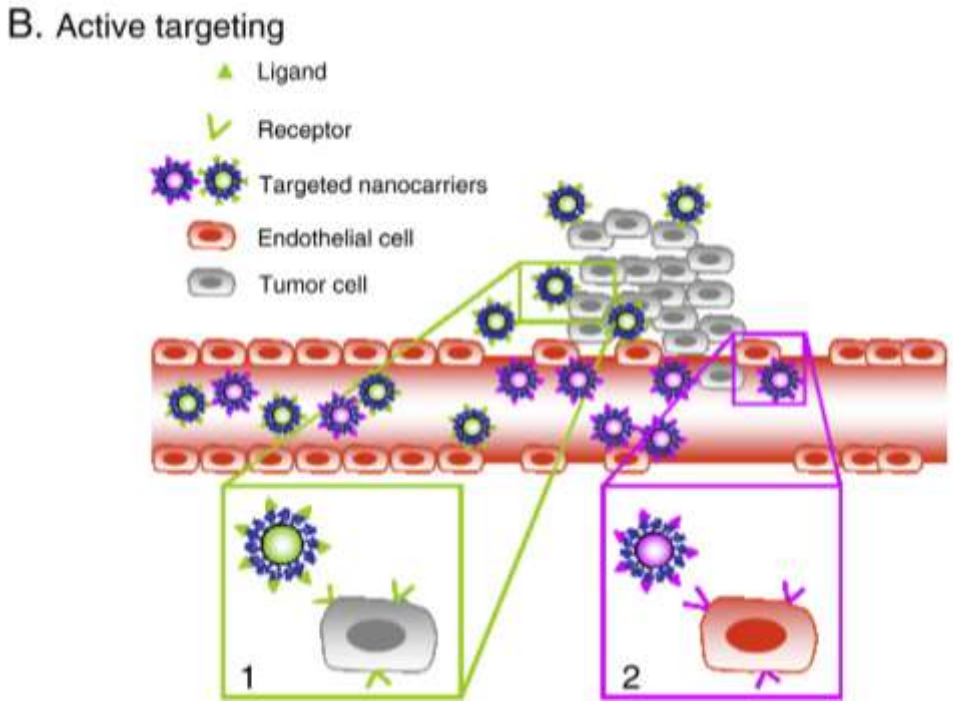

Figure 2: *Active targeting strategies. Ligands grafted at the surface of nanocarriers bind to receptors (over)expressed by* ***(1)*** *cancer cells or* ***(2)*** *angiogenic endothelial cells.*

1.3.3 Triggered drug targeting

Another promising mechanism of drug targeting to tumours is triggered targeting, where the nanoparticles release their payloads by exposing them to an external stimulus, such as an electric or magnetic field, ultrasound, hyperthermia or light (Lammers, 2012). The main disadvantage of these kinds of nanoformulations is that they are not easy to prepare. Moreover, they can release amounts of drug without being triggered or even fail to release their load at the conditions required to induce drug release. However, much effort is being made to solve these limiting shortcomings (Tagami, 2011a; Tagami 2011b).

1.4 Investigated nanocarriers for cancer therapy

The main limitations in cancer therapies are related to their lack of specificity and subsequent toxicity. Moreover, in many cancers, there are specific biological barriers, such as the MDR (multi drug resistance) mechanisms, which limit the efficacy of the treatments (Gottesman, 2002; Ehdaie, 2007). Finally, from the formulation point of view, most of the anticancer drugs suffer from poor water solubility and instability. Over recent decades, different nanoparticle delivery systems (liposomes, polymeric nanoparticles, polymeric micelles, polymer-drug conjugate nanoparticles or lipid-drug conjugate nanoparticles) have been developed. Some of them are already on the market and others are still under clinical and preclinical research. Our work was focused on three different formulations applicable to cancer therapy: liposomes, solid lipid nanoparticles and nanocapsules.

1.4.1 Liposomes

Liposomes are spherical, self-closed structures formed by one or several concentric lipid bilayers with an aqueous phase inside and between the lipid bilayers. They have been widely used since Bargham discovered them 40 years ago (Bangham, 1964) for their attractive properties:

• Liposomes are biocompatible.

• Liposomes can entrap water-soluble (hydrophilic) pharmaceutical agents in their internal water compartment and water-insoluble (hydrophobic) pharmaceuticals into the membrane.

• Liposome-incorporated pharmaceuticals are protected from the inactivating effect of external conditions, yet do not cause undesirable side reactions.

• Liposomes provide a unique opportunity to deliver pharmaceuticals into cells or even inside individual cellular compartments.

• Size, charge and surface properties of liposomes can be easily changed simply by adding new ingredients to the lipid mixture before liposome preparation and/or by variation of preparation methods.

Research on liposome technology has progressed from **conventional vescicles** ("first-generation liposomes") to "second-generation liposomes", in wich long-circulating liposomes are obtained by modulating the lipid composition, size and charge of the vesicle. A significant step in the development of long circulating liposomes came with inclusion of the synthetic polymer poly-ethylene glycol (PEG) in liposome composition (**stealth liposomes**). The mechanism whereby steric stabilization of liposomes increases their longevity in circulation has been extensively discussed (Drummond, 1999). The basic concept is that a hydrophilic polymers such as PEG, possessing a flexible chain that occupies the space immediately adjacent to the liposome surface ("periliposomal layer"), tends to exclude other macromolecules from this space. Consequently, access and binding of blood plasma opsonins to the liposome surface are hindered, and thus interactions of MPS (mononuclear phagocyte system) macrophages with such liposomes are inhibited. The most evidentcharacteristic of PEGylated liposomes is their circulation longevity determined by pharmacokinetic evaluation as reported by Immordino et al. (Immordino, 2003)

for liposomes containing docetaxel. By reducing MPS uptake long-circulating liposomes can passively accumulate inside other tissues or organs. This technology has resulted in a large number of liposome formulations encapsulating active molecules, with high target efficiency and activity.

To increase liposomal drug accumulation in the desired tissues, producing higher and more selective therapeutic activity, the use of **targeted liposomes** has been suggested. This involves the coupling of targeting moieties capable of recognizing target cells, binding to them, and inducing the internalization of liposomes or encapsulated drugs. Targeting moieties include monoclonal antibodies (MAb) or fragments, peptides, growth factors, glycoproteins, carbohydrates, or receptor ligands (Lopes De Menezes, 1999; Sapra, 1999; Medina , 2004). Targeted liposomes offer various advantages over individual drugs targeted by means of polymers or antibodies. One of the most compelling advantages is the dramatic increase in drug amount that can be delivered to the target. Furthermore, the number of ligand molecules exposed on the liposome surface can be increased, improving ligand avidity and degree of uptake. Immunoliposomes also provide a "bystander killing" effect, because the drug molecules can diffuse into adjoining tumor cells (Immordino, 2006).

Thus far, just four formulations based on liposomes have been clinically approved: Doxil® (Caelyx® in Europe), Myocet®, DaunoXome® and DepoCyt® (Hofheinz, 2005). The first two formulations include doxorubicin, which has dangerous side effects related to its cardiotoxicity at therapeutic concentrations when administered in a standard formulation, which limits its dosage (Singal, 1998). DaunoXome® is a non-PEGylated liposomal daunorubicin. It was demonstrated to be a safe and effective in therapy for advanced AIDS-related Kaposi's sarcoma (Gill, 1996). To date, the last liposomal formulation on the market is DepoCyt®, the commercial name of a non-PEGylated liposomal cytarabine, a hydrophilic chemotherapeutic drug. In addition to the previous formulations on the market, a huge variety of antineoplastic liposomes are still under clinical research and many of them have been elaborated with PEG. As reported in Table 2 also targeted liposomes are under clinical studies. The first formulation (MBP-426) incorporates oxaliplatin in a liposome consisting of transferrin conjugated to N-glutarylphosphatidylethanolamine (NGPE). MBP-426 is currently in a phase II clinical trial after demonstrating a favourable safety profile, with thrombocytopenia as the main side effect, together with improved efficacy (Sankhala, 2009). MCC-465, an immunoliposome encapsulating doxorubicin, was compared to Doxil® in a phase I trial, indicating similar pharmacokinetic results, however the adverse events related to Doxil® were reduced. The novelty of this promising formulation is that it is tagged with PEG and a fragment of the human monoclonal antibody, able to identify cell surface molecules of different cancer cell lines (Matsumura, 2004). A stimuli-responsive promising liposomal formulation is Thermodox™; this novel formulation is a thermally sensitive PEGylated liposome entrapping doxorubicin, activated by the application of localised hyperthermia. Thus, it releases its payload when reaching temperatures between 39 and 42°C. Therefore, this delivery system enables higher concentrations of the chemotherapeutic agent at the tumour site. Thermodox™ is currently being tested in a phase II

study to evaluate its efficacy in combination with radiofrequency ablation (RFA) in patients with hepatocellular carcinoma, compared to those receiving RFA alone (www.clinicaltrials.gov).

Name	Formulation	Drug	Indication	Status
Doxil® (Caelyx®)	PEGylated liposome	Doxorubicin	Breast cancer, ovarian cancer, multiple myeloma, Kaposi's sarcoma	Market
Myocet®	Non-PEGylated liposome	Doxorubicin	Breast cancer	Market
DaunoXome®	Non-PEGylated liposome	Daunorubicin	Kaposi's sarcoma	Market
DepoCyt®	Non-PEGylated liposome	Cytarabine	Lymphomatus meningitis, leukemia, glioblastoma	Market
Lipoplatin	PEGylated liposome	Cisplatin	Various malignancies	Phase III
S-CKD602	PEGylated liposome	CKD-602	Various malignancies	Phase I/II
NL CPT-11	PEGylated liposome	Irinotecan (CPT-11)	Glioma	Phase I
CPX-1	Liposome	Irinotecan	Colorectal cancer	Phase II
LE-SN38	Liposome	SN-38	Colorectal cancer	Phase II
MBP-426	Tf-NGPE-liposome	Oxaliplatin	Various malignancies	Phase II
MCC-465	Human antibody fragment (GAH)-PEG-liposome	Doxorubicin	Gastric cancer	Phase I
Thermodox™	Heat-activated PEGylated liposome	Doxorubicin	Liver cancer, breast cancer	Phase III
CPX-351	Liposome	Cytarabine+ daunorubicin	Acute myeloid leukaemia	Phase II
SGT-53	Transferrin-targeted DNA plasmid liposome	P53 gene	Various solid malignancies	Phase I

Table 2: *Liposomes on the market and in clinical development (Egusquiaguirre, 2012).*

1.4.2 Solid lipid nanoparticles

Solid lipid nanoparticles (SLN) were introduced in 1991 and represent an alternative carrier system to traditional colloidal carriers, such as emulsions, liposomes and polymeric micro- and nano-particles (Muller, 1995). SLN have been designed to overcome the main problems of membrane stability and drug leakage associated with liposomes and conventional emulsions (Ruckmani, 2006). SLN are characterized as being colloidal particles made of lipid that remain in solid state at room and body temperature, wich are generally recognized as safe (GRAS) or have a regulatory accepted status. They present sizes from 50 to 500 nm, depending on the method and materials employed for the manufacturing process (Figure 3).

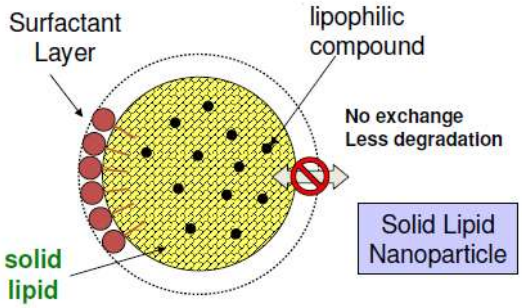

Figure 3: *Schematic representation of solid lipid nanoparticles.*

General ingredients include solid lipid(s), emulsifier(s) and water. The term lipid is used here in a broader sense and includes triglycerides (e.g. tristearin), partial glycerides (e.g. Imwitor), fatty acids (e.g. stearic acid), steroids (e.g. cholesterol) and waxes (e.g. cetyl palmitate). All classes of emulsifiers (with respect to charge and molecular weight) have been used to stabilize the lipid dispersion. The lipid matrix is made from physiological lipids which decreases the danger of acute and chronic toxicity. The choice of the emulsifier depends on the administration route and is more limited for parenteral administrations.

Clear advantages of SLN include the possibility of controlled drug release and drug targeting, increased drug stability, absence of biotoxicity of the carrier, avoidance of organic solvents, no problems with respect to large scale production and sterilization (Mehenert, 2012).

There are two main production techniques for SLN: the high pressure homogenization (HPH) (Muller, 1995) and the microemulsion technique (Gasco, 1993). Alternatively, several other processes have been used for the production of these systems, in order to attempt cheaper and easier ways of production, e.g., ultrasound technique (US), solvent-based techniques or cold homogenization (Sarmento, 2007; Kristl, 2003; Gokce, 2008; Wang, 2005; Zhang, 2006).

Since early 1990's, a number of SLN-based systems for the delivery of cytotoxic drugs have been successfully formulated and tested. Compared to many other drug delivery systems, the history of SLN is relatively short: there is still a lack of clinical studies of the use of SLN for cancer management and to date there is no SLN product for cancer therapy on the market. Nevertheless,

the findings in the preclinical studies using cell culture systems or animal models have so far been very promising. Table 3 provides a list of drugs formulated in these systems.

Group	Examples
Alkaloids	Mitotic inhibitor: *Vinorelbine* Topoisomerase I inhibitor: *Camptothecin*
Alkylating agents	Nitrogen mustard: *Chlorambucil*
Alkyl Lysophospholipids	*Edelfosine*
Anthracyclines	*Doxorubicin, Idarubicin*
Antimetabolites	Folic acid analog: *Methotrexate* Pyrimidine analog: *5-Fluorouracil*
Hormonal agents	Estrogen receptor antagonist: *Tamoxifen*
Podophyllotoxin derivatives	*Etoposide*
Taxanes	*Paclitaxel, Docetaxel*
Others	*All trans retinoic acid* *Beta-elemene* *Cholesteryl butirate* *Cisplatin* Topoisomerase II inhibitor: *Mitoxantrone*

Table 3: *Classification of antineoplastic agents vectorized in SLN (Hestella-Ermoso, 2009).*

In vivo studies with Ehrlich ascite carcinoma (EAC) were carried out by Ruckmany et al. They administered methotrexate-loaded SLN made of stearic acid intraperitoneally for 9 days. After 9 days, mean survival time for the mice treated with SLN was nearly 30% higher than that of the mice treatedwith methotrexate solution (Ruckmany, 2006). In another study, mitoxantrone-loaded SLN also showed efficacy lymph node metastases. The treatment with SLN gave a mean size of lymph node three times smaller than that of the mitoxantrone solution (Lu, 2006). In addition many *in vitro* studies performed with doxorubicin loaded SLN have clearly show the efficacy of the system. In all tested tumor cell lines, doxorubicin-loaded SLN inhibited cell growth more strongly than the free solution. Cytotoxicity of paclitaxel-loaded SLN has also been widely assayed (Serpe, 2004; Yuan, 2008; Chen, 2001). Different authors have discovered that the cellular uptakes of different types of SLN are time-dependent, concentration-dependent and that the intracellular accumulation of drugs may be further optimized though receptor-mediates endocytosis of the drug-loaded SLN.

1.4.3 Nanocapsules

Nanocapsules, first developed by Couvreur et al. (Couvreur, 1977), offer unique opportunities with the pourpose of improving the biological profile of drugs in terms of transport across biological barriers, biodistribution and cellular uptake. They have a vesicular organization whose internal

reservoir can be composed of aqueous or oily components, and they are surrounded by a polymeric coating (Legrand, 1999; Couvreur, 2002). This reservoir system offers the possibility of great loadings of either lipophilic or hydrophilic drugs, depending on the nature of the liquid core (Figure 4). Additionally, the core has the role of protecting the drug from the physiological environment. Finally, the liquid nature of nanocapsules and, thus, their elasticity, may facilitate the contact of the nanostructures with the ephithelia and further internalization.

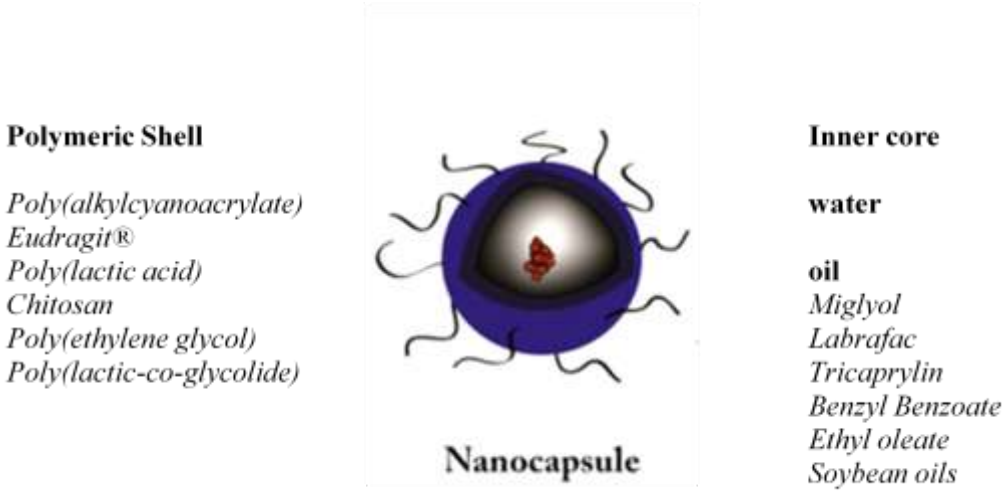

Figure 4: *Schematic diagram of nanocapsules containing an aqueous or oily core.*

Moreover, nanocapsules have shown to be capable of inhibiting multidrug resistance cellular mechanisms, especially important in cancer therapy. Several methods have been developed to date for the production of nanocapsules and the encapsulation of drugs. These methods are based on different physicochemical principles including (i) interfacial polymerization (Couvreur, 1977), (ii) interfacial deposition or solvent displacement (Fessi, 1989), (iii) phase inversion temperature (Heurtault, 2002) and (iv) polymer adsorption onto a preformed emulsion (Prego, 2006; Lozano, 2008).

The choice of the most appropriate materials and methods for the preparation of the nanocapsules is critical. The size and large surface-to-volume ratios of the nanocapsules facilitate their accumulation in the tumor by the well-known enhanced permeability and retention effect (EPR) (Iyer, 2006; Greish 2007) and their capacity to be internalized by the tumor cells. Moreover, it has been shown that lipid nanocapsules behave as a MDR-inhibiting system (Brigger, 2002; Garcion, 2006).

There are a number of reports showing the advantages of nanocapsules for specific anticancer drugs. For example, Lenaerts et al. (Lenaerts, 1995) encapsulated phtalocyanines, important agents in photodynamic tumor therapy, in poloxamer surface modified-PACA nanocapsules. They found that the presence of some types of poloxamer significantly decreased the uptake of nanocapsules by organs rich in phagocytic cells and increased the accumulation of phtalocyanines in primary tumors The concentration of photosensitizers in the tumor was maximal 12 h post-administration, these carriers allowing a 200-fold higher accumulation in the tumor.

In different reports it has been shown that lipid nanocapsules are adequate vehicles for the delivery of taxanes. More specifically, the encapsulation of paclitaxel into lipid nanocapsules led to a significant concentration increase in the tumoral tissue, and significantly reduced the tumor mass compared to the commercial product (Taxol ®) (Garcion, 2006). Additionally, *in vivo* studies in rats have shown that lipid nanocapsules enhanced around 3-fold the oral bioavailability of the anticancer drug, in comparison with the commercial product (Peltier, 2006; Lacoeuille, 2007). Docetaxel is another taxane that has been encapsulated into lipid nanocapsules; these nanocapsules showed an enhanced drug deposition in mice tumors which was characterized by a 5-fold increase in the area under the curve of the tumor (AUCtumor) when compared to the control formulation (Taxotere®) (Khalid, 2006).

An alternative carrier for the intracellular delivery of docetaxel consisting of oligomer chitosan nanocapsules (Lozano, 2008) has been proposed. The results have shown that chitosan nanocapsules are able to facilitate the rapid internalization of the drug into the cancer cells, leading to a significant increase of the antiproliferative effect of the drug.

Overall, the results presented here indicate that nanocapsules represent an alternative for the intracellular delivery of hydrophobic anticancer drugs. This potential is related to their capacity to be internalized by the cells and inhibit the MDR mechanisms, thus maximizing the antitumoral drug effects.

A new generation of nanocapsules, named **lipid nanocapsules**, were first prepared by the group of Benoit (Heurtault, 2002). These systems consist of an oil core surrounded by a thick polymeric shell, made of PEG-hydroxystearate and phosphatidylcholine. These nanocapsules can be prepared via a solvent-free, phase inversion process. In this process, all the components of the system are mixed together with the aqueous phase and, then, exposed to several cycles of heating and cooling (usually between temperatures around 65 and 85ºC). The size and polydispersity of the nanocapsules decrease as a function of the number and temperature cycles and a thick interfacial layer is created with this cycling process, since the surfactant is forced to overconcentrate at the interface of the oily droplets (Anton, 2007). Finally, the process is quenched at a temperature below the phase inversion temperature (o/w emulsion), followed by addition of cold water. This fast cooling-dilution process led to the formation of lipid nanocapsules with particle sizes between 20 and 100 nm (Heurtault, 2003).

1.4.3.1 Polyaminoacids as coating materials for nanocarriers

Polyaminoacids are biodegradable materials composed of long chains of amino acids. They can be obtained by natural or synthetic route and have raised great expectancy in the development of nanocarriers for anticancer drugs. Polyaminoacids have been found to render nanocarriers surface more hydrophilic and flexible to prevent the uptake by the mononuclear phagocytic system (MPS) (Danhier, 2010; Huynh, 2010; Yoshizawa, 2011). An interesting property of polyaminoacids relies

on the possibility to conjugate them with poly(ethylene glycol) (PEG). Among them, the anionic polymer poly-L-glutamic acid (PGA) is a promising candidate because of its properties.

Polyglutamic acid (PGA) is a highly anionic polyaminoacid composed of naturally occurring L-glutamic acid linked by peptide bonds. Two different isoforms of this polyaminoacid exist: α and γ isoforms. Isoform γ is obtained by bacterial fermentation and it is made up of L-glutamic acid monomers linked via amino bonds between γ-carboxyl and α-amino groups of adjacent monomer. This isoform is rarely used in pharmaceutical technology due to their limited availability. Isoform α, structurally different and obtained by synthesis, consists of L-glutamic acid units linked through amide bonds (Figure 5). γ free carboxyl groups are negatively charged favoring its solubility in water. Furthermore, α carboxyl groups can be used to bind other polymers, such as PEG, in order to obtain diblock or grafted structures. PGA is highly biocompatible and readily biodegradable by digestion with lysosomal enzymes. It is a suitable material for drug delivery designed not only owing to its safety profile but also because it renders the surface of the nanocarriers more hydrophilic avoiding the uptake by the mononuclear phagocytic system. This enhanced circulation times are important to achieve enhanced accumulation of the anticancer drug at the tumor site by the EPR effect, as it has been observed for PGA-paclitaxel® conjugates.

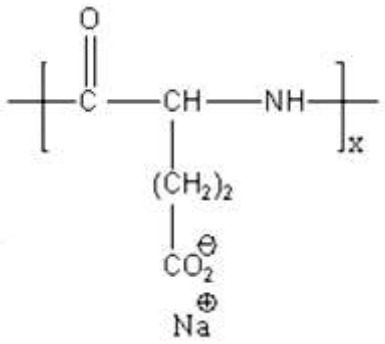

Figure 5: *Chemical structure of isoform α of poly-L-glutamic acid.*

PGA has been already included in carrier system relevant to cancer therapy. Xyotax® (PGA-conjugated paclitaxel) has become the first polymer-drug conjugated for the delivery of cytotoxic chemotherapeutic agent to advance to clinical Phase III trials (Jack, 2005).

Also in 2008 Phase I and II studies of PGA derivate, polyglutammate-camptothecine conjugated (CT 2106) were successfully carried out (Homsi, 2007).

1.5 Selected model drugs

The role of natural products as a source for remedies has been recognized since ancient times (Farnsworth, 1985; Cragg, 1997). An analysis of the number of chemotherapeutic agents and their sources indicates that over 60% of approved drugs are derived from natural compounds (Cragg, 1997). Numerous natural products have been studied to determine the molecular pathways for cancer prevention and treatment (Bachrach, 2002; Narayan, 2004; Jagtap, 2009; Lee, 2011).

The development of novel agents from natural sources presents obstacles that are not usually met when one deals with synthetic compounds. For instance, there may be difficulties in accessing the source of the samples, obtaining appropriate amounts of the sample, in the identification and isolation of the active compound in the sample, and problems in synthesizing the necessary amounts of the compound of interest. In addition their poor solubility and bioavailability have severely limited their use. Our work was focused on formulation of different natural (curcumin and artemisinin) and semisynthetic (docetaxel and dihydroartemisinin) compounds for cancer therapy, to overcome the shortcomings described.

1.5.1 Docetaxel

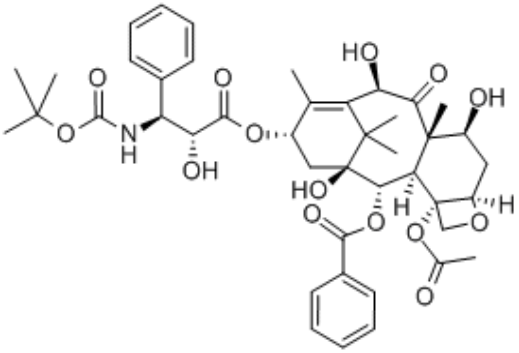

Figure 6: *Chemical structure of docetaxel.*

Docetaxel (Figure 6) is one of the most important cytotoxic chemotherapeutic agents used today in the treatment of breast, lung, ovarian, gastric, and prostate cancer. Phase III clinical trials in other solid tumours, such as squamous-cell head and neck cancers and transitional-cell carcinoma of the urothelium, are further defining the role of docetaxel in these cancers (Montero, 2005).

Docetaxel is a semisynthetic taxane, a class of anticancer agents that bind to β tubulin, thereby stabilizing microtubules and inducing cell-cycle arrest and apoptosis. Taxanes (paclitaxel and docetaxel) have a different mechanism of action from that of any other class of anticancer.

Paclitaxel was originally isolated from the bark of the yew tree *Taxus brevifolia* (Wani, 1971), a finite source of the compound. It took some years to develop a semi-synthetic analog (docetaxel) which is derived from a renewable source, the leaves of *Taxus baccata* (Cortes, 1995). Currently, total synthesis has been achieved for both agents and drug supply is no longer a problem.

Although these novel chemotherapeutics have led to improvements in survival, they are associated with numerous drug-related toxicities. Docetaxel has been associated with a significant increase in neutropenia, febrile neutropenia, leucopenia, stomatitis, edema, fatigue and/or asthenia, and diarrhea (Montero, 2005). These effects are due in part to the high doses used to achieve the desired anti-tumor effect, which are necessary because of the non-specific distribution of both novel and traditional chemotherapies, with only a small fraction of drugs reaching the tumor. The drugs can accumulate in healthy organs, and there is a fine line between tolerability and severe morbidity, e.g., in the case of doxorubicin, a DNA intercalator that produces cardiotoxicity (Olson, 1990).

These drugs are characterized by their hydrophobic character and a resulting necessity to use solubilizer for their intravenous administration. So far, Cremophor EL and Tween80®, both of wich combined with ethanol, have been the only pharmaceutical formulation vehicles used for administration of paclitaxel and docetaxel, respectively. These veicles, however are responsible for severe side effects wich limit the amount of drug that can be safely administered (Van Zuylen, 2001; Engels, 2006).

The commercial formulation of docetaxel, Taxotere®, is formulated with a high concentration of Tween 80® (40 g/L), which has been found to have severe side effects, including hypersensitivity reactions, cumulative fluid retention, and nausea and which has shown incompatibility with commonly used polyvinyl chloride intravenous administration sets (Ma, 2011). Taken together, these factors compromise the curative potential of anticancer drugs, and more effective methods for their delivery to tumors are required (Blanko, 2011). To overcome these problems, alternative nanotechnology-based formulation, which do not require solubilization, have recently been proposed. These formulation consist of nanostructures, such as polymer conjugates, polymeric micelles, liposomes or nanoparticles (Heath, 2008; Peer, 2007).

1.5.2 Curcumin

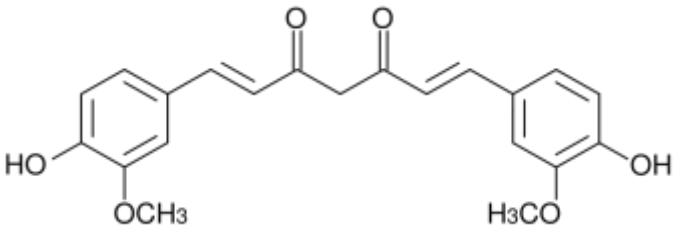

Figure 7: *Chemical structure of curcumin.*

The polyphenol curcumin (Figure 7) is the active ingredient in the herbal remedy and dietary spice turmeric *Curcuma longa* Linn. This yellow spice, derived from the rhizome of the plant, has a long history of use in traditional medicines of China and India (Ammon, 1991). Research has revealed that curcumin has a surprisingly wide range of beneficial properties, including anti-inflammatory, antioxidant, chemopreventive and chemotherapeutic activity. These activities have been demonstrated both in cultured cells and in animal models, and have paved the way for ongoing human clinical trials (Hatcher, 2008). The pleiotropic activities of curcumin derive from its complex chemistry as well as its ability to influence multiple signaling pathways. Curcumin inhibits cancer development and progression, targeting multiple steps in the pathway to malignancy (Figure 8). Curcumin has activity as both a blocking agent, inhibiting the initiation step of cancer pressing agent, inhibiting malignant cell proliferation during promotion and progression of carcinogenesis (Duvoix, 2005).

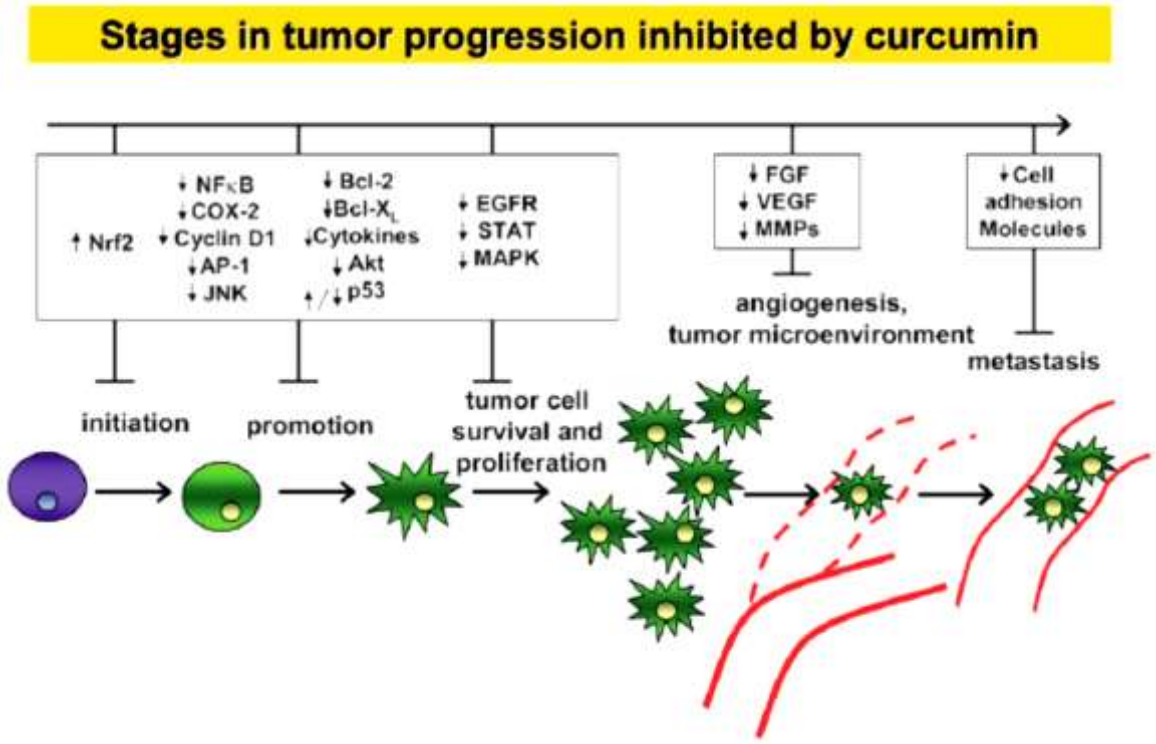

Figure 8: *Stages in tumor progression inhibited by curcumin (Arbiser, 1998).*

Curcumin has been shown to interfere with many of the processes involved in angiogenesis (Arbiser, 1998). Early studies demonstrated that curcumin inhibits fibroblast growth factor (FGF)-induced neovascularization (Gururaj, 2002). Additional effects of curcumin on angiogenesis and metastasis may be mediated by its ability to regulate cell adhesion molecules such as intracellular adhesion molecule-1 (ICAM-1), vascular cell adhesion molecule-1 (VCAM-1), and endothelial leukocyte adhesion molecule-1 (ELAM-1), cell surface proteins involved in tumor metastasis (Bhandarkar, 2007). Curcumin is a potent inhibitor of ligand-induced activation of epidermal growth factor receptor (EGFR), suggesting the potential to block the cascade of intracellular signals associated with mutagenesis and cell proliferation (Korutla, 1995). Among signaling pathways affected by curcumin are key survival pathways regulated by NF-kB and Akt, as well as cytoprotective pathways dependent on Nrf2.

Owing to its valuable properties, almost 100 pharmaceutical and chemical companies are producing various curcumin products in the form of tablets, capsules, coloring agents, creams, drinks, extracts, gels, nasal sprays, and so on for daily and medical needs (Goel, 2008). Various clinical trials are underway or have been completed to judge the efficacy of curcumin as a therapeutic molecule in medicine (www.clinicaltrials.gov/curcumin).

A major limiting factor of curcumin is its low solubility in water (i.e. $0.4x10^{-3}$ mg/ml at pH 7.3). Many preclinical and clinical studies in mice, rats and humans revealed a low bioavailability of curcumin (Goel, 2008; Aggarwal, 2007). Although 10 or 12 g/ml of curcumin administered orally in humans showed curcumin levels in serum to be approximately 50 ng/ml, this resulted in a minimum availability of curcumin in the blood circulation to achieve its therapeutic effects (Lao,

2007). A simple way of solving the limiting factors of curcumin is to improve its bioavailability, protect it from degradation and metabolism, and increase its targeting capacity toward cancer tumor(s).

Various types of nanocarriers are suitable and have been investigated for the delivery of an active form of curcumin to tumors (Muqbil, 2011). Stable self-emulsifying liquid formulations of curcumin with particles size of approximately 30 nm and approximately 99% curcumin loading have successfully been developed (Setthacheewakul, 2010). These formulations have a 10–14-fold greater absorption rate in male Wistar-strain rats given an oral treatment of 50 mg/kg of curcumin, compared with the same oral dose of free curcumin.

D-a tocopheryl polyethylene glycol 1000 succinate (TPGS) stabilized curcumin nanosuspension (CUR-NS) crystal formulation has been evaluated for the pharmacokinetics and biodistribution of curcumin after intravenous administration in rabbits and mice (Gao, 2010). The area under the plasma concentration (AUC; 0–1) of CUR-NS (700.43±281.53 mg/ml min) was 3.8-fold greater than for a curcumin solution (145.4±9.29 mg/ml min). The mean residence time was 11.2-fold longer with CUR-NS compared with a curcumin solution (194.57±32.18 min versus 15.88±3.56 min).

Co-administration of curcumin and paclitaxel nanoemulsion formulations are capable of overcoming MDR in SKOV-3 (TR) human ovarian adenocarcinoma cells by inhibiting NF-kB activity, downregulating P-gp and promoting apoptotic responses (Ganta, 2009). Additionally, curcumin nanoemulsion increases the bioavailability of paclitaxel up to 5.2-fold, and there is a 3.2-fold increase in its accumulation at the tumor site in an oral administration to SKOV-3 tumor-bearing xenograft mice models. This resulted from downregulation of intestinal P-gp and cytochrome P450 3A2 (CYP3A2) protein levels (Ganta, 2010).

A combined glycerol monooleate and pluronic F-127 polymer nanocarrier is also well suited to the delivery of curcumin to various types of cancer cell (i.e. PANC-1, MiaPaCa-2, K-562, MCF-7, A549 and HCT-16) (Mohanty, 2010). This formulation has shown significant anticancer properties at all concentrations (5–30 mM) compared with free curcumin. These improved effects are correlated with the inhibition of phosphorylation and activation of the Akt pathway, which inactivates NF-kB and inhibits the proliferation and induction of apoptosis.

Safe toxicological profiles of the various curcumin nanoformulations and their efficacy in the cell-line models highlight their potential for evaluation in *in vivo* models. Human trials need to be conducted to establish their effectiveness in clinical applications as an improved therapeutic modality for cancer treatment.

1.5.3 Artemisinin and Dihydroartemisinin

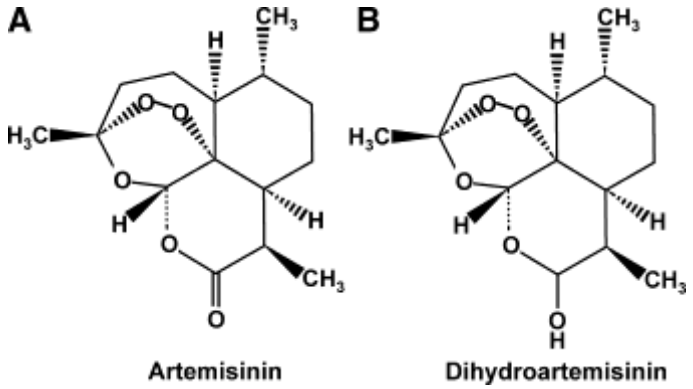

Figure 9:*Chemical structure of artemisinin* ***(A)*** *and dihydroartemisinin* ***(B)****.*

Artemisinin (Figure 9) a sesquiterpene lactone derived from the sweet wormwood plant *Artemisia annua* is widely used as an antimalarial drug (Hsu, 2006; Miller, 2011; Tu, 2011). Recently, more and more evidences have emerged to elucidate that artemisinin and its derivatives show potent anticancer activities in a variety of human cancer cells (Hou, 2008; Chen, 2009; Morrisey, 2010; O'Neill, 2010). Molecular, cellular and physiological studies have demonstrated that, depending on the tissue type and experimental system, artemisinin and its derivatives arrest the growth, induce an apoptotic response, alter hormone responsive properties and/or inhibit angiogenesis of human cancer cells. One proposed mechanism by which artemisinin targets cancer cells is cleavage of the endoperoxide bridge by the relatively high concentrations of iron in cancer cells, resulting in free radicals such as ROS and subsequent oxidative damage as well as iron depletion in the cells. This mechanism resembles the action of artemisinin in malarial parasites (Bustos, 1994). In addition to possessing higher iron influx via transferrin receptors, cancer cells are also sensitive to oxygen radicals because of a relative deficiency in antioxidant. In details it has been postulated that bioactivation of artemisinin occurs in the endosome after pH-induced release of iron from internalized transferrin. Iron activated-artemisinin generates carbon-centered radicals which may mediate lysosomal disruption and generation of ROS resulting in mitochondrial damage, activation of caspases, and cell death. Alternatively, it has been suggested that only specific activation of artemisinin by heme or heme-bound protein generates cytotoxic carbon-centered radicals. In the mitochondrion, these adducts interfere with the electron transfer chain (ETC) by interacting with heme or heme-bound proteins leading to generation of ROS and apoptosis. ROS harboring may induce ER stress and genotoxicity (Crespo-Ortiz, 2012) (Figure 10).

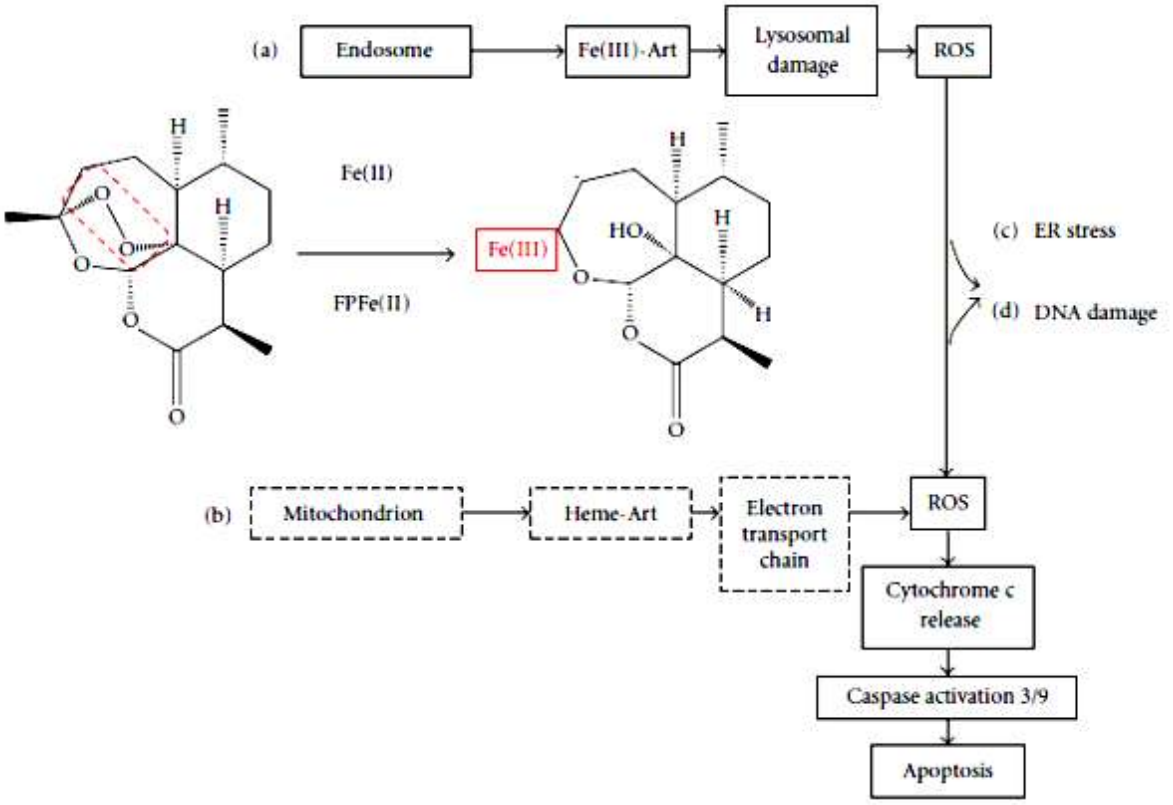

Figure 13: *Postulated anticancer mechanisms of action of artemisinins (Crespo-Ortiz, 2012)*

Despite its efficacy artemisinin has pharmacokinetic limitations. Artemisinin has low solubility in water or oil, making it difficult to administrate through intravenous injection, it has poor bioavailability, and a short half-life *in vivo* (~2.5 h) (Ashton, 1998; Li, 2007). To overcome some of these problems, generations of artemisinin-like endoperoxides including semisynthetic derivatives and fully synthetic compounds have been developed. Semisynthetic artemisinins are obtained from dihydroartemisinin (DHA), the main active metabolite of artemisinin (Haynes, 2002; Klayman, 1985).

Dihydroartemisinin (Figure 9) is an artemisinin derivative with the C-10 lactone group replaced by hemiacetal. DHA has been widely used as an antimalarial drug due to its efficacy and easy production with less synthetic steps and a lower cost (Wilairatana, 1998). In recent years, DHA has also been shown to be effective in killing cancer cells (Lai, 1995; Efferth, 2001; Efferth, 2004; Sing, 2001; Golenser, 2006; Nakase, 2008). One study that tested 55 cell lines from the Developmental Therapeutics Program of the National Cancer Institute (NCI) showed that dihydroartemisinin has remarkable antineoplastic activity against pancreatic, leukemic, osteosarcoma, and lung cancer cells (Lu, 2009). Studies have shown that DHA inhibits cell proliferation, and/or induces apoptosis in various human cancer cell lines via downregulating cyclin (D1,E), Bcl-2, Bcl-xL, caspase (3,9), and VEGF, while upregulating P21, P27, and Bax (Chen 2003; Mu, 2008; Fujita, 2008; Hou, 2008). Recent studies also indicate that DHA inhibits cell growth, induces cell cycle arrest, and promotes apoptosis in pancreatic cancer cells both *in vitro* and *in vivo* (Chen, 2009).

However, DHA has poor water-solubility and low bioavailability for oral administration due to slow drug dissolution and decomposition in the stomach and intestine (Gabriels, 2004). Furthermore, the half-life of DHA is very short (34–90 min) (Batty, 1996). It has been demonstrated that intravenous delivery of DHA results in the highest availability to body as compared to all other routes (Li, 1998). Therefore, the development of the new formulation of DHA that enables quickavailability to the body is in great need.

A novel N/O/W submicron emulsion with high drug loading capacity was prepared for intravenous administration of DHA. The pharmacokinetics of N/O/W emulsion is characterized by the significantly prolonged half-life and slow plasma clearance compared with conventional O/W emulsion and DHA solution. Presumably due to the improved PK profiles, the toxic effect of DHA was greatly reduced. Furthermore, the antitumor efficacy was demonstrated *in vivo* studies using a hepatic H22 tumor transplanted mouse model. (Wang, 2012).

A solvent diffusion method in an aqueous system was employed to prepare DHA-NLC; the formulation was optimized using response surface methodology central and the drug release *in vitro* exhibited a sustained release over 48 h (Zhang, 2010a).

The pharmacokinetics and tissue distribution after intravenous administration of DHA in nanostructured lipid carrier (NLC) and in solution were then compared. The mean residence times (MRT) of the DHA-NLC was much longer than that of the DHA solution. In the tested organs, the AUC values of the DHA-NLC were higher than that of the DHA solution in liver, spleen, lung, brain and muscle, and lower than the DHA solution in heart and kidney. DHA-NLC prepared in this study is a promising sustained-release and drug-targeting system for antitumor drugs. It may also allow a reduction in dosage and a decrease in systemic toxicity (Zhang, 2010b).

1.6 REFERENCES

Aggarwal, B.B. et al., Curcumin: the Indian solid gold. Adv. Exp. Med. Biol. 2007, 595: 1–75.

Allen T.M., Ligand-targeted therapeutics in anticancer therapy. Nat. Rev. Cancer. 2002, 2, 750–763.

Allen T.M., Long-circulating (sterically stabilized) liposomes for targeted drug-delivery. Trends Pharmacol. Sci. 1994, 15: 215–220.

Ammon H., et al., Pharmacology of Curcuma longa. Planta Med. 1991, 57: 1–7.

Anton N., et al., Nano-emulsions and nanocapsules by the PIT method: An investigation on the role of the temperature cycling on the emulsion phase inversion. Int J Pharm. 2007, 344: 44-52.

Antony A.C., The biological chemistry of folate receptors. Blood. 1992, 79: 2807–2820.

Arbiser J., et al., Curcumin is an in vivo inhibitor of angiogenesis. Mol. Med. 1998, 4: 376–383.

Ashton M., et al., Artemisinin kinetics and dynamics during oral and rectal treatment of uncomplicated malaria, Clinical Pharmacology and Therapeutics. 1998, 63, 4: 482–493.

Bachrach U., et al., Cancer therapy and prevention by green tea: Role of ornithine decarboxylase. Amino Acids. 2002, 22: 1-13.

Bangham A.D., et al., Negative staining of phospholipids and their structural modifi cation by surface-active agents as observed in the electron microscope. J Mol Biol. 1964, 8:660–668.

Batty K.T., et al., Selective high performance liquid chromatographic determination of artesunate and α- and β dihydroartemisinin in patients with falciparum malaria. Journal of Chromatography B. 1996, 677: 345–350.

Bhandarkar S.S., et al., Curcumin as an inhibitor of angiogenesis. Adv. Exp.Med. Biol. 2007, 595: 185–195.

Blanco E., et al., Nanomedicine in cancer therapy: Innovative trends and prospects. Cancer Sci. 2011, 102, 1247–1252.

Brigger I., et al., Nanoparticles in cancer therapy and diagnosis. Adv Drug Deliv Rev. 2002, 54: 631-651.

Bustos M.D., et al., In-vitro tests on Philippine isolates of Plasmodium falciparum against four standard antimalarials and four qinghaosu derivatives. Bulletin of the World Health Organization. 1994, 72: 729-735.

Chen D.B., et al., In Vitro and in Vivo Study of Two Types of Long-Circulating Solid Lipid Nanoparticles Containing Paclitaxel. Chem. Pharm. Bull. 2001, 49(11): 1444—1447.

.

Chen H.H., et al., Inhibition of human cancer cell line growth and human umbilical vein endothelial cell angiogenesis by artemisinin derivatives in vitro. Pharmacol. Res. 2003, 48: 231–236.

Chen T., et al., Dihydroartemisinin induces apoptosis and sensitizes human ovarian cancer cells to carboplatin therapy. J Cell Mol Med. 2009, 13: 1358–1370.

Cho K., et al., Therapeutic nanoparticles for drug delivery in cancer. Clin Cancer Res. 2008, 14:1310–1316.

Cortes J.E., et al., Docetaxel. J Clin Oncol. 1995, 13:2643-2655.

Couvreur, P., et al., Nanocapsule technology: A review. Crit Rev Ther Drug Carrier Syst. 2002, 19: 99-134.

Couvreur, P., et al., Nanocapsules: a new type of lysosomotropic carrier. FEBS Lett. 1977, 84: 323-326.

Cragg G.M., et al., Natural products in drug discovery and development. J Nat Prod. 1997, 60: 52-60.

Crespo-Ortiz M., et al., Antitumor activity of artemisinin and its derivatives: from a well-know antimalarial agent to a potential anticancer drug. Journal of Biomedicine and Biotechnology. 2012.

Danhier F., et al., To exploit the tumor microenvironment: Passive and active tumor targeting of nanocarriers for anti-cancer drug delivery. J Controlled Release 2010, 148(2):135-146.

Das, M. et al. Ligand-based targeted therapy for cancer tissue. Drug Delivery. 2009, 6: 285–304.

Drummond D.C., et al., Optimizing liposomes for delivery of chemotherapeutic agents to solid tumors. Pharmacol Rev. 1999, 51: 691–743.

Duvoix A., et al., Chemopreventive and therapeutic effect of curcumin. Cancer Lett. 2005, 223: 181–190.

Efferth T., et al., Enhancement of cytotoxicity of artemisinins toward cancer cells by ferrous iron. Free Radical Biology & Medicine. 2004, 37: 998–1009.

Efferth T., et al., The anti-malarial artesunate is also active against cancer. International Journal of Oncology. 2001, 18: 767–773.

Egusquiaguirre S.P., et al., Nanoparticle delivery systems for cancer therapy: advances in clinical and preclinical research. Clin Transl Oncol. 2012, 14:83-93.

Ehadaie B., Application of Nanotechnology in Cancer Research: Review of Progress in the National Cancer Institute's Alliance for Nanotechnology. Int J Biol Sci. 2007, 3(2):108-110.

Engels F.K., et al., Influence of high dose ketoconazol on the pharmacokinetics of docetaxel. Cancer Biol Ther. 2006, 5: 833–9.

Farnsworth N.R., et al., Medicinal plants in therapy. Bull World Health Organ. 1985, 63: 965-981.

Ferrari M., Cancer nanotechnology: opportunities and challenges. Nat. Rev. Cancer. 2005, 5: 161–171.

Fessi H., et al., Nanocapsule formation by interfacial polymer deposition following solvent deplacement. Int J Pharm. 1989, 55: 25-28.

Fujita T., et al., Human fortilin is a molecular target of dihydroartemisinin, FEBS Lett. 2008, 582: 1055–1060.

Gabriëls M., et al., Design of a dissolution system for the evaluation of the release rate characteristics of artemether and dihydroartemisinin from tablets. International Journal of Pharmaceutics. 2004, 274: 245–260.

Ganta S., et al., Curcumin enhances oral bioavailability and anti-tumor therapeutic efficacy of paclitaxel upon administration in nanoemulsion formulation. J. Pharm. Sci. 2010, 99: 4630–4641.

Ganta S., et al., Coadministration of paclitaxel and curcumin in nanoemulsion formulations to overcome multidrug resistance in tumor cells. Mol. Pharm. 2009, 6: 928–939.

Gao Y., et al., Preparation, characterization, pharmacokinetics, and tissue distribution of curcumin nanosuspension with TPGS as stabilizer. Drug Dev. Ind. Pharm. 2010, 36: 1225–1234.

Garcion E., et al., A new generation of anticancer, drug-loaded, colloidal vectors reverses multidrug resistance in glioma and reduces tumor progression in rats. Mol Cancer Ther. 2006, 5: 1710-1722.

Gasco M.R., Method for producing solid lipid microspheres having a narrow size distribution. United States of America Patent, 1993.

Gill P.S., et al., Randomized phase III trial of liposomal daunorubicin versus doxorubicin, bleomycin, and vincristine in AIDS-related Kaposi's sarcoma. J Clin Oncol. 1996, 14: 2353–2364.

Goel A., et al., Curcumin as 'curecumin': from kitchen to clinic. Biochem. Pharmacol. 2008, 75: 787–809.

Gokce E.H., et al., Cyclosporine A loaded SLNs: evaluation of cellular uptake and corneal cytotoxicity. Int. J. Pharm. 2008, 364: 76–86.

Golenser J., et al., Current perspectives on the mechanism of action of artemisinins. International Journal for Parasitology. 2006, 36: 1427–1441.

Gottesman M.M., et al., Multidrug resistance in cancer: Role of ATP-dependent transporters. Nat. Rev. Cancer. 2002, 2: 48–58.

Greish K., et al., Enhanced permeability and retention of macromolecular drugs in solid tumors: A royal gate for targeted anticancer nanomedicines. J Drug Target. 2007, 15: 457-464.

Gullotti E., et al., Extracellularly activated nanocarriers: a new paradigm of tumor targeted drug delivery. Mol. Pharm. 2009, 6: 1041–1051.

Gururaj A., et al., Molecular mechanisms of antiangiogenic effect of curcumin. Biochem. Biophys. Res. Commun. 2002, 297: 934–942.

Hanahan D. et al., The hallmarks of cancer. Cell. 2000, 100: 57–70.

Hatcher H., et al., Curcumin: from ancient medicine to current clinical trials. Cell Mol Life Sci. 2008, 65:1631–1652.

Haynes R.K., et al., C-10 ester and ether derivatives of dihydroartemisinin - 10-α artesunate, preparation of authentic 10-β artesunate, and of other ester and ether derivatives bearing potential aromatic intercalating groups at C-10. European Journal of Organic Chemistry. 2002,1: 113–132.

Heat J.R., et al., Nanotechnology and cancer, Annu. Rev. Med. 2008. 59: 251–65.

Hestella-Ermoso de Mendoza A., et al., Lipid Nanomedicine for Anticancer Drug Therapy. Journal of Biomedical Nanotechnology. 2009, 5: 1-21.

Heurtault B., et al., A novel phase inversion-based process for the preparation of lipid nanocarriers. Pharm Res. 2002, 19: 875-880.

Heurtault B., et al., Interfacial stability of lipid nanocapsules.Colloids Surf B Biointerfaces. 2003, 30: 225-235

Hofheinz R.D., et al., Liposomal encapsulated anti-cancer drugs. Anticancer Drugs. 2005, 16: 691–707.

Homsi J., et al., Phase I Trial of Poly-l-Glutamate Camptothecin (CT-2106) Administered Weekly in Patients with Advanced Solid Malignancies. Clinical Cancer Research. 2007, 13 (19): 5855-5861.

Hou J., et al., Experimental therapy of hepatoma with artemisinin and its derivatives: in vitro and in vivo activity, chemosensitization, and mechanisms of action. Clin Cancer Res. 2008, 14: 5519-5530.

Hsu E., et al., The history of qing hao in the Chinese materia medica. Trans R Soc Trop Med Hyg. 2006, 100: 505–508.

Huynh N.T., et al., The rise and rise of stealth nanocarriers for cancer therapy: passive versus active targeting. Nanomedicine 2010, 5(9):1415-1433.

Immordino M.L. et al., Stealth liposomes: review of the basic science, rationale, and clinical applications, existing and potential. Int J Nanomedicine. 2006, 1(3): 297–315.

Immordino M.L., et al., Preparation, characterization, cytotoxicity and pharmacokinetics of liposomes containing docetaxel. J Control Release, 2003, 91: 417–29.

Ishida O., et al., Liposomes bearing polyethyleneglycol-coupled transferrin with intracellular targeting property to the solid tumors in vivo. Pharm. Res. 2001, 18: 1042–1048.

Iyer A.K., et al., Exploiting the enhanced permeability and retention effect for tumor targeting. Drug Discov Today. 2006, 11: 812–818.

Jack W.S., Paclitaxel poliglumex (XYOTAX™, CT-2103): A macromolecular taxane. J Control Release. 2005, 109(1–3): 120-126.

Jagtap S., et al., Chemoprotective mechanism of the natural compounds, epigallocatechin-3-O-gallate, quercetin and curcumin against cancer and cardiovascular diseases. Curr. Med. Chem. 2009, 16: 1451-1462.

Jain R.K., Barriers to drug-delivery in solid tumors. Sci. Am. 1994, 271: 58–65.

Jain R.K., et al., Delivering nanomedicine to solid tumors. Nat Rev Clin Oncol. 2010, 7: 653–664.

Khalid M.N., et al., Long circulating poly(ethylene glycol)-decorated lipid nanocapsules deliver docetaxel to solid tumors. Pharm Res. 2006, 23: 752-758.

Klayman D.L., et al., Qinghaosu (artemisinin): an antimalarial drug from China. Science, 228, 4703: 1049–1055, 1985.

Kohandel M., et al., Dynamics of tumor growth and combination of anti-angiogenic and cytotoxic therapies. Phys Med Biol. 2007, 52: 3665–3677.

Korutla L., et al., Inhibition of ligand-induced activation of epidermal growth factor receptor tyrosine phosphorylation by curcumin. Carcinogenesis. 1995, 16: 1741–1745.

Kristl J., et al., Interactions of solid lipid nanoparticles with model membranes and leukocytes studied by EPR. Int. J. Pharm. 2003, 256: 133–140.

Kukowska-Latallo J.F., et al., Nanoparticle targeting of anticancer drug improves therapeutic response in animal model of human epithelial cancer. Cancer Res. 2005, 65: 5317–5324.

Lacoeuille F., et al., *.In vivo* evaluation of lipid nanocapsules as a promising colloidal carrier for paclitaxel. Int J Pharm. 2007, 344: 143-149.

Lai H., et al., Selective cancer cell cytotoxicity from exposure to dihydroartemisinin and holotransferrin. Cancer Letters. 1995, 91: 41–46.

Lammers T., et al., Drug targeting to tumors: principles, pitfalls and (pre-) clinical progress. J Control Release (in press).

Lao C.D. et al., Dose escalation of a curcuminoid formulation. BMC Complement. Altern. Med. 2007, 6: 10.

Lee K.W., et al., Molecular targets of phytochemicals for cancer prevention. Nat. Rev. Cancer. 2011, 1: 211-218.

Legrand, P., et al., Polymeric nanocapsules as drug delivery systems: A review. STP Pharm. Sci.1999, 9: 411-418.

Lenaerts V., et al., Nanocapsules with a reduced liver uptake: Targeting of phthalocyanines to EMT-6 mouse mammary tumor *in vivo*. Eur J Pharm Biopharm. 1995, 41: 38-43.

Li G., et al., Pharmacokinetics and bioavailability of dihydroartemisinin, arteether, artemether, artesunic acid and artelinic acid in rats, Journal of Pharmacy and Pharmacology. 1998, 50: 173–182.

Li Q., et al., Pharmacokinetic and pharmacodynamic profiles of rapid-acting artemisinins in the antimalarial therapy, Current Drug Therapy. 2007, 210–223.

Liu K., et al., Preparation and characterization of 10-hydroxycamptothecin loaded nanostructured lipid carriers. Drug Dev. Ind. Pharm. 2008, 34: 465–471.

Lopes De Menezes D.E., et al., Cellular traff icking and cytotoxicity of anti-CD19-targeted liposomal doxorubicin in B lymphoma cells. J Liposome Res. 1999, 199–228.

Lozano M.V., et al., Highly Efficient System To Deliver Taxanes into Tumor Cells: Docetaxel-Loaded Chitosan Oligomer Colloidal Carriers. Biomacromolecules, 2008. 9(8): 2186-2193.

Lu B., et al., Solid lipid nanoparticles of mitoxantrone for local injection against breast cancer and its lymph node metastases. European Journal of Pharmaceutical Sciences. 2006, 28 (2): 86-95.

Lu Y.Y. et al., Dihydroartemisinin (DHA) induces caspase-3-dependent apoptosis in human lung adenocarcinoma ASTC-a-1 cells. Journal of Biomedical Science. 2009, 16,1.

Luo J. et al., Principles of cancer therapy: oncogene and non-oncogene addiction. Cell. 2009, 136: 823–837.

Ma Y., et al., Novel docetaxel-loaded nanoparticles based on PCL-Tween 80 copolymer for cancer treatment. Int J Nanomedicine. 2011, 6: 2679–2688.

Maeda H., et al., The enhanced permeability and retention (EPR) effect in tumor vasculature: the key role of tumor-selective macromolecular drug targeting. Adv Enzyme Regul. 2001, 41: 189–207.

Malam Y., et al., Liposomes and nanoparticles: nanosized vehicles for drug delivery in cancer. Trends Pharmacol. Sci. 2009, 30: 592–599.

Matsumura Y., et al., Phase I and pharmacokinetic study of MCC-465, a doxorubicin (DXR) encapsulated in PEG immunoliposome, in patients with metastatic stomach cancer. Ann Oncol. 2004, 15: 17–525.

Matsumura Y., et al., Phase I clinical trial and pharmacokinetic evaluation of NK911, a micelle encapsulated doxorubicin. Br J Cancer. 1999, 91: 1775–1781.

Medina O.P., et al., Targeted liposomal drug delivery in cancer. Curr Pharm Des. 2004, 10:2981–9.

Mehenert W., et al., Solid Lipid Nanoparticles: Production, characterization and applications. Advanced Drug Delivery Reviews. 2012, 64: 83–101.

Miller L.H., et al., Artemisinin: Discovery from the Chinese Herbal Garden. Cell. 2011, 146: 855–858.

Mohanty C., et al., The in vitro stability and in vivo pharmacokinetics of curcumin prepared as an aqueous nanoparticulate formulation. Biomaterials. 2010, 31: 6597–6611.

Montero A., et al., Docetaxel for treatment of solid tumours: a systematic review of clinical data The Lancet Oncology. 2005, 6, 4: 229-239.

Morrissey C., et al., Effect of artemisinin derivatives on apoptosis and cell cycle in prostate cancer cells. Anti-Cancer Drugs. 2010, 21: 423–432.

Mu D., et al., The role of calcium, P38 MAPK in dihydroartemisinin-induced apoptosis of lung cancer PC-14 cells. Cancer Chemother. Pharmacol. 2008, 61: 639–645.

Müller R.H., et al., Solid lipid nanoparticles (SLN)—an alternative colloidal carrier system for controlled drug delivery. Eur. J. Pharm. Biopharm. 1995, 41: 62–69.

Muqbil I., et al., Progress in nanotechnology based approaches to enhance the potential of chemopreventive agents. Cancer. 2011, 3: 428–445.

Nakase I., et al., Anticancer properties of artemisinin derivatives and their targeted delivery by transferrin conjugation. International Journal of Pharmaceutics. 2008, 354: 28–33.

Narayan S., et al., Curcumin, a multi-functional chemopreventive agent, blocks growth of colon cancer cells by targeting beta-catenin-mediated transactivation and cell-cell adhesion pathways. J. Mol. Histol. 2004, 35: 301-307.

O'Neill P.M., et al., The molecular mechanism of action of artemisinin–the debate continues. Molecules. 2010, 15: 1705–1721.

Olson R.D., et al., Doxorubicin cardiotoxicity: analysis of prevailing hypotheses. FASEB J. 1990, 4: 3076–3086.

Padera T.P., et al., Lymphatic metastasis in the absence of functional intratumor lymphatics. Science. 2002, 296:1883- 1886.

Parveen S. et al., Nanomedicine: clinical applications of polyethylene glycol conjugated proteins and drugs. Clinical Pharmacokinetics. 2006, 45: 965–988.

Parveen S. et al., Polymeric nanoparticles for cancer therapy. Journal of drug targeting. 2008, 16: 108–123.

Peer D., et al., Fluoxetine and reversal of multidrug resistance. Cancer Lett. 2006, 237: 180–187.

Peer D., et al., Nanocarriers as an emerging platform for cancer therapy. Nat Nanotechnol. 2007, 2 (12): 751-60.

Peer D., et al., Selective gene silencing in activated leukocytes by targeting siRNAs to the integrin lymphocyte function-associated antigen-1. Proc. Natl Acad. Sci. 2007, 104: 4095–4100.

Pelicano H., et al., Glycolysis inhibition for anticancer treatment. Oncogene. 2006, 25: 4633–4646.

Peltier S., et al., Enhanced oral paclitaxel bioavailability after administration of paclitaxel-loaded lipid nanocapsules. Pharm Res. 2006, 23: 1243-1250.

Prego C., et al., Chitosan nanocapsules: A new carrier for nasal peptide delivery. JDDST.2006, 16: 331-337.

Prost A.C., et al., Differential transferrin receptor density in human colorectal cancer: A potential probe for diagnosis and therapy. Int. J. Oncol. 1998, 13: 871–875.

Ruckmani K., et al., Methotrexate loaded solid lipid nanoparticles (SLN) for effective treatment of carcinoma. J Nanosci Nanotechnol. 2006, 6 (9-10): 2991-5.

Sanfilippo J.S., et al., Quantitative analyses of epidermal growth factor receptors, HER-2/neu oncoprotein and cathepsin D in nonmalignant and malignant uteri. Cancer. 1996, 77: 710–716.

Sankhala K.K., et al., A phase I pharmacokinetic (PK) study of MBP-426, a novel liposome encapsulated oxaliplatin. J Clin Oncol. 2009, 27: 2535.

Sapra P., et al., Ligand-targeted liposomal anticancer drugs. Prog Lipid Res. 1999, 42: 439–62.

Sarmento B., et al., Oral insulin delivery by means of solid lipid nanoparticles. Int. J. Nanomed. 2. 2007, 743–749.

Serpe L., et al., Cytotoxicity of anticancer drugs incorporated in solid lipid nanoparticles on HT-29 colorectal cancer cell line.European Journal of Pharmaceutics and Biopharmaceutics. 2004, 58 (3): 673-680.

Setthacheewakul S., et al. Development and evaluation of selfmicroemulsifying liquid and pellet formulations of curcumin, and absorption studies in rats. Eur. J. Pharm. Biopharm. 2010, 76: 475–485.

Singal P.K., et al., Doxorubicin-induced cardiomyopathy. N Engl J Med. 1998, 339: 900–905.

Singh N.P., et al., Selective toxicity of dihydroartemisinin and holotransferrin toward human breast cancer cells. Life Science. 2011, 70: 49–56.

Tagami T., et al., Efficient tumor regression by a single and low dose treatment with a novel and enhanced formulation of thermosensitive liposomal doxorubicin. J Control Release. 2011b, 152: 303–309

Tagami T., et al., Optimization of a novel and improved thermosensitive liposome formulated with DPPC and a Brij surfactant using a robust in vitro system. J Control Release. 2011a, 154: 290–297.

Torchilin V., Recent advances with liposomes as pharmaceutical carriers. Nat. Rev. Drug Discov. 2005, 4: 145–160.

Tu Y., et al., The discovery of artemisinin (qinghaosu) and gifts from Chinese medicine. Nat Med. 2011, 17: 1217–1220.

Van Zuylen., et al., Role of formulation vehicles in taxane pharmacology. Invest. New Drugs. 2001, 19: 125–141.

Wang S., et al., An injectable hybrid nanoparticle-in-oil-in-water submicron emulsion for improved delivery of poorly soluble drugs.Nanoscale Research Letters. 2012, 7:219.

Wang Y., et al., Characterization and body distribution of beta-elemene solid lipid nanoparticles (SLN), Drug Dev. Ind. Pharm. 2005, 31: 769–778.

Wani M.C., et al., Plant antitumor agents. VI. The isolation and structure of taxol, a novel antileukemic and antitumor agent from Taxus brevifolia. J Am Chem Soc. 1971, 93: 2325-2327.

Wilairatana P., et al., A comparison of three different dihydroartemisinin formulations for the treatment of acute uncomplicated falciparum malaria in Thailand. International Journal for Parasitology. 1998, 28: 1213–1218.

World Health Organization (2011) Cancer. Fact Sheet 297

Yoshizawa Y., et al., PEG liposomalization of paclitaxel improved its *in vivo* disposition and anti-tumor efficacy. Int J Pharm; In Press, Corrected Proof.

Yuan H., et al., Cellular uptake of solid lipid nanoparticles and cytotoxicity of encapsulated paclitaxel in A549 cancer cells. International Journal of Pharmaceutics. 2008, 348: 137-145

Zhang N., et al., Lectin-modified solid lipid nanoparticles as carriers for oral administration of insulin. Int. J. Pharm. 2006, 327: 153–159.

Zhang X., et al., Dihydroartemisinin loaded nanostructured lipid carriers (DHA-NLC): evaluation of pharmacokinetics and tissue distribution after intravenous administration to rats. Pharmazie, 2010, 65(9):670-8.

Zhang X., et al., Formulation optimization of dihydroartemisinin nanostructured lipid carrier using response surface methodology. Powder Technology. 2010, 197, 1–2: 120–128.

CHAPTER 2

Solid lipid nanoparticles for oral delivery of curcumin

2.1 INTRODUCTION

Curcumin is a yellow-colored phenolic natural constituent derived from the rhizome of the spice herb *Curcuma longa* widely known as turmeric. It has a broad spectrum of biological and pharmacological activity. Clinical trials have shown that curcumin has antioxidant (Sharma, 1976; Selvam, 1995; Ruby, 1995) anti-inflammatory (Menon, 2007; Rao, 1982), antibacterial (Negri, 1997), antifungal (Sharma, 2010) and anticarcinogenic activity (Devasena, 2003; Park, 2010). In particular it has been received considerable attention because of its putative cancer prevention and anti-cancer activities which are mediated through influencing multiple signaling pathways. Curcumin helps modulate 33 different proteins, including thioredoxin reductase, cyclooxygenase-2 (COX-2), protein kinase C (PKC), 5-lipoxygenase, and tubulin. Other molecular targets modulated by this agent include transcription factors, growth factors and their receptors, cytokines, enzymes, and genes regulating cell proliferation and apoptosis (Aggarwal, 2003; 2007; 2009). The most compelling and key rationale for the therapeutic use of curcumin is its good safety profile. To date, no studies in either animals or humans have demonstrated any toxicity associated with the use of curcumin, even at high doses (Shankar 1980; Lao; 2006). Despite multiple medicinal benefits its therapeutical utility is strongly limited by its poor aqueous solubility and low oral bioavailability. The latter is attributed to poor absorption, extensive intestinal and hepatic metabolism, rapid elimination and clearance from the body (Pan, 1999; Anand, 2007). Formulating curcumin for clinical efficacy has presented many challenges due to its poor physicochemical properties. Inspite of the numerous formulation challenges, several strategies such as nanoparticles, liposomes, complexation with phospholipids and cyclodextrins and solid dispersions have been developed to improve the bioavailability of curcumin (Bisht, 2007; Maiti, 2007; Tiyaboonchai, 2007).

Our work was focused on the development and characterization of SLN for the encapsulation of curcumin for oral administration used as antitumoral treatment. Oral curcumin administration has been found to inhibit the development of chemically-induced cancer in animal models of oral (Krishnaswamy, 1998; Li, 2002), stomach (Ikezaki, 2001; Huang, 1994), liver (Chuang, 2000), and colon (Pereira, 1996; Rao, 1995; Kawamori, 1995) cancer. Phase II clinical trials of curcumin in patients with colorectal cancer are currently under way. A phase II clinical trial in patients with advanced pancreatic cancer found that curcumin exhibited some anticancer activity in two out of 21 patients; however, bioavailability of curcumin was extremely poor (Dhillon, 2008). Oral route is the most common and preferred for drug administration. This choice is mainly related with its non-invasiveness and ease of administration, which increases patient's compliance and therapeutic success. However, the hydrophilic environment of the gastrointestinal tract (GIT) can limit the bioavailability of lipophilic and/or other poorly water-soluble compounds. The trend in drug discovery toward lipophilic molecules has increased the need to develop alternative oral delivery systems for poorly soluble compounds. Lipid-based drug delivery systems are promising, since lipids are known oral drug absorption enhancers (Porter, 2008; Chakraborty, 2009) and can be prepared with low particle size (Jia, 2005; Pouton, 2006). Solid lipid nanoparticles (SLN) combine these two features: they are colloidal carriers of submicron sizes, composed of lipids that are solid

at body and room temperature. These carriers can be made of physiologic or inert substances generally recognized as safe (GRAS), which means that they have low or total absence of toxicity in humans (Müller, 1995). Moreover, they retain the advantages of traditional colloidal systems, while circumventing some of their disadvantages (Müller, 2000): this includes enhanced physical stability; protection of drug molecules from degradation in the body; controlled drug release; organ or tissue specific targeting; biocompatibility; laboratory to industrial-scalability. Due to the characteristic configuration of SLNs, that consists of a biocompatible lipid core and an amphiphilic surfactant as an outer shell, the amount of drug in the outer shell and on the particle surface is released in the form of a burst and thus rapid onset of action is firstly observed. On the other hand, the drug incorporated into the particle core is released in a prolonged way. This makes the controlled release from these carriers possible which becomes an important tool when it is necessary to supply the drug over a prolonged period of time (Muller, 2000; Reddy, 2005). The aim of the present study was to investigate the feasibility of the inclusion of the water-insoluble drug curcumin into SLNs. Ultrasound technique was employed to prepare SLNs and formulation parameters as sonication time and drug concentration were evaluated. The physicochemical characterization of curcumin-loaded SLNs, in terms of particle size, drug loading capacity, drug entrapment efficiency, and *in vitro* drug release, was carried out. Transcellular permeability by the non-cell based assay PAMPA was also evaluated.

2.2 MATERIALS AND METHOD

2.2.1 Materials

Compritol® 888 ATO (glyceryl behenate, tribehenin), a mixture of mono-, di- and triglycerides of behenic acid (C22), was a gift of Gattefossè (Milan, Italy). Curcumin, Pluronic F68 and 1,7 octadiene were purchased from Sigma Aldrich corporation (St. Louis, MO, USA). All the solvents used were HPLC grade from Merck (Darmstadt, Germany); 85% formic acid was provided by Carlo Erba (Milan, Italy). Water was purified by a Milli-Q_{plus} system from Millipore (Milford, MA). Lecithin was kindly provided by Galeno (Comeana, Italy). Cholesterol was analytical grade from Sigma Aldrich (Milan, Italy). 96-well MultiScreen PAMPA filter plate were purchased from Millipore corporation.

2.2.2 Ultrasonication method

Blank and drug loaded SLN were prepared using hot homogenization process followed by ultrasonication (Castelli, 2005). Table 1 show the three different formulations investigated. Briefly different amounts of curcumin, (respectively 75, 150 and 225 mg) were weighted accurately and added to Compritol® 888 ATO (7.5 g) previously melted at 80ºC. Pluronic F 68 was dissolved in double distilled water (2.7 % w/w) and heated up to 80ºC in a beaker. When a clear homogenous lipid phase was obtained, the hot aqueous surfactant solution was added to hot lipid phase and

homogenization was carried out at 12.000 rpm, by using a high-speed stirrer (Ultra Turrax T25,IKA-WerkeGmbH&Co. KG, Staufen, Germany) for five minutes. The temperature was maintained at 80ºC during the homogenization step. The coarse emulsion was then subjected to probe sonication (Bandelin, Berlin, Germany) by TT13 probe for different times in amplitude of 70 % and potence of 100 W. To prevent temperature increase, the probe sonicator was inactive in 2-s intervals. Sonication was applied maximum for 15 minutes to avoid metal contamination. To prevent recrystallization during homogenization and ultrasonication, production temperature was kept at least 5ºC above the lipid melting point. After ultrasonication the obtained emulsion (O/W) was cooled in an ice bath in order to solidify the lipid matrix and to form SLN. Blank and drug loaded SLN were prepared and characterized as well. SLN dispersions were stored at 4ºC for further analyses.

Formulation	Curcumin (g)	Compritol® 888 ATO (g)	Pluronic F 68 (g)	Water (g)
SLN-1	0.075	7.5	3.75	138
SLN-2	0.150	7.5	3.75	138
SLN-3	0.225	7.5	3.75	138

Table 1: *Composition of different solid lipid nanoparticles formulations. SLN-1: solid lipid nanoparticles loaded with 1% of curcumin. SLN-2: solid lipid nanoparticles loaded with 2% of curcumin. SLN-3: solid lipid nanoparticles loaded with 3% of curcumin.*

2.2.3 Particle size analysis and zeta potential measurements

Mean diameter of the main population and polydispersity index (P.I.) as a measure of the width of particle size distribution were assessed by photon correlation spectroscopy (PCS) using a Zetasizer Nano ZS (Malvern Instruments, UK). Samples were prepared diluting 10µl of SLN suspension with 2 ml of deionized water. All measurements were done in triplicate. The surface charge was determined by measuring the zeta potential of SLN based on the Smoluchowski equation:

$$\nu = \left(\frac{\varepsilon\, E}{\eta}\right)$$

where ν is the measured electrophoretic velocity, η is the viscosity, ε is the electrical permittivity of the electrolytic solution, and E is the electric field.

2.2.4 Determination of encapsulation efficiency

The percentage of curcumin entrapped in the lipid matrix was determined as follows: a fixed amount of SLN dispersion was submitted to exhaustive dialysis using a membrane (MW=12.400). An amount of retained material was then freeze-dried at −40ºC for 24 h. The pre-freezing and freeze drying time were optimized to recover completely dried nanoparticles. Sample obtained were

dissolved in MeOH under sonication, centrifuged for 30 minutes at 14.000 rpm and the supernatant obtained was analyzed by HPLC/DAD analysis using curcumin as external standard. Calibration curves for the validated method were performed on six solutions in the concentration range 1.38–138 µg/ml. The correlation coefficient was >0.99. Curcumin encapsulation efficiency was expressed as drug recovery and calculated from:

$$Drug\ recovery\ (\%) = \frac{mass\ of\ active\ in\ nanoparticles}{mass\ of\ active\ fed\ to\ the\ system}\ x\ 100$$

The drug loading content was the ratio of incorporated drug to lipid (w/w):

$$Drug\ loading\ (\%) = \frac{mass\ of\ active\ in\ nanoparticles}{weight\ of\ lipid}\ x\ 100$$

Possible lipid interferences during UV determination of curcumin were also investigated: no lipid interference occurred (data not show). Curcumin loaded concentration was assayed by HPLC/DAD analysis performed using a HP 1100 Liquid Chromatograph (Agilent Technologies, Palo Alto, CA, USA) equipped with a HP 1040 Diode Array Detector (DAD), an automatic injector, an auto sampler and a column oven and managed by a HP 9000 workstation (Agilent Technologies, Palo Alto, CA, USA). The UV-Vis spectra were recorded between 220–500 nm and the chromatographic profiles was registered at 420 nm. Separations were performed on a reversed phase column Luna C18 (150 x 4.6 mm, 5 µm, Phenomenex) maintained at 27°C. The eluents were H_2O at pH 3.2 by formic acid (Solvent A) and acetonitrile (Solvent B). The multi-step linear gradient applied is described on Table 2.

Time (min.)	Solvent A	Solvent B
0.10	72	18
10	56	44
13	56	44
27	52	48
32	20	80
35	72	18

Table 2: *HPLC method for curcumin quantification*

2.2.5 Differential scanning calorimetry (DSC)

DSC was carried out using a Mettler TA4000 apparatus equipped with a DSC 25 cell. A mass of 10 mg samples were accurately weighted (Mettler M3 Microbalance) directly in pierced aluminium

pans and scanned between 30 and 250°C at a heating rate of 10 K min^{-1} under static air. DSC thermograms of pure curcumin, Compritol® ATO 888, and curcumin-loaded SLN were compared.

2.2.6 Wide angle X-ray scattering (WAXS)

X-ray diffraction patterns were obtained using the wide-angle X-ray scattering (WAXS, 2θ= 4-40º) on a Philips PW 1830 X-ray generator (Philips, Amedo, The Netherlands) with a copper anode (Cu-Kαradiation, λ = 1.5418 nm) using a Goniometer PW18120 as a detector. Data of the scattered radiation were recorded with a blend local-sensible detector using an anode voltage of 40 kV, a current of 25mA and a scan rate of 0.5º per minute.

2.2.7 Transmission electron microscopy (TEM)

The morphological characterization of the systems was performed using the transmission electron microscopy technique (TEM, CM12 Philips, Netherlands). Samples were stained with 2% (w/v) phosphotungstic acid solution and placed on copper grids with Formvar films for viewing by TEM.

2.2.8 In vitro release studies

Dialysis bag method was performed to study the drug release using a mixture of PBS and EtOH (50:50 v/v), pH 6.8, as the dissolution medium. Release was monitored for 24. The dialysis bags were hydrated in PBS before use. Two milliliter of SLN dispersion was poured into the dialysis bag. The bag was placed in a beaker containing 200 mL of dissolution medium maintained at 37ºC and stirred at a rate of 100 rpm. Aliquots of the dissolution medium were withdrawn at different time intervals and were replaced with the same volume of fresh medium to maintain the sink conditions. The samples were suitably diluted and analyzed for curcumin spectrophotometrically. All the operations were carried out in triplicate.

2.2.9 Stability studies

Stability of curcumin solid lipid nanoparticles was studied over 1 month. Solid lipid nanoparticles were kept at 4±1°C and at fixed time intervals they were assayed for their physical stability. Physical stability was checked by monitoring of size, zeta potential and polidispersity in time, by DLS.

2.2.10 Parallel artificial membrane permeability assay (PAMPA)

The PAMPA assay is a method for predicting passive intestinal absorption. The assay is carried out in a 96-well, MultiScreen-IP PAMPA (Millipore corporation) filter plate. The ability of compounds to diffuse from a donor compartment, through a PVDF membrane filter pretreated with a lipid-containing organic solvent, into an acceptor compartment is evaluated. A mixture of lecithin (1%

w/v) and cholesterol (0.8 w/v) in 1,7 octadiene was prepared and sonicate to ensure complete dissolution. 5 µL of the lipidic mixture were added to the filter of each well. Immediately after the application of the artificial membrane, 150 µL of drug containing donor solutions (free drug or curcumin SLNs diluted in 5% DMSO, PBS) were added to each well of the donor plate. 300 µL of buffer (5% DMSO in PBS, pH 7.4) were added to each well of the acceptor plate. The acceptor plate was then placed into the donor plate (Figure 1) , ensuring that the underside of the membrane was in contact with buffer. The plate was covered and incubated at room temperature under shaking for 24 hours and permeation was evaluated at fixed time interval of 1, 2, 4, 6, 19, 24 hours.

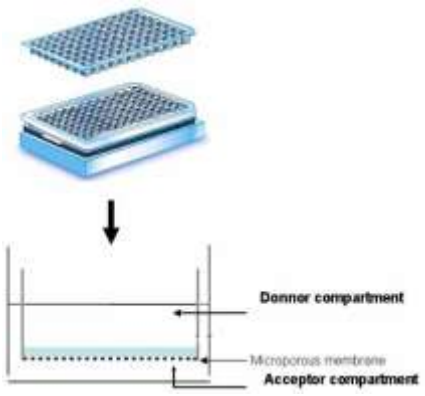

***Figure 1**: PAMPA model in a 96-well plate and detail of a well*

2.3 RESULTS AND DISCUSSION

Due to the increasing life expectancy, majority of people in the older age dwell with multiple disorders, thus creating a need to look upon molecules with multiple targets. Curcumin obtained from the rhizome of *C. longa* Linn. is a lipid-soluble antioxidant constituent. Curcumin targets multiple chemotherapeutic and inflammatory pathways and has demonstrated safety and tolerability in humans; however, the clinical literature lacks conclusive evidence supporting its use as a therapeutic agent due to its low bioavailability (Kakkar, 2011). Its insolubility in most biocompatible solvents has made curcumin very difficult to deliver into the body through conventional routes, including orally or by an intravenous or intramuscular injection. The aim of this study was to develop and characterize lipid nanoparticles wich can circumvent these problems for the encapsulation of curcumin for oral administration used for antitumoral treatment.

2.3.1 Preparation of SLN

SLN made of Compritol® 888 ATO as the core material were stabilized with Pluronic F68. Compritol® ATO 888 was selected because is a mixture of monoglycerides, diglycerides, and triglycerides. In the nanoparticle structure, the lipid that results in a highly crystalline structure with a perfect lattice would lead to drug expulsion. On the other hand, the imperfections (lattice defects)

of the lipid structure could offer more loading space to accommodate drugs. As a result, the structure of less ordered arrangement in the nanoparticles would be beneficial to the drug loading capacity. Pluronics® are class of non-ionic surfactants that are well known for their very low toxicity. Pluronic F68 has been used also for development of injectables and ophthalmic solutions. The emulsification-ultrasonication method was found to be efficient and quick to produce SLNs; a great advantage of this method is the fact that the equipment is common in every lab and the production can easily be done. Three different formulations with increasing amount of curcumin (1, 2 and 3% w/w respect to the lipid phase) were prepared and fully characterized. Effect of different process variables on size, P.I, zeta potential and encapsulation efficiency are discussed in the following section and presented on Table 3. **Homogenization time** was fixed at ten minutes, in fact as already reported (Das, 2011), this variable did not show any effect on particle size. This should be expected as homogenization step is only for emulsification of lipid in aqueus phase; it is an intermediate step and did not produce final particles.

Sonication time showed huge influence on particle size. Size significantly decreased with increasing sonication time and we obtained a decreasing of P.I. values in the formulations SLN-1 and SLN-2. These observations are reasonable as sonication was responsable for final particle size of SLNs, which broke the coarse emulsion drops to nanoemulsion droplets. Longer sonication time put more sonication energy to the SLN dispersions, which reduced size of the nanoemulsion droplets and decreased size distribution. The zeta potential indicates the degree of repulsion between close and similarly charged particles in the nanodispersion. High zeta potential indicates highly charged particles. Generally, high zeta potential negative or positive prevents aggregation of the particles due to electric repulsion and electrically stabilizes the nanoparticle dispersion. Zeta potential more than |30| mV indicates stable nanodispersion. The negative zeta potential of SLNs was attributed to the presence of behenic acid onto the lipid matrix surface; values were around -30/-40 mV indicating a stable system, however a small decreasing of zeta potentials values was found with increasing sonication time. Encapsulation efficiency was not significantly different among the groups. We can observe higher values of zeta potential in the case of loaded nanoparticles that confirm the incapsulation of curcumin in the carrier.

Particle size slightly increased with higher **drug concentration** (2 and 3% of curcumin); this is probably due to the presence of curcumin on the lipidic core. Zeta potential were comparable in all cases which suggests good stability of the SLN dispersions. In general we obtained good values of encapsulation efficiency around 70 %; such values may be due to the highly lipophilic nature of the drug and good solubility in glyceryl behenate.

As lipid has certain drug loading capacity, addition of excess drug led to increase of unencapsulated drug; it was observed for formulation loaded with 3% w/w of curcumin that showed a macroscopic precipitate after only few hours after preparation. The formulation selected for the best properties in terms of size, P.I. and zeta potential was SLN-2-15; it showed also good values of encapsulation efficiency (80%) and was selected for further investigation

Formulation	Time of sonication (min)	Curcumin (% w/w)	Size (nm)	P.I.	ζ Potential (mV)	Encapsulation efficiency (%)	Drug loading (%)
Blank SLN	5	-	333±1	0.28±0.02	-36±3	-	-
	10	-	254±6	0.25±0.01	-24±2	-	-
	15	-	241±9	0.33±0.03	-10±1	-	-
SLN-1-5	5	1	320±18	0.31±0.03	-45±2	76.4±4.9	0.76
SLN-1-10	10	1	238±4	0.31±0.04	-34±4	74.2±16	0.74
SLN-1-15	15	1	199±23	0.26±0.02	-39±4	76.4±4.6	0.76
SLN-2-5	5	2	415±6	0.31±0.08	-39±3	70.7±2	1.41
SLN-2-10	10	2	313±13	0.33±0.01	-29±4	77.8±8	1.56
SLN-2-15	15	2	270±15	0.29±0.01	-33±3	80.2±2	1.60
SLN-3-5	5	3	345±20	0.31±0.02	-40±4	66.3±6.4	1.99
SLN-3-10	10	3	278±19	0.33±0.05	-39±2	82.5±11.6	2.48
SLN-3-15	15	3	227±11	0.32±0.04	-28±7	86.5±8.2	2.60

Table 3: *Characterization of developed blank and curcumin loaded SLNs; effect of sonication time and amount of curcumin on size, P.I., encapsulation efficiency and drug loading. SLN-1, SLN-2 and SLN-3 are solid lipid nanoparticles loaded respectively with 1, 2 and 3% of curcumin. 5, 10 and 15 indicates sonication time.*

2.3.2 TEM analysis

The morphology of solid lipid nanoparticles determined by TEM was shown in Figure 2. The TEM study demonstrated that the particles had almost spherical and uniform shapes and did not stick to each other. The mean diameter was in the range of 250-300 nm.

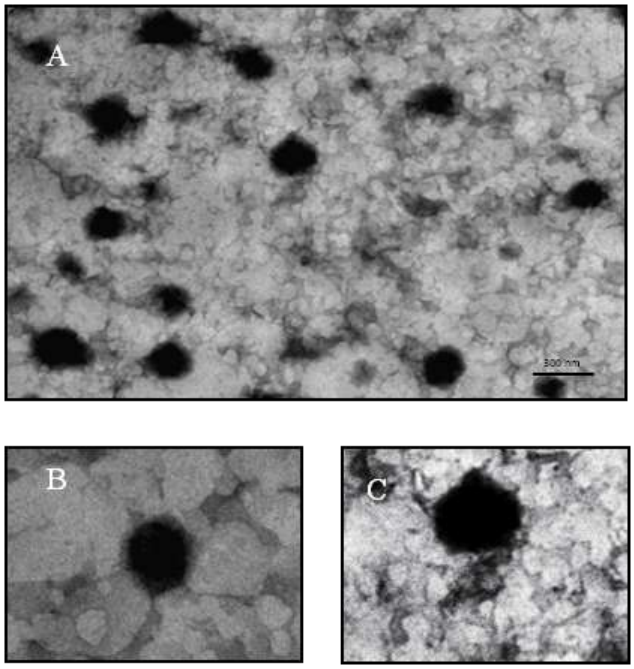

Figure 2: *TEM morphology of curcumin solid lipid nanoparticles with details of single SLNs.*

2.3.3 DSC and X-ray diffractometry assays

Lipid nanoparticles were analysed by DSC and X-ray diffractometry to investigate the crystal pattern of both curcumin and lipids, because this aspect could influence the *in vitro* and *in vivo* release of the drug from the systems. To investigate this effect, analysis was performed on the following samples: curcumin, Compritol®888 ATO; unloaded solid lipid nanoparticle and loaded solid lipid nanoparticles. Figure 3 depicts the DSC thermograms obtained. As Compritol®888 ATO is not composed of pure triacylglycerols, the observed melting peak at 72.1ºC might be due to a mixture of metastable polymorphic β and β' forms. The heating run showed also a relatively small endothermic shoulder at around 55ºC; this small shoulder corresponds to the melting of a very unstable modification of Compritol®888 ATO which is the α modification (Souto, 2006), that clearly disappears after the treatment for nanoparticle preparation. DSC analysis of curcumin showed the drug melting peak at 173.17ºC. In the DSC thermograms of blank SLN (unloaded) and loaded SLNs, a small endothermic peak was observed at 50ºC. This peak indicates the presence of Pluronic either in the form of coating surrounding the nanoparticles or as residue after dyalisis and lyophilization. X-ray diffraction studies showed that diffraction pattern of bulk Compritol®888 ATO (Figure 4) has two main typical signals at 21.5 (2θ) and 23.5 (2θ) that are significantly modified when formulated into nanoparticles. Besides, when nanoparticles are formulated, another signal arises at 19.4 (2θ) which corresponds to the most stable polymorphic form of triacylglycerols β (Souto, 2006). These results might indicate that the final formulation is composed of the most stable polymorphic state of Compritol®888 ATO: solid lipid nanoparticles seem to lose part of their

crystalline state transforming from a mixture of β and β' polymorphs to the most stable β polymorph, permitting curcumin to fit in the molecular gaps.

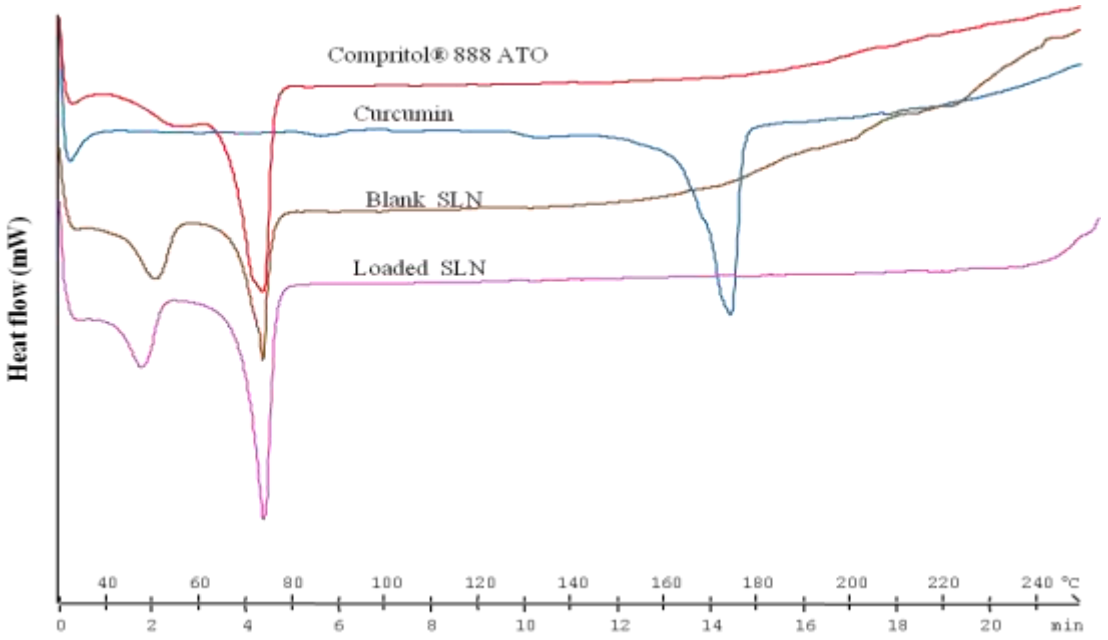

Figure 3: *DSC thermographs of Compritol®888 ATO; pure curcumin; blank and loade solid lipid nanoparticles.*

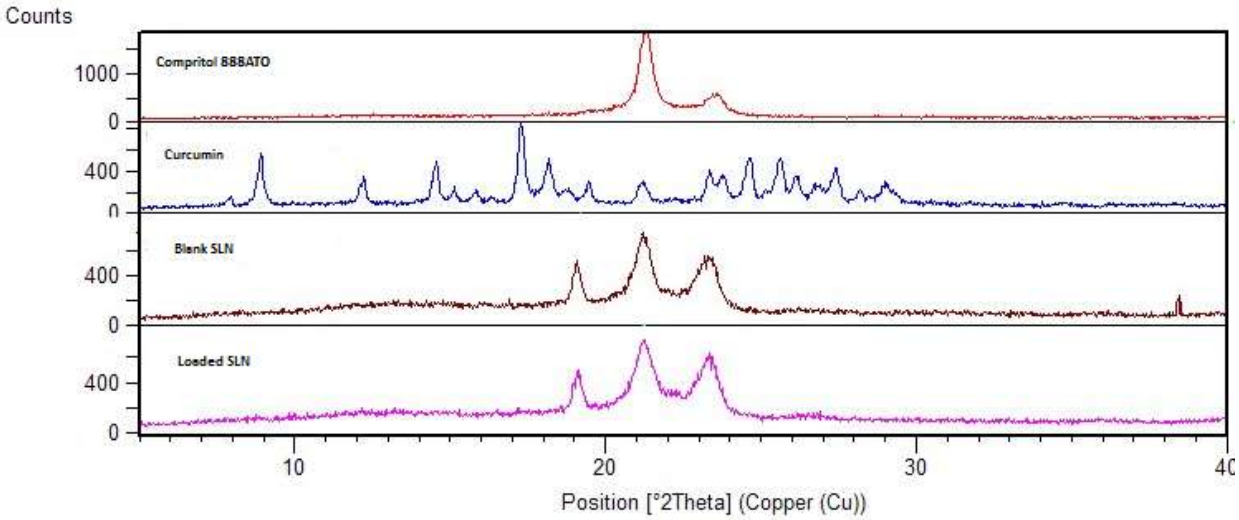

Figure 4: *X-ray diffraction pattern of Compritol®888 ATO; pure curcumin; blank and loaded solid lipid nanoparticles.*

2.3.4 In vitro release studies

The prepared particles were further evaluate for *in vitro* release of curcumin. The choice of dissolution medium and the sink condition have always been a problem for the low solubility drugs such as curcumin. For these compounds, an aqueus solution containing a surfactant or solvent in

which the drug is soluble may be used to enhance its solubility. In the present case solubility of curcumin in water and simulated gastric fluid at room temperature has been determined to be $3x10^{-3}$ and $5.7x10^{-3}$ µg/ml (Kakkar, 2011). Thus, to provide sink condition, 50% v/v ethanol in which the solubility of curcumin is 0.693±0.13 mg/ml was chosen as the receptor medium. The use of this receptor medium has been already described in literature (Kakkar, 2011; Mulik, 2010). Drug released from the SLNs and diffused through the dialysis membrane into the release media, while the dialysis bag retained the SLN. Hence, drug released from the SLN were measured by determining drug concentration in the release media. Percent cumulative drug release versus time was plotted to demonstrate the drug release pattern (Figure 5). A rapid release was observed in the first 6 hours that reached about 30% of the overall curcumin released from the formulation, which could be due to the drug-enriched shell around the particles and the consequence short diffusion distance for the drug. Although the release rate of SLN could be influenced by complex factors, it was reported that among the factors that contribute to a fast release are the large surface area, a high diffusion coefficient due to small molecular size or low viscosity in the matrix. The subsequent phase of delayed release may be attribute to the fact that the curcumin dispersed within the core is being released slowly from the lipidic solid matrices through diffusion and dissolution.

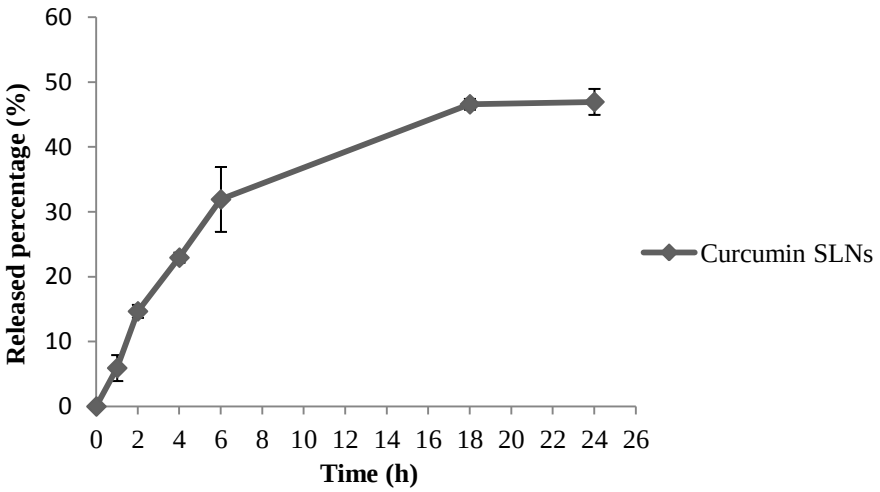

Figure 5: *In vitro release profile of curcumin from solid lipid nanoparticles by dialysis method, 50% ethanol was used as the release medium. Each data represent the mean ± standard deviation of three experiments.*

2.3.5 Stability studies

Stability of curcumin solid lipid nanoparticles was studied over 1 month. Physical stability was checked by monitoring of size, zeta potential and P.I. in time, by DLS measurements. There was no modification on the particle size neither on the zeta potential of the solid lipid nanoparticles, which maintained their original values throughout the study (Figure 6). Furthermore, polydispersity was stable over time. That means that no vesicle size alterations occurred over the whole period.

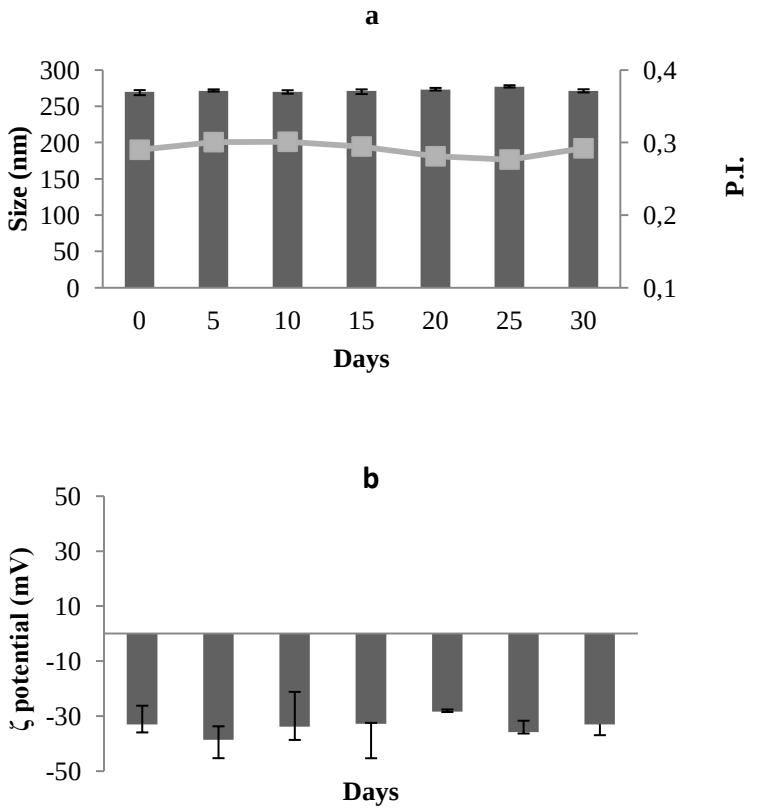

Figure 6: *Particle size and P.I* ***(a)*** *and zeta potential* ***(b)*** *evolution of curcumin solid lipid nanoparticles at storage condition (1 month, 4ºC). (Mean±S.D.; n=3).*

2.3.6 Parallel artificial membrane permeability assay (PAMPA)

An approach for rapid assessment of absorption potential include the parallel artificial membrane permeability assay (PAMPA) (Kansy, 2004). Pampa is based on a 96-well microplate technology and allows reasonable throughput, although it lacks similarity to natural membranes in that it does not posses pores or active transport mechanism. It enables fast determination of the trends in the ability of the compounds to permeate membrane by passive diffusion and is thus suited for the screening of large libraries. A caveat of the PAMPA approaches is to remember that they will underestimate the absorption of compound subject to active or paracellular transport *in vivo* and

overestimate the absorption of compound subject to efflux pump transport. The experiment was carried out measuring the ability of curcumin to diffuse from our SLN suspension to a donor compartment through a PVDF membrane. Solid lipid nanoparticles suspension was diluted to a final concentration of 160 μg of curcumin in each donor compartment. A saturated solution of curcumin in DMSO 5%/PBS (0.2 μg of curcumin solubilized in each donor compartment) was used as control. Results obtained (Figure 7) showed a strong increasing of the amount of curcumin permeated in the case of SLN suspension if compared with the saturated solution of curcumin used as control. We can observe that in the case of solid lipid nanoparticles after 6h, 19h and 24h respectively 2.6%, 4.9% and 5.8% of curcumin present in the donor compartment permeated to the acceptor compartment. In the case of saturated solution after 6h, 19h and 24h respectively 10%, 10% and 14% of curcumin present in the donor compartment permeated to the acceptor compartment. We can observe also that the amount of free curcumin permeated is constant during all the time while in SLNs the amount of curcumin permeated increase in time. This confirm the sustained release of our nanocarriers and it is also in accordance with the results obtained by releasing profile.

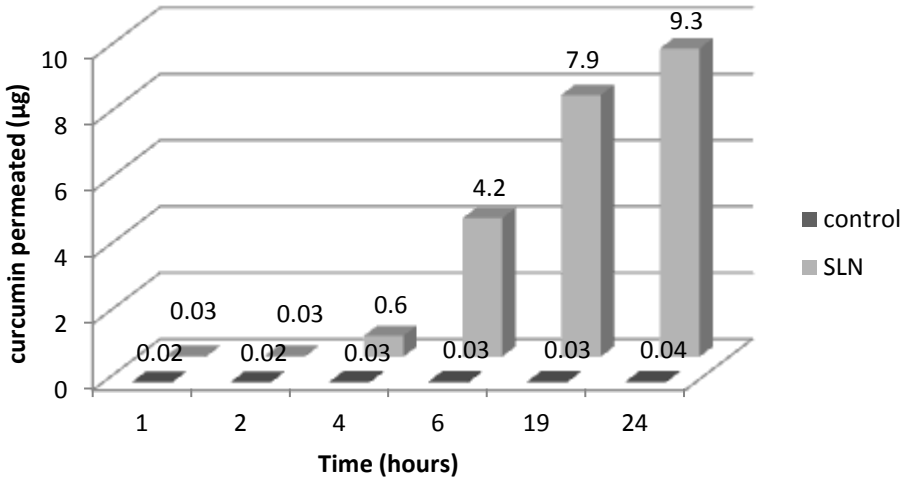

Figure 7:*Permeation profile of free curcumin and curcumin loaded SLNs by Parallel artificial membrane permeability assay (PAMPA). Each data represent the mean of three experiments. Amount of curcumin is referred to each well.*

2.4 CONCLUSIONS

In this study the poorly-soluble drug curcumin was incorporated into SLN by homogenization and ultrasound technique. Compritol® 888 ATO demonstrated good curcumin solubilization and the effect on the formulation of variables like amount of drug and time of sonication were evaluated. Selected formulation showed good values of encapsulation efficiency, size, P.I., zeta potential and stability was confirmed over one month on storage condition. The presence of round shape SLN with homogeneus size distribution was confimed by TEM analysis. In particular the average particle size of nanoparticles was maintained below 300 nm, it helps bypassing the liver first pass metabolism that has been reported to be the major site of curcumin degradation. Like other formulations, such as microemulsions or submicron emulsions, reduction in the particles size is a key factor for improving the peroral performance of poorly soluble drugs. In SLN formulations the particle size range was reduced resulting in an increase in surface area and saturation solubility. An increase in saturation solubility and, consequently, an increase in the release rate of the drug allows it to reach high concentrations in the gastrointestinal tract. In addition, use of surfactants such Pluronic F68 in the preparation of SLNs may contribute toward an increase in the permeability of the intestinal membrane or affinity between lipid particles and intestinal membrane, and may also exhibit bioadhesion to the GI tract wall. It was confirmed by Parallel artificial membrane permeability assay (PAMPA) that showed a considerable increasing in curcumin permeation by SLN. Also, by incorporation into SLN, curcumin is embedded into a solid lipid matrix that reduce the exposure to enzymatic degradation during the process of absorption. We observe also a prolonged release profile that suggest that curcumin molecules are solubilized throught the solid lipid matrix. Advantages of SLN is the fact that they can be freeze-dried and converted into solid dosage forms, such as tablets, capsules, pellets or powders in sachets, and they can also be transferred to a powder (by spray-drying or lyophilization) and added to the tabletting powder mixture. The obtained powders can be used to produce classic solid dosage forms, can be redispersed in water or juice prior to administration, and can also be used for the filling of hard gelatine capsules. Further investigations will be carried out to optimize freeze-dried process for oral delivery of developed SLNs. We can conclude that SLNs offer a promising delivery system for enhancing the oral absorption of poorly soluble drugs like curcumin.

2.5 REFERENCES

Aggarwal B.B., et al., Anticancer potential of curcumin: preclinical and clinical studies. Anticancer Res. 2003. 23: 363−398.

Aggarwal B.B., et al., The molecular targets and therapeutics of curcumin in health and disease; Springer Publication. 2007. Vol. 995.

Aggarwal B.B., et al., Molecular targets of nutraceuticals derived from dietary spices: potential role in suppression of inflammation and tumorigenesis. Exp. Biol. Med. 2009. 234: 825−849.

Anand P., et al., Bioavailability of curcumin: problems and promises. Mol. Pharm. 2007. 4: 807–818.

Bisht S., et al., Polymeric nanoparticle-encapsulated curcumin (‘‘nanocurcumin’’): a novel strategy for human cancer therapy. J. Nanobiotechnol. 2007. 5: 3.

Castelli F., et al., Characterization of indomethacin-loaded lipid nanoparticles by differential scanning calorimetry. Int. J. Pharm. 2005. 304: 231–238.

Chakraborty S., et al., Lipid – an emerging platform for oral delivery of drugs with poor bioavailability. Eur. J. Pharm. Biopharm. 2009. 73: 1–15.

Chuang S.E., et al., Curcumin-containing diet inhibits diethylnitrosamine-induced murine hepatocarcinogenesis. Carcinogenesis. 2000. 21(2): 331-335.

Das S., et al., Formulation design, preparation and physicochemical characterizations of solid lipid nanoparticles containing a hydrophobic drug: effects of process variables. Colloids Surf B Biointerfaces. 2011. 88(1): 483-9.

Devasena T., et al., Anticarcinogenic effect of bis-1,7-(2-hydroxyphenyl)-hepta-1,6-diene-3,5-dione a curcumin analog on DMH-induced colon cancer model. Pharmacol Res. 2003. 47(2): 133–140.

Dhillon N., et al., Phase II trial of curcumin in patients with advanced pancreatic cancer. Clin Cancer Res. 2008. 14(14): 4491-4499.

Huang M.T., et al., Inhibitory effects of dietary curcumin on forestomach, duodenal, and colon carcinogenesis in mice. Cancer Res. 1994. 54(22): 5841-5847.

Ikezaki S., et al., Chemopreventive effects of curcumin on glandular stomach carcinogenesis induced by N-methyl-N'-nitro-N-nitrosoguanidine and sodium chloride in rats. Anticancer Res. 2001. 21(5): 3407-3411

Jia L., et al., Nanoparticle formulation increases oral bioavailability of poorly soluble drugs: approaches experimental evidences and theory. Curr. Nanosci. 2005. 1: 237–243.

Kakkar V., et al., Exploring solid lipid nanoparticles to enhance the oral bioavailability of curcumin. Mol Nut Food Res. 2011. 55(3):495-503.

Kansy M., et al., Advances in screening for membrane permeability: high-resolution PAMPA for medicinal chemists. Drug discovery todays: Technologies. 2004. 1 (4): 349-355.

Kawamori T., et al., Chemopreventive effect of curcumin, a naturally occurring anti-inflammatory agent, during the promotion/progression stages of colon cancer. Cancer Res. 1999. 59(3): 597-601.

Krishnaswamy K., et al., Retardation of experimental tumorigenesis and reduction in DNA adducts by turmeric and curcumin. Nutr Cancer. 1998. 30(2):163-166.

Lao C.D., et al., Dose escalation of a curcuminoid formulation. BMC Complement Altern Med. 2006. 17; 6:10

Li N., et al., Inhibition of 7,12-dimethylbenz[a]anthracene (DMBA)-induced oral carcinogenesis in hamsters by tea and curcumin. Carcinogenesis. 2002. 23(8):1307-1313.

Maiti K., et al., Curcumin phospholipid complex: preparation, therapeutic evaluation and pharmacokinetic study in rats. Int. J. Pharm. 2007. 330: 155–163.

Menon V.P., et al., Antioxidant and anti-inflammatory properties of curcumin. Adv Exp Med Biol. 2007. 595: 105-125.

Mulik R.S. et al., Transferrin mediated solid lipid nanoparticles containing curcumin: enhanced in vitro anticancer activity by induction of apoptosis. Int J Pharm. 2010. 5 (1-2): 190-203.

Müller R.H., et al., Solid lipid nanoparticles (SLN) for controlled drug delivery—a review of the state of the art. Eur. J. Pharm. Biopharm. 2000. 50: 161–177.

Müller R.H., et al., Solid lipid nanoparticles (SLN)—an alternative colloidal carrier system for controlled drug delivery. Eur. J. Pharm. Biopharm. 1995. 41: 62–69.

Negri P.S., et al., Antibacterial activity of turmeric oil: a byproduct from curcumin manufacture. J Agric Food Chem. 1999. 47(10): 4297–4300.

Pan M.H., et al., Biotransformation of curcumin through reduction and glucuronidation in mice. Drug Metab. Dispos. 1999. 27: 486–494.

Park J., et al., Anti-carcinogenic properties of curcumin on colorectal cancer. World J Gastrointest Oncol. 2010. 2(4): 169–176.

Pereira M.A., et al., Effects of the phytochemicals, curcumin and quercetin, upon azoxymethane-induced colon cancer and 7,12-dimethylbenz[a]anthracene-induced mammary cancer in rats. Carcinogenesis. 1996. 17(6): 1305-131.

Porter C.J., et al., Lipid-based systems for the enhanced delivery of poorly water soluble drugs. Adv. Drug Deliv. Rev. 2008. 60: 615–616.

Pouton C., et al., Formulation of poorly water-soluble drugs for oral administration: physicochemical and physiological issues and the lipid formulation classification system. Eur. J. Pharm. Sci. 2006. 29: 278–287.

Rao C.V., et al., Chemoprevention of colon carcinogenesis by dietary curcumin, a naturally occurring plant phenolic compound. Cancer Res. 1995. 55(2): 259-266.

Rao T.S., et al., Anti-inflammatory activity of curcumin analogues. Indian J Med Res. 1982. 75: 574-578.

Reddy L.H., et al., Etoposide-loaded nanoparticles made from glyceride lipids: formulation, characterization, in vitro drug release, and stability evaluation. AAPS PharmSciTech. 2005. 6: (2): 24.

Ruby A.J., et al., Anti-tumour and antioxidant activity of natural curcuminoids. Cancer Lett. 1995. 94(1): 79-83.

Selvam R., et al., The anti-oxidant activity of turmeric (Curcuma longa). J Ethnopharmacol. 1995, 47(2): 59-67.

Sharma M., et al., Antifungal curcumin induces reactive oxygen species and triggers an early apoptosis but prevents hyphae development by targeting the global repressor TUP1 in Candida albicans. Biosci Rep. 2010. 30(6): 391-404.

Shankar T.N., et al., Toxicity studies on turmeric (Curcuma longa): acute toxicity studies in rats, guineapigs & monkeys. Indian J Exp Biol.1980. 18(1):73-5

Sharma O. P., Antioxidant activity of curcumin and related compounds. Biochem Pharmacol. 1976. 25(15): 1811-1812.

Souto et al., Polymorphic behaviour of Compritol888 ATO as bulk lipid and as SLN and NLC. J.Microencapsul. 2006. 23 (4): 417–433.

Tiyaboonchai W., et al., Formulation and characterization of curcuminoids loaded solid lipid nanoparticles. Int. J. Pharm. 2007. 337: 299–306

CHAPTER 3

Polymeric nanocapsules for docetaxel delivery: development and characterization

This work was carried out in collaboration with NOEMI CSABA[1], MARTA ALONSO[1], MARIA JOSE' ALONSO[1]

[1]*Department of Pharmaceutics and Pharmaceutical Technology, School of Pharmacy, Research Center on Molecular Medicine (CIMUS), University of Santiago de Compostela, Spain.*

3.1 INTRODUCTION

The clinical use of most anticancer drugs is associated to severe side effects and decreased quality of life for the patients. These effects are related to the biodistribution of large fractions of the drugs to non-target tissues, where they result in toxic effects to normal cells (Park, 2008). Interestingly, the side effects of many anticancer treatments are not only related to the active ingredient, but also to the excipients used for formulating them for parenteral administration. This is due to the extreme water insolubility of many anticancer drugs that requires the use of organic solvents to prepare conventional parenteral formulations. Typical organic solvents used in these formulations are Cremophor® EL/ethanol mixtures that have been deemed responsible of serious adverse effects including acute hypersensitivity reactions characterised by dyspnoea, flushing, rash, chest pain, tachycardia, hypotension, angio-edema and generalised urticarial (Gelderblom, 2001).

The limitations of conventional therapies have resulted in a great interest for the use of nanocarriers for anticancer drug delivery. From a technological perspective, the ideal nanocarrier should be well tolerated and capable of encapsulating highly hydrophobic drugs. Among the different delivery strategies, polymeric nanocapsules present many positive features for this application (Mora-Huertas, 2010; Couvreur, 2002; Garcion, 2006).

The oily core of polymeric nanocapsules is an ideal environment to encapsulate most antitumor drugs at high payloads, with good encapsulation efficacies and in a stable environment. On the other hand, the polymeric shell can be chosen to improve the biodistribution and the pharmacokinetic profile of the nanocarrier and to increase the intracellular penetration. Polyglutamic acid (PGA) is a highly anionic polyaminoacid composed of naturally occurring L-glutamic acid linked by peptide bonds. PGA is highly biocompatible and readily biodegradable by digestion with lysosomal enzymes. It is a suitable material for drug delivery design not only owing to its safety profile but also because it renders the surface of the nanocarriers more hydrophilic avoiding the uptake by the mononuclear phagocytic system (Dash, 2010).

The research group of Prof. M.J. Alonso has developed in previous studies highly efficient polymeric nanocapsulese to deliver docetaxel into tumor cells; these nanocarriers are characterized by the presence of soybean lecithin and cationic surfactant that drive the interaction between nanoemulsion and polymer. Natural surfactant like lecithin present significant variability of content and purity with risk of poor reproducibility of results. Moreover it has been established that ionic surfactants show higher toxicity value that non-ionic ones, and that cationic surfactants are more potent than their anionic counterparts as demonstrated by cytotoxicity test on HeLa cells (Vlachy, 2009).

Taking into account this information, the aim of this work was to evaluate the potential of innovative PGA nanocapsules as vehicles for docetaxel as model drug (I) avoiding use of lecithin as surfactant to overcome stability and variability problems (II) decreasing the amount of cationic surfactants to reduce the toxicity of the formulation. The disadvantage with the use of surfactants in drug delivery system is their potential toxicity at higher concentration. Surfactants are capable of causing distruption in biological membranes and display significant interaction with certain proteins

and a high concentration of surfactant over a long period of time may disturb some bodily processes (Buckton, 1995).

Tween80® and PEG40-stearate were selected as non ionic surfactants (Figure 1). Tween 80® is a polyethylene sorbitol ester, with a calculated molecular weight of 1310 Da, assuming 20 ethylene oxide units, one sorbitol, and one oleic acid as the primary fatty acid. It is widely used as pharmaceutical surfactants in various oral and parenteral delivery system. Its application intravenously is also approved by the US Food and Drug Administration as well as the European Medicine Agency. Alternatively, we have also explored the possibility of modulating the surface properties of the nanocapsules by using PEG-stearate on the shell composition. The presence of PEG40-stearate as stabilizer reduced significantly the surface hydrophobicity and prolonging circulation time *in vivo*. Mononuclear phagocyte system can opsonize colloidal drug carriers and so rapid clearance of drug may cause reduction of its effectiveness. To enhance the plasma half-life and circulation of nanoparticles, many researchers have recommended PEG modification of nanoparticles (Kajiwara, 2007; Han, 2007).

Two different cationic surfactants were selected for nanocapsules preparation: stearylamine and hexadecyltrimethylammonium bromide (CTAB)**,** already used in the formulations previously developed. Stearylamine has been reported to have lower toxicity after oral administration if compared with CTAB (CTAB in rat LD 50 oral 410 mg/Kg and SA 1395mg/Kg) (Ramadan, 2011).

Docetaxel has demonstrated anticancer effects both *in vitro* and *in vivo* against a variety of tumors including lung, ovaries, breast, leukemia, malignant melanoma (Saloustros, 2008; Haas, 2008). It was selected as model drug. It is characterized by hydrophobic character and result necessary the of use solubilizer (i.e. Cremophor®EL and ethanol) for its intravenous administration with severe side effects.

In this work different innovative PGA nanocapsules were designed for the delivery of docetaxel; blank and DCX-loaded nanocapsules were prepared and physicochemically characterized. An *in vitro* release study was carried out and a qualitative uptake study in A549 cells confirmed the possibility to use the two selected formulation as efficient carriers to deliver docetaxel to cancer cells.

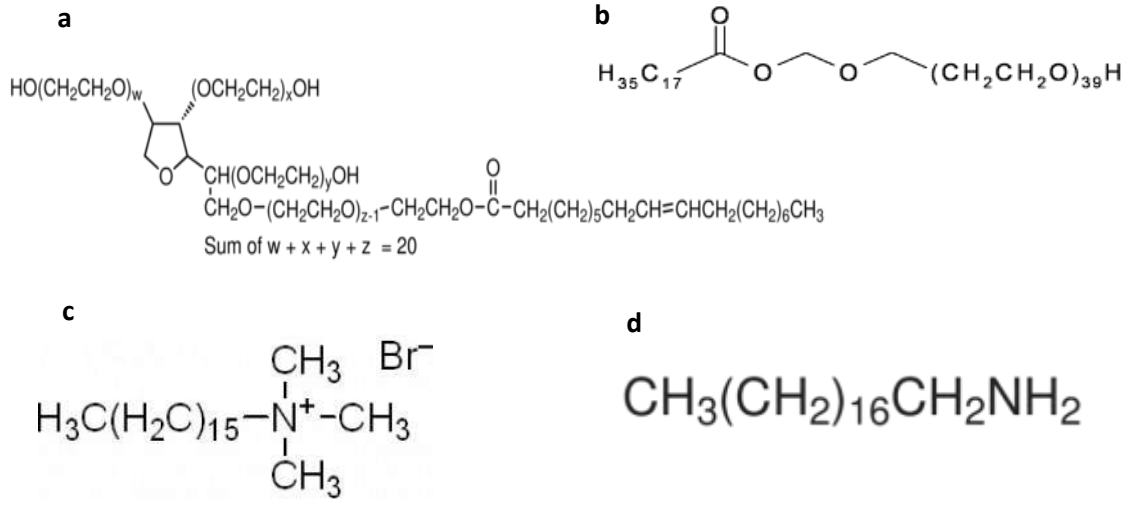

Figure 1*:Molecular structure of the components used for the preparation of the nanoparticles. Non ionic surfactants:* ***(a)*** *Tween®80 and* ***(b)*** *PEG40-stearate. Cationic surfactants:* ***(c)*** *hexadecyltrimethylammonium bromide (CTAB) and* ***(d)*** *octadecylamine (stearylamine).*

3.2 MATERIALS AND METHODS

3.2.1 Chemicals

Poly-L-glutamic acid (PGA) (Mw 15-50 KDa), docetaxel (DCX), Tween80®, hexadecyltrimethylammonium bromide (CTAB), octadecylamine (stearylamine) were purchased from Sigma, Spain. Miglyol 812®, a neutral oil formed by esters of caprylic and capric fatty acids and glycerol, was a kind gift from Sasol Germany GmbH (Germany). Poly(ethyethyleneglycol)-stearate of a degree of polymerization of 40 henceforth designated as PEG40-stearate (Simulsol M 52) was provided by Seppic, France; DAPI (4'-6-diamidino-2-phenylindole) and 1,1′-dioctadecyl-3,3,3′,3′-tetramethylindodicarbocyanine perchlorate (DiD) (DiD Em 644 nm; Ex 664 nm) were obtained from Molecular Probes-Invitrogen (USA). All other reagents used were HPLC grade.

3.2.2 Preparation of nanocapsules

The preparation of PGA nanocapsules was based on a modification of the solvent displacement technique as previously reported (Calvo, 1997). The method involved a polymer ionic interaction after solvent diffusion. Blank nanocapsules were obtained by two different methods: one-step and two step-techniques.

One step technique: Briefly, an organic phase was formed by dissolving 12 mg of anionic surfactant (Tween 80® or PEG40-stearate) in 0.250 ml of ethanol, followed by 62.5 µl of Mygliol®812 and different amounts of cationic surfactant (0.9 mg of CTAB or 0.5 mg of stearylamine) in 4.75 ml of acetone solution. This organic phase was immediately poured over 5ml

of a water solution of PGA (0.5 mg/ml). Finally, solvents were evaporated under vacuum from the suspension to a final constant volume of 5 ml.

Nanoemulsions were also obtained by the method previously described. Unlike nanocapsules, nanoemulsions are only formed by the hydrophobic cores without the polymer cover. We prepare anionic and cationic nanoemulsions which differ for the presence of the cationic surfactants stearylamine or CTAB.

Two step technique: The primary nanoemulsion obtained as previously described was incubated with PGA solution (1-2 mg/ml) in 5:1 ratio under magnetic stirring for 30 min, obtaining the PGA coated nanocapsules.

3.2.3 Characterization of PGA nanocapsules

Particle size and polydispersion index were determined by photon correlation spectroscopy (PCS). Samples were diluted to an appropriate concentration with filtered water (60 µl of sample in 2 ml of water) and each analysis was carried out at 25ºC with an angle detection of 173º. Zeta potential values were calculated from the mean electrophoretic mobility values, which were determined by laser Doppler anemometry. Samples were diluted with KCl 0.1 mM. Analyses were performed in triplicate using a zetasizer NanoZS® (Malvern Instruments, Malvern, UK). The morphological characterization of the systems was performed using the transmission electron microscopy technique (TEM, CM12 Philips, Netherlands). Samples were stained with 2% (w/v) phosphotungstic acid solution and placed on copper grids with Formvar films for viewing by TEM.

3.2.4 Docetaxel encapsulation into nanocapsules

In order to achieve the incorporation of DCX into PGA nanocapsules, 50 µl of the DCX stock ethanol solution (conc. 1 mg/ml) were added to the organic phase and the process was continued as described previously. PGA nanocapsules were concentrated up to a final volume of 5 ml in order to obtain a final drug concentration of 10 µg/µl.

The encapsulation efficiency of DCX in PGA nanocapsules was determined indirectly by the difference between the total amount of DCX in the formulation and the free drug measured in the subnatant of the nanocapsules. Therefore, the total amount of drug was estimated by dissolving an aliquot of non-isolated DCX loaded PGA nanocapsules with acetonitrile. This sample was centrifuged during 20 min at 4000g and the supernatant was measured with a high-performance liquid chromatography (HPLC) system. The non-encapsulated drug was determined by the same method following separation of PGA nanocapsules from the aqueous medium by ultracentrifugation at 30000 rpm, 15°C, 1h.

DCX was assayed by a slightly modified version of the method proposed by Lee et al. (Lee, 1999). The HPLC system consisted of an Agilent 1100 Series instrument equipped with a UV detector set at 227 nm and a reverse phase Zorbax Eclipse® XDB-C8 column (4.6 x 150 mm i.d., pore size 5 µm Agilent USA). The mobile phase consisted of a mixture of acetonitrile and 0.1% v/v

ortophosphoric acid (55:45 v/v) and the flow rate was 1 ml/min. The standard calibration curves of docetaxel were linear ($r^2 = 0.999$) in the range of concentrations between 10-0.5 µg/ml

The encapsulation efficiency (E.E.) was calculated as follows:

$$E.E.\% = [(A-B)/A] \times 100$$

Where A is the experimental total drug concentration and B is the drug concentration measured in the external aqueous medium, corresponding to unloaded drug.

3.2.5 Fluorescent DiD encapsulation

Fluorescent labeled formulations were obtained replacing 0.5 ml of ethanol of the organic phase with 0.250 ml of DiD stock solution in ethanol (2.5 mg/ml). The final concentration of DiD in the nanocarriers was approximately 125 µg/ml. DiD encapsulation efficiency in all the systems was determined indirectly by the difference between the total amount of fluorescent probe in the formulations and the free dye measured in the subnatant of the nanocapsules after ultracentrifugation (30000 rpm, 15°C, 1h). At the end of the ultracentrifugation aliquots of subnatant were diluted with acetonitrile and analyzed by UV spectrophotometry (646 nm). To determinate the total amount of the probe present in the systems aliquots of nanocapsules suspension were diluted with acetonitrile and analyzed at λ=646 nm.

3.2.6 In vitro release study

The release of DCX from PGA nanocapsules was performed by incubating a sample of each formulation with phosphate buffer at an appropriate concentration to assure sink conditions (4.9 µg/ml). The vials were placed in an incubator at 37º C with horizontal shaking. An aliquot of 4 ml of the suspension was collected at different time intervals (1, 4, 8, 24, 48 h), and ultracentrifuged in Herolab® tubes (Herolab GmbH, Germany). The amount of drug released was calculated indirectly by determining the amount of free drug in the aqueous phase as described above. As a control, the total amount of drug in the suspension was also determined.

3.2.7 Stability studies

The stability of loaded PGA nanocapsules suspension at 37°C in phosphate buffer under stirring was followed for a period of 7 days by measuring the particle size and polidispersity index of the colloidal system. Stability of two selected formulations was also evaluated for 48h in two different cell culture media: Opti-MEM® (Reduced Serum Medium) and DMEM supplemented with 10% FBS.

3.2.8 Cell culture

The human lung carcinoma derived A549 cell line was cultured on 80 cm^2 flasks (Nunc, Denmark) using Dulbecco's modified Eagle medium-high glucose (DMEM) supplemented with 10% FBS, 1% L-glutamine, 1% non-essential amino acids (x100), penicillin (100U/ml) and streptomycin (100 µg/ml) (all obtained from Sigma-Aldrich). Cells were maintained at 37ºC in a humidified atmosphere with 5% CO_2. The culture medium was changed every two days for approximately 5-6 days until cells reached approximately 80-90% confluence. Then, cells were trypsinized, subcultured and seeded at $2.5x10^5$ cells per flask.

3.2.9 Qualitative uptake studies

A549 cells were seeded at a density of 5 x 10^4 cells/cm^2 on sterile coverslips placed in 6-well plates; after this, the apical culture medium was removed and cells were incubated with the fluorescent nanosystems. After incubation for 4 hours, cells were washed three times with PBS (Sigma-Aldrich, Spain). Then, the cells were fixed for 10 min with 4% p-formaldehyde in PBS at room temperature, rinsed twice with fresh PBS and nuclei was staided with DAPI. Living cells were analyzed by confocal microscopy (Leica).

3.2.10 Statistical analysis

The design of experiments was formulated using the statistical software NEMRODW. Particle size, P.I. and zeta potential were statistically analyzed by the analysis of variance (ANOVA). Differences were considered to be significant at level of $p < 0.05$.

3.3 RESULTS AND DISCUSSION

As indicated in the introduction, the purpose of this work was to optimize innovative nanocapsules that overcome stability problems due to the use of lecithin and characterized by a lower amount of cationic surfactant. The rationale for selecting PGA as the coating polymer was its biocompatibility and its potential ability to provide stealth properties to the carrier . Four different formulations were optimized to load the anticancer molecule docetaxel. We discuss the preparation of these nanocarriers, their physicochemical characterization, their capacity to load and release docetaxel and a qualitative cell uptake study.

3.3.1 Optimization of non ionic nanoemulsion by solvent displacement technique

Non ionic nanoemulsions were obtained according to a modified solvent displacement technique; different amounts of non ionic surfactant (Tween80® and Peg40-stearate), referred to 5 ml of formulation, were tested. Blank nanoemulsions (Table 1) formed a homogeneous population of a mean particle size around the 200 nm with a narrow size distribution (polydispersity index = 0.1 or

0.2). The two nanoemulsions with smaller amount of non ionic surfactant (12 mg of Tween80® and 12 mg of PEG40-stearate) were selected to develop relative cationic nanoemulsions.

Tween80® (mg)	Size (nm)	P.I.	ζ Potential (mV)
12	172±7	0.1	-15±1
24	179±4	0.1	-17±1
48	185±4	0.1	-20±1

1A

PEG40-St (mg)	Size (nm)	P.I.	ζ Potential (mV)
12	226±3	0.2	-2±1
24	237±12	0.2	-6±1
48	266±6	0.2	-6±2

1B

Table 1*: Characterization of blank non ionic nanoemulsions developed using Tween80®* ***(A)*** *or PEG40-stearate* ***(B)*** *as non ionic surfactants. P.I.: polydispersity index, Values are given as mean ± SD; n=3.*

3.3.2 Development of blank nanocapsules by two step technique: optimization of polymer and cationic surfactant amounts

Nanocapsules were obtained according to a modified solvent displacement technique where the coating polymer is deposited onto the oily core by electrostatic interaction. A similar approach had successfully been used before by the group to prepare chitosan and polyarginine nanocapsules (Lozano, submitted; Calvo, 1997). In this case, the inclusion of a cationic surfactant (CTAB or stearylamine) was required to drive the interaction between PGA and the nanoemulsion (Figure 2): the PGA coating around the positive surface was formed due to the ionic-polar interactions between the positively amine groups of surfactant agent and the lateral chain of PGA.

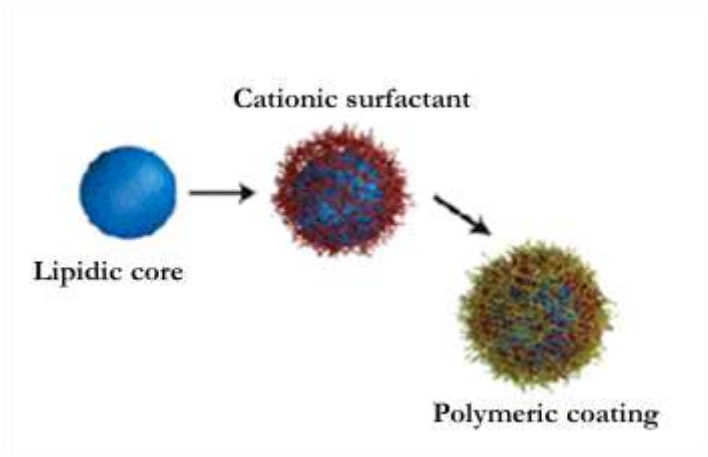

Figure 2: *Illustration of the structure and preparation method of PGA nanocapsule*

In the first step of our work several cationic nanoemulsion were developed and characterized in terms of size, P.I and zeta potential in order to optimize the amount of cationic surfactant used. Cationic nanoemulsions were then incubated with water solution of PGA at two different concentrations: 1 mg/ml and 2 mg/ml in order to optimize the amount of polymer used. The mean particle size of PGA nanocapsules was approximately 200 nm, corresponding to a monomodal and narrow size distribution (polydispersity index=0.1). The zeta potential was indicative of the different composition of these systems. PGA nanocapsules exhibited a polyanionic charge, whereas nanoemulsion have net positive charge. Considering that nanoemulsion has the same composition as compared to PGA nanocapsules except for the polymer coating, this charge inversion suggests that the electrostatically driven coating process is successful.

Cationic nanoemulsions prepared using Tween80® as non ionic surfactant and CTAB as cationic surfactant showed good values of size, P.I and zeta potential (Table 2); relative nanocapsules, obtained after incubation with a water solution of PGA, showed an inversion of zeta potential values that confirm the process coating. We observe a strong decreasing of zeta potential values comparing nanocapsules prepared with 0.9 mg of CTAB (-30 mV) with nanocapsules prepared with 0.5 mg of CTAB (-8 mV). The amount of PGA hasn't been so influent for the physical characteristics of the preparation (Figure 3). We obtained a similar profile also for nanocapsules prepared with the same method using PEG40-stearate as non ionic surfactant (Table 3, Figure 4). Thaking into account these results 0.9 mg of CTAB was the minimum amount of cationic surfactant selected to obtain a stable system by one step technique. Cationic nanoemulsions prepared using Tween80® as non ionic surfactant and stearylamine as cationic surfactant showed higher values of zeta potential (Table 4); relative nanocapsules obtained by two step technique showed good values of zeta potential also using 0.5 mg of stearylamine (-20 mv) (Figure 5). We obtained a similar profile also for nanocapsules prepared with PEG40-stearate and stearylamine as cationic surfactant (Table 5; Figure 6): nanocapsules with 0.5 mg of stearylamine and 1 mg/ml PGA showed a zeta potential of -25 mV that assure good stability of the system. 0.5 mg of stearylamine was the amount selected for nanocapsules preparation by one step technique.

Cationic Nanoemulsion	Size (nm)	P.I.	ζ Potential (mV)
1. Tween80®/0.9 mg CTAB	203±3	0.1	+34±2
2. Tween80®/0.5 mg CTAB	203±4	0.1	+25±1
3. Tween80®/0.3 mg CTAB	193±1	0.1	+17±1

***Table 2**: Characterization of blank cationic nanoemulsion prepared using Tween80® as non ionic surfactant and CTAB as cationic surfactant. P.I.: polydispersity index, Values are given as mean ± SD; n=3.*

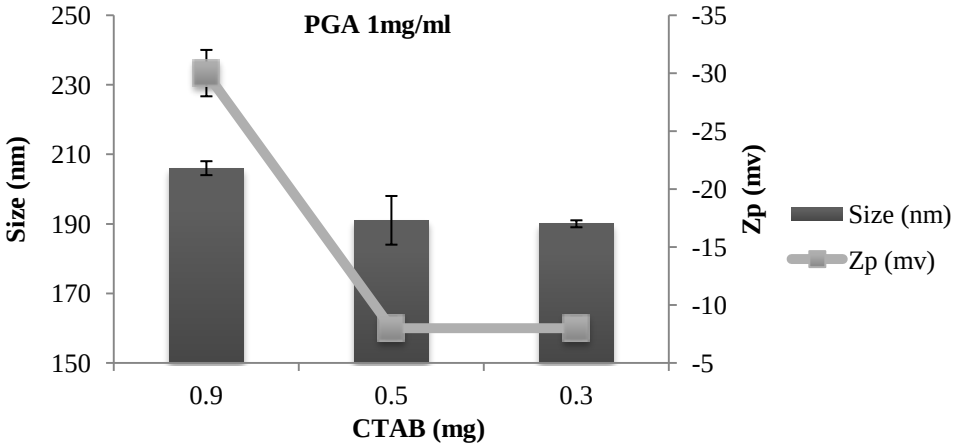

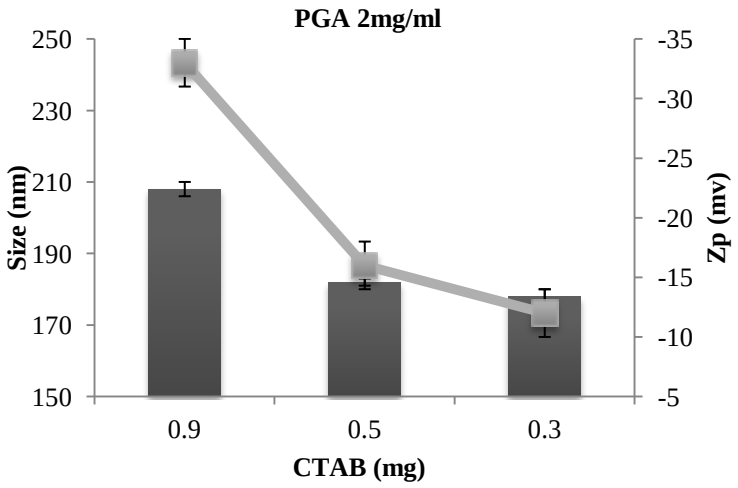

***Figure 3:** Characterization of blank cationic nanocapsules prepared by two step technique with different amount of PGA (1 mg/ml and 2 mg/ml) using Tween80® as non ionic surfactant and CTAB as cationic surfactant. Values are given as mean ± SD; n=3.*

Cationic Nanoemulsion	Size (nm)	P.I.	ζ Potential (mV)
4. PEG40-St/0.9 mg CTAB	215±4	0.1	+44±1
5. PEG40-St/ 0.5 mg CTAB	216±4	0.1	+35±2
6. PEG40-St/0.3 mg CTAB	218±6	0.2	+28±2

Table 3: *Characterization of blank cationic nanoemulsion prepared using Peg-40 stearate as non ionic surfactant and CTAB as cationic surfactant. P.I.: polydispersity index, Values are given as mean ± SD; n=3.*

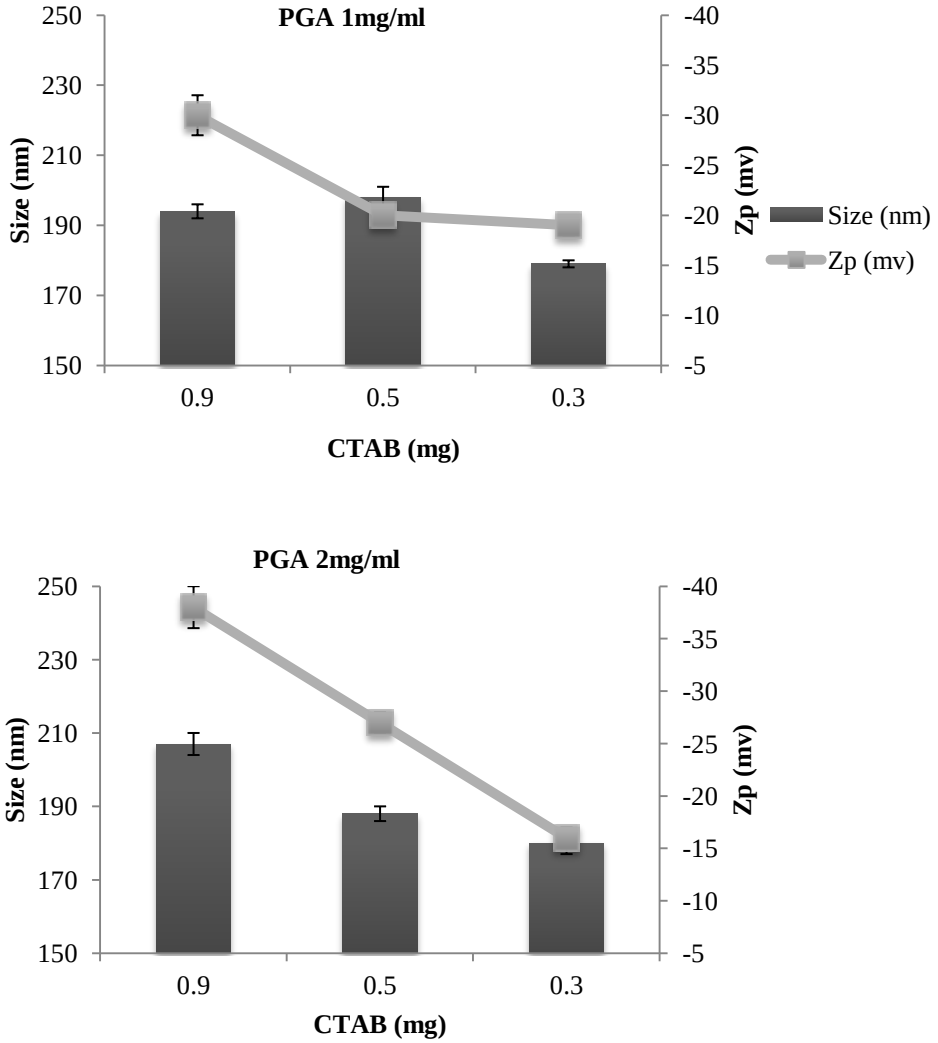

Figure 4: *Characterization of blank cationic nanocapsules prepared by two step technique with different amount of PGA (1 mg/ml and 2 mg/ml) using Peg-40 stearate as non ionic surfactant and CTAB as cationic surfactant. Values are given as mean ± SD; n=3.*

Cationic Nanoemulsion	Size (nm)	P.I.	ζ Potential (mV)
7. Tween80®/0.9 mg Stearylamine	236±11	0.1	+49±1
8. Tween80®/0.5 mg Stearylamine	209±9	0.1	+39±2
9. Tween80®/0.3 mg Stearylamine	208±2	0.1	+26±1

Table 4: *Characterization of blank cationic nanoemulsion prepared using Tween80® as non ionic surfactant and Stearylamine as cationic surfactant. P.I.: polydispersity index, Values are given as mean ± SD; n=3.*

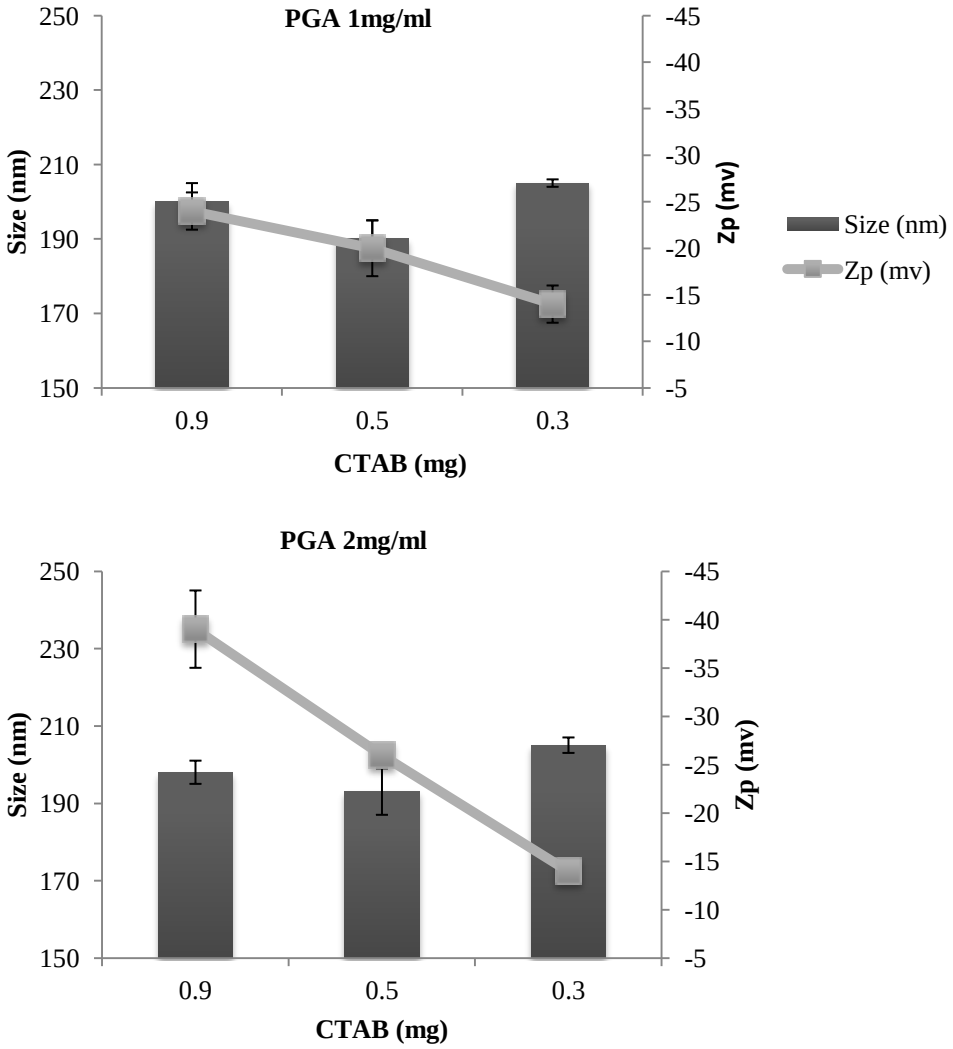

Figure 5: *Characterization of blank cationic nanocapsules prepared by two step technique with different amount of PGA (1 mg/ml and 2 mg/ml) using Tween80® as non ionic surfactant and Stearylamine as cationic surfactant. Values are given as mean ± SD; n=3.*

Cationic Nanoemulsion	Size (nm)	P.I.	ζ Potential (mV)
10. PEG40-St/0.9 mg Stearylamine	253±13	0.2	+52±2
11. PEG40-St/0.5 mg Stearylamine	246±10	0.2	+48±1
12. PEG40-St/0.3 mg Stearylamine	241±4	0.2	+40±2

Table 5: *Characterization of blank cationic nanoemulsion prepared using Peg40-stearate as non ionic surfactant and Stearylamine as cationic surfactant. P.I.: polydispersity index, Values are given as mean ± SD; n=3.*

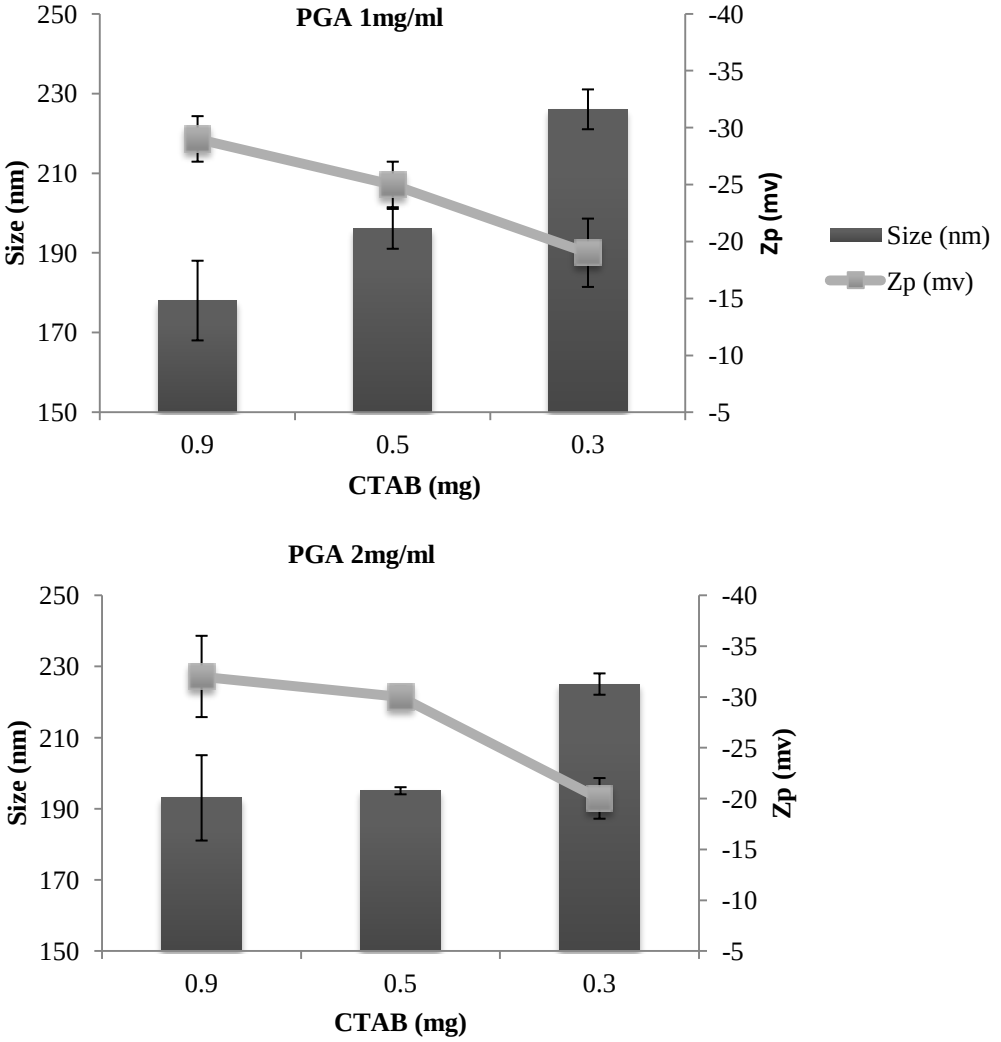

Figure 6: *Characterization of blank cationic nanocapsules prepared by two step technique with different amount of PGA (1 mg/ml and 2 mg/ml) using Peg-40 stearate as non ionic surfactant and Stearylamine as cationic surfactant. Values are given as mean ± SD; n=3.*

3.3.3 Preparation and characterization of blank PGA nanocapsules by one step technique

Blank nanocapsules, using the amounts of cationic surfactants selected, were prepared by solvent displacement techniques in one step as previously described.

Considering the results obtained during the preliminary studies (section 3.3.2) and confirmed by experimental designed (section 3.3.11), we decided to test two concentration of PGA in water: 1 mg/ml and 0.5 mg/ml. Nanocapsules obtained were fully characterized as reported in Table 6. As can be noted, the use of adequate concentrations of polymer and cationic surfactant results in the formation of homogenous populations of nanocapsules between 170-215 nm.

The results showed that the different amount of PGA did not affect markedly size and zeta potential values of the systems so we select 0.5 mg/ml as concentration of PGA to obtain a stable system reducing the cost of the formulation. Formulations number 1, 3, 5, and 7 were selected for further investigations.

Formulation	PGA conc. (mg/ml)	Size (nm)	P.I.	ζ Potential (mV)
1. NCs Tween80®/CTAB	**0.5**	**171±2**	**0.2**	**-25±1**
2. NCs Tween80®/CTAB	1	198±6	0.1	-24±4
3. NCs PEG40-St/CTAB	**0.5**	**179±5**	**0.1**	**-20±1**
4. NCs PEG40-St/CTAB	1	193±4	0.1	-25±2
5. NCs Tween80®/Stearylamine	**0.5**	**190±3**	**0.1**	**-19±3**
6. NCs Tween80®/Stearylamine	1	186±3	0.1	-15±2
7. NCs PEG40-St/Stearylamine	**0.5**	**217±6**	**0.1**	**-18±5**
8. NCs PEG40-St/Stearylamine	1	215±15	0.1	-22±1

Table 6: *Physic characteristics of blank PGA nanocapsules (Mean ± S.D.; n=3). NCs: nanocapsules. PEG40-St: PEG40-Stearate*

3.3.4 Preparation and characterization of docetaxel-loaded PGA nanocapsules

The four formulations selected were loaded with DCX at concentration of 10 µg/ml and fully characterized. The Table 7 summarized the characterization of loaded and blank nanocapsules. The mean particle size of PGA nanocapsules was approximately 200 nm, corresponding to a monomodal and narrow size distribution (polydispersity index=0.1 or 0.2). PGA nanocapsules exhibited a negative zeta potential between -20 and -25 mV. Docetaxel-loaded nanocarriers showed similar physicochemical properties than unloaded ones. This might be related to an efficient incorporation of the drug in the oily core of the nanocarriers (Teixera, 2005). Values of encapsulation efficiency are between 40-50 % with slightly higer values in the case of stearylamina. Values of encapsulation efficiency compared with systems previously developed (Lozano, 2008) were lower probably due to the absence of a lipophilic surfactant like lecithin.

Formulation	Size (nm)	P.I.	ζ Potential (mV)	EE (%)
NCs Tween80®/CTAB	171±2	0.2	-25±1	
NCs Tween80®/CTAB-DCX	**200±6**	**0.1**	**-23±1**	**41.1±1.5**
NCs PEG40-St/CTAB	179±5	0.1	-20±1	
NCs PEG40-St/CTAB-DCX	**185±4**	**0.2**	**-19±1**	**45.9±4.2**
NCs Tween80®/Stearylamine	190±3	0.1	-19±3	
NCs Tween80®/Stearylamine-DCX	**186±2**	**0.1**	**-19±1**	**51.3±1.8**
NCs PEG40-St/Stearylamine	217±6	0.1	-18±5	
NCs PEG40-St/Stearylamine-DCX	**205±9**	**0.1**	**-18±2**	**45.2±2.5**

Table 7: *Physicochemical characteristics of blank and DXC-loaded PGA nanocapsules. P.I.: polydispersity index, Values are given as mean ± SD; n=3. NCs: nanocapsules and PEG40-St: PEG40-stearate*

3.3.5 Stability of docetaxel-loaded PGA nanocapsules

For assessing the stability of the different formulations in *in vitro* conditions PGA nanocapsules preparations were incubated at 37ºC in phosphate buffere for one week (Figure 7). Different parameters were assessed at different time point: macroscopic aspect; particle size, polydispersity and zeta potential. The macroscopic aspect is important to exclude dramatic aggregation or phase separation processes, including drug precipitation. The preservation of the nanocapsules particle size and polydispersity is critical to ensure that system is suitable for administration, but also that it will maintain its pharmacokinetic properties that can change with nanocarrier size. The macroscopic analysis showed evidence of aggregation and sedimentation in the samples prepared with PEG40-stearate as non ionic surfactant after only one day. The precipitate was observed both in the unloaded and loaded formulations, probably not due to the presence of DCX.

Instead the two formulations with Tween80® as non ionic surfactant showed a good stability, no significant differences on the mean particles size were observed during 7 days. Polydispersity determinations confirm chemical and physicochemical stability of the system (data not shown). The two stable formulations prepared with Tween80® as non ionic surfactant were selected for further studies.

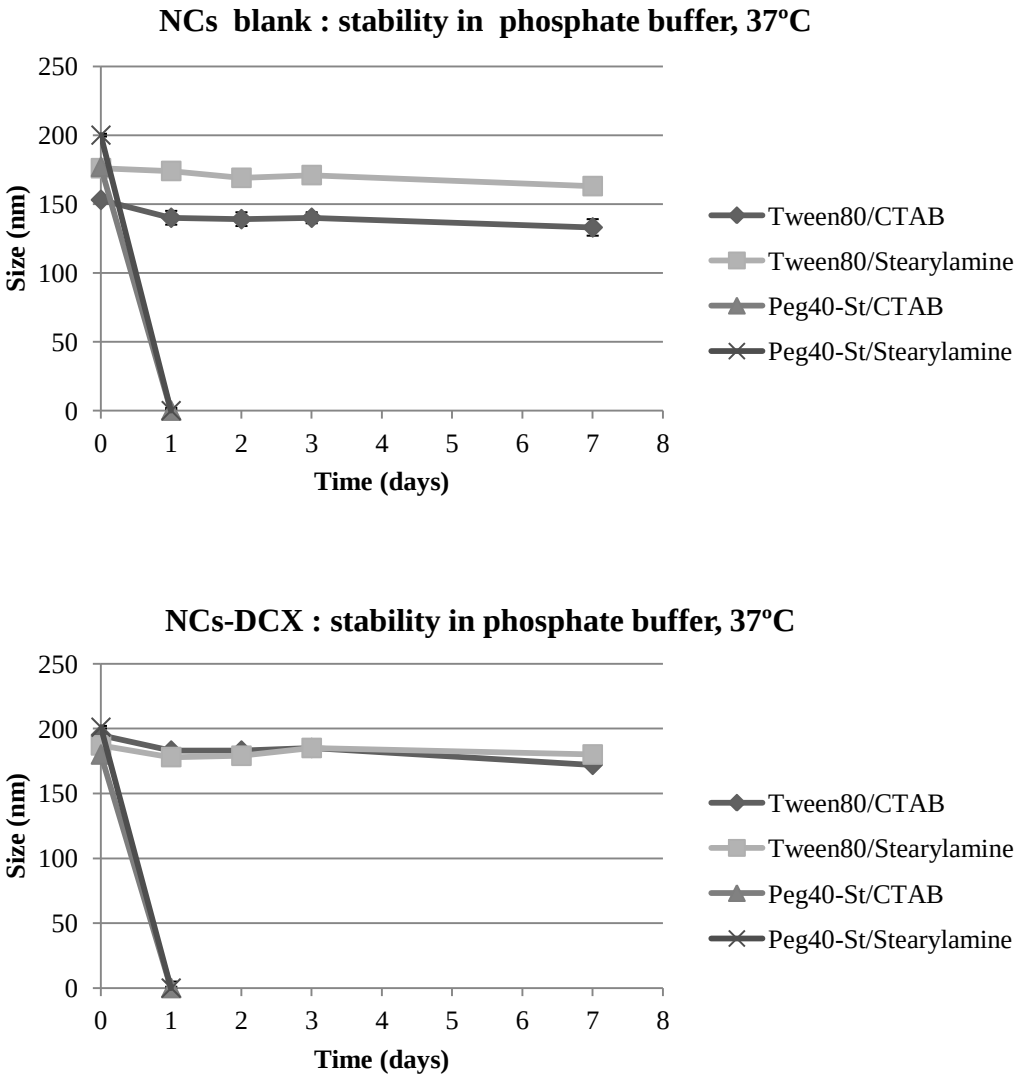

Figure 7: *Stability of blank and loaded nanocapsules at 37ºC in phosphate buffer. Data represents means ±SD, n=3*

3.3.6 Transmission electron micrograph of PGA nanocapsules

TEM images confirmed the approximate values of particle size for PGA nanocapsules as measured by PCS, and supported the homogeneity of the particle size distribution (Figure 8). TEM images indicated also that nanocapsules have a rounded and regular morphology, with the presence of a polymeric outer layer.

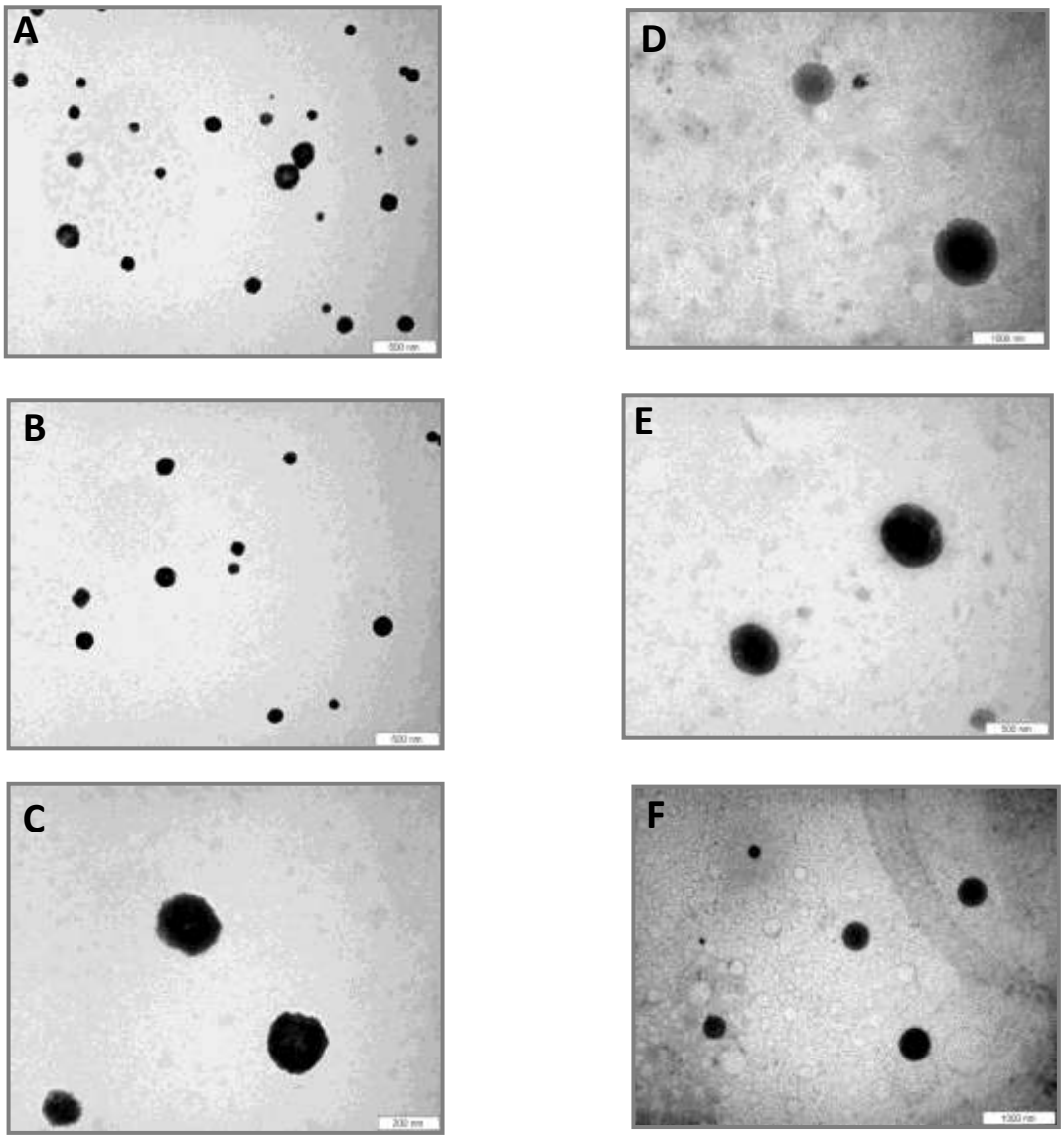

Figure 8: *TEM images of PGA nanocapsules loaded with docetaxel. PGA nanocapsules with stearylamine* ***(A, B, C)*** *or CTAB* ***(D, E, F)*** *as cationic surfactant and Tween80® as non ionic surfactant.*

3.3.7 In vitro release studies

The release pattern of docetaxel from PGA nanocapsules was studied upon incubation in phosphate buffer (Figure 9). After one hour nanocapsules with CTAB as cationic surfactant were shown to release around 45% of their cargo and nanocapsules with stearylamine around 60%. Afterwards, no further release could be observed for the remaining time of the experiment (48 h). This *in vitro* release profile presents the typical biphasic release characterized by an initial burst until partition equilibrium is reached with the external aqueous phase. The fact that a significant fraction of the drug remained in the nanocapsules despite the high dilution is a further indication of the high affinity of docetaxel for the oily core of the nanocapsules (Lozano, 2008; Calvo, 1997). Stability of free drug in the same condition was confirmed (data not shown).

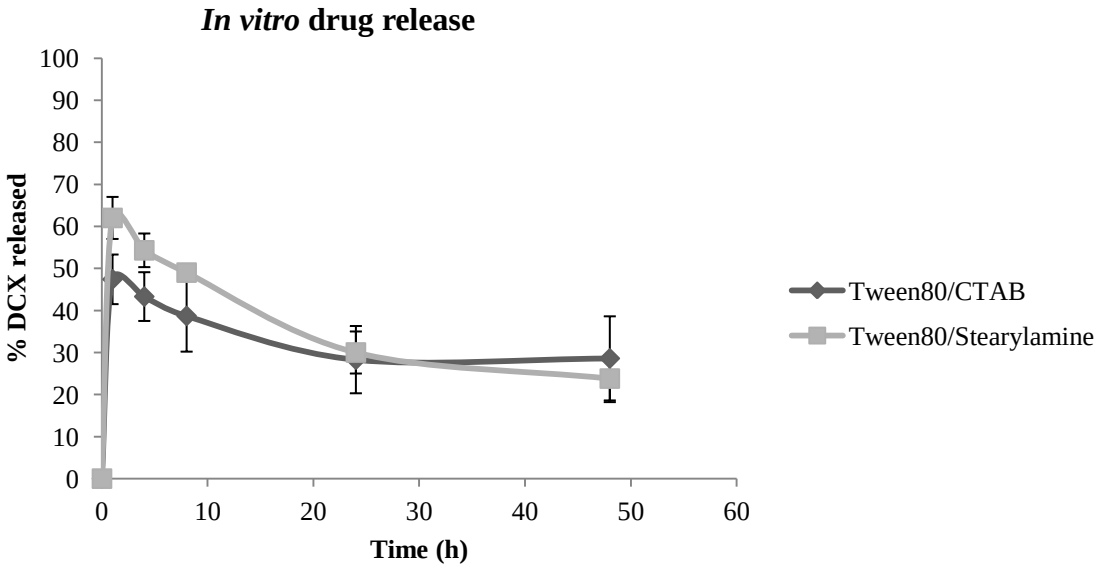

***Figure 9**: In vitro drug release from docetaxel-loaded nanocapsule formulations in phosphate buffer, pH=7, 37 ºC. PGA nanocapsules with stearylamine as cationic surfactant (□); PGA nanocapsules with CTAB as cationic surfactant (♦). Data represents the mean ±SD, n=3.*

3.3.8 Stability in cell culture media

Stability studies were performed in two different cell culture media (Opti-MEM®: Reduced Serum Medium and DMEM supplemented with 10% FBS) in order to carry out a preliminary cellular uptake study. The two selected formulations showed a good stability in both cells culture media until 24 h, with an increasing in size at 48 h in NCs loaded with docetaxel and Tween80® as non ionic surfactant (Figure 10).

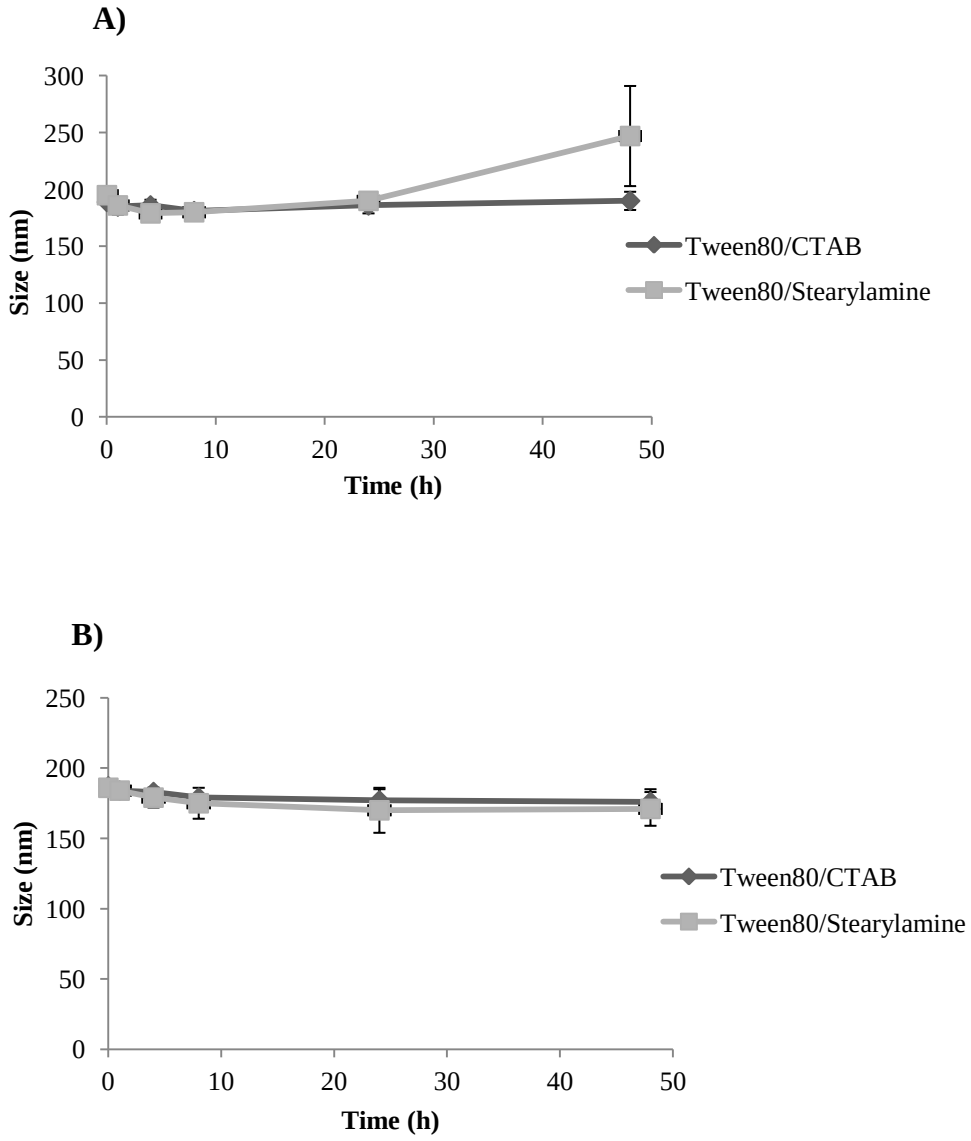

Figure 10: *Evolution of the particle size of PGA nanocapsules measured after incubation at 37ºC in cell culture media* ***A)*** *Opti-MEM® and* ***B)*** *DMEM supplemented with 10% FBS. PGA nanocapsules with CTAB as cationic surfactant (♦) PGA nanocapsules with stearylamine as cationic surfactant (□). Values are presented as mean ±SD, n=3.*

3.3.9 Fluorescent DiD encapsulation into nanocapsules

The results obtained indicate that the fluorescent probe was efficiently encapsulated (59-76 %) without altering the original characteristics of nanocapsules (Table 8). Values of encapsulation efficiency were higher in nanocapsules prepared using stearylamine as surfactant; it was probably due to the more lipophilic properties of this surfactant in comparison with CTAB.

Formulation	Size	P.I.	ζ Potential (mV)	EE (%)
NCs Tween80®/CTAB-DiD	187±5	0.1	-24±2	59±6
NCs Tween80®/Stearylamine-DiD	170±6	0.1	-18±2	76±3

Table 8: *Physicochemical characteristics of DiD-loaded PGA nanocapsules. P.I.: polydispersity index. EE: encapsulation efficiency. Values are given as mean ± SD; n=3.*

3.3.10 Uptake analysis

Fluorescence microscopy studies were conducted to test the intensity of uptake by A549 cells of the encapsulated fluorescent probe DiD. The uptake was significantly fast and after only 4 hours nanocapsules showed cellular uptake. Uptake didn't increase with longer incubation time: after 24 hours cells showed the same amount of fluorescence and no differences among the two types of nanocapsules could be detected (data not shown). Fluorescence microscopy showed that the dye localization inside the cell was in the cytoplasm (Figure 11).

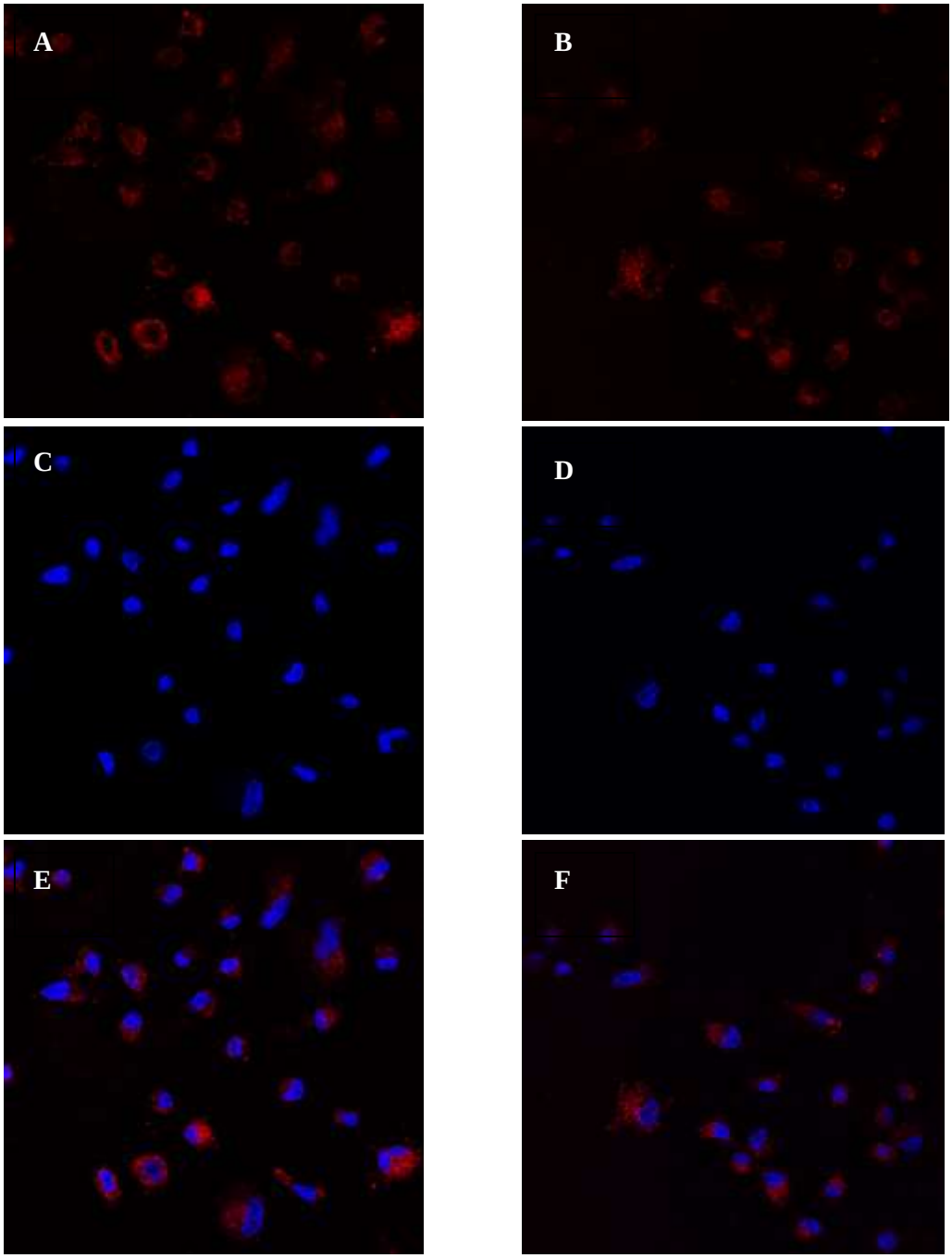

Figure 11: *Confocal microscopy of A549 cells after incubation with DiD-loaded carriers. Cells were incubated for 4 h with 0.5 µg/ml of incapsulated fluorescent probe. They were subsequently processed by staining nuclear DNA (DAPI). A, C, E: NCs Tween80®/CTAB-DiD; B, D, F: NCs Tween80®/Stearylamine-DiD. Red label corresponds to fluorescent carriers loaded with DiD. Nuclei stained with DAPI (blue). Merged imagine of nuclei stained with DAPI (blue) and fluorescent nanocapsules (red).*

3.3.11 Study of formulation variables by experimental designed

Statistical experimental design methodologies are powerful, efficient and systematic tools in the design of pharmaceutical dosage forms, allowing a rational study of the influence of formulation and/or processing parameters on the selected responses with a shortening of the experiment time and an improvement in the research and development work (Schwartz, 1997; Lewis, 1999; Gabrielsson, 2002). The main objective of the experimental design strategies is to plan experiments in order to obtain the maximum information regarding the considered experimental domain with the lowest number of experiments (Lunsted, 1998). Moreover, the multi-varied strategy of experimental design enables the simultaneous evaluation of the influence of the different variables involved in any process, being therefore particularly useful when, as in the case of pre-formulation studies, multiple factors have to be evaluated contemporaneously. The aim of the present section was to evaluate, by means of a multi-varied experimental design methodology, the influence of both the amount and type of cationic surfactant and the amount of polymer on the physical characteristics of nanocapsules prepared by two steps technique. Tween80® and PEG40-stearate were selected as non ionicic surfactants. The selected response variables were size, P.I. and zeta potential of nanocapsules. The software NEMRODW was used for generation and evaluation of the statistical experimental design (Mathieu, 2000). Blank nanocapsules were prepared by two step-technique and fully characterized as previously described (Section 4.2).

The parameters selected as response variables to describe and optimize characteristics of nanocapsules were:

Y_1: size

Y_2: zeta potential

Y_3: P.I.

The effect of different levels of each independent variable on the considered responses was studied. The variables evaluated for each examined cationic surfactant (CTAB, stearylamine) and for each considered non ionic surfactant (Tween80® and PEG40-stearate) and their respective levels were:

U1: amount of PGA (mg/ml)

U2: amount of cationic surfactant (mg) (referred to 5 ml of formulation).

A qualitative model (Broudiscou, 1996) was hypothesized among response and factors under study that contained one constant plus, for each factor, a number of terms equal to its number of levels minus one:

$$y=b_0+A_1x_1+B_1x_2+B_2x_2$$

In particular, A_1 is the coefficient relative to the effect on the response of the level change of the factor U_1 and B_1-B_2 are the coefficients relative to the changes of level of the factor U_2. In order to evaluate the effects on the response of variations in the factor levels, an asymmetric screening design was used (Lewis, 1999; Addelman, 1962). The asymmetric screening design allows a rapid examination of factors at different numbers of levels, thus it can be used when the number of levels of each factor is different. In the present case, the D-optimal design contained six experiments (Table 9). Four independent studies were performed, according to the same general experimental

plan (Table 9).The experimental plans and the obtained responses for the two examined non ionic surfactants are reported in Tables 10 and 11. Effect on the response statistically significative were evaluated by analysis of variance (Table 12). Statistical evaluation of the experimental results processed with the NEMRODW software made it possible to obtain the desired information about the weight of each level of each factor on the considered responses. In particular, the graphic analysis of the effects (Mathieu, 1996) was used to evaluate the different effect of factor levels and determine the suitable level of the variable to be selected for optimising the considered response. The results of the graphic analysis of the investigated are presented in Figure 12-15. It must be pointed out that for the statistic treatment of the data zeta potential values was expressed in absolute values. Graphic analysis of effects is a simple experimental design tool in which the changes of levels that are active on the response correspond to the bars that exceed the dotted vertical lines, which represent the experimental error (Figure 12-15 a). In particular, coefficient A1 indicates the effect on the response moving from level 1 to level 2 of factor U1. Coefficient B1 indicates the effect on the response moving from level 1 to level 2 of factor U2; B2 indicates for the same factor the effect on the response moving from level 1 to the level 3; B3 refers to the 2–3 level change. Once the active level changes are pointed out, it is possible to individuate the suitable levels with another graph in which the effects of each tested level on the response are reported (Figure 12-15 b). In this graph the length of the bars is correlated with the effect of the level on the response: the bars with maximum length are those relative to the levels that determine a maximization of the response. Bars with similar length indicate that the change in the factor levels is not statistically significant for the observed response (Mathieu, 2006). Starting from these figures, it is possible to select, for each drug, the best level of each factor for each considered response. In particular, for each variable, the level to select is indicated by the highest or lowest bar, depending on the considered response have to be maximized (zeta potential) or minimized (size), respectively.

Trials	Variable U_1 (mg PGA)	Variable U_2 (mg of cationic surfactant)
1	1	0.3
2	2	0.3
3	1	0.5
4	2	0.5
5	1	0.9
6	2	0.9

Table 9: *Six run asymmetric screening matrix*

Trials	U_1 (mg)	U_2 (mg)	Cationic surfactant: CTAB			Cationic surfactant: stearylamine		
			Size (nm)	Zeta potential (mv)	P.I.	Size (nm)	Zeta potential (mv)	P.I.
1	1	0.3	189	-9	0.1	205	-14	0.1
2	2	0.3	178	-13	0.1	205	-13	0.1
3	1	0.5	190	-8	0.1	190	-20	0.1
4	2	0.5	182	-16	0.1	193	-26	0.1
5	1	0.9	205	-30	0.1	200	-24	0.1
6	2	0.9	208	-33	0.1	198	-39	0.1

Table 10: *Experimental plan and observed responses for Tween80®/CTAB and Tween80®/stearylamine nanocapsules with cationic surfactant and polymer at different concentrations.*

Trials	U_1(mg)	U_2(mg)	Cationic surfactant: CTAB			Cationic surfactant: stearylamine		
			Size (nm)	Zeta potential (mv)	P.I.	Size (nm)	Zeta potential (mv)	P.I.
1	1	0.3	179	-19	0.1	226	-19	0.1
2	2	0.3	180	-17	0.2	225	-20	0.1
3	1	0.5	198	-20	0.1	196	-25	0.2
4	2	0.5	188	-27	0.1	194	-30	0.2
5	1	0.9	194	-30	0.2	178	-28	0.2
6	2	0.9	206	-38	0.2	193	-31	0.2

Table 11: *Experimental plan and observed responses for PEG40-Stearate/CTAB and PEG40-Stearate/stearylamine nanocapsules with cationic surfactant and polymer at different concentrations.*

Formulation	Surfactant concentration			PGA concentration		
	Size	Zp	P.I.	Size	Zp	P.I.
1.NCs Tween80®/CTAB	◙	◙				
2.NCs Tween80®/Stearylamine	◙	◙			◙	
3.NCs Peg40-St/CTAB		◙				
4.NCs Peg40-St/Stearylamine	◙	◙				

Table 12: *Results of analysis of variance. Variables: surfactant concentration and PGA concentration. Response of interest : Size, zeta potential and P.I. Differences were considered to be significant at a level of $p < 0.05$.*

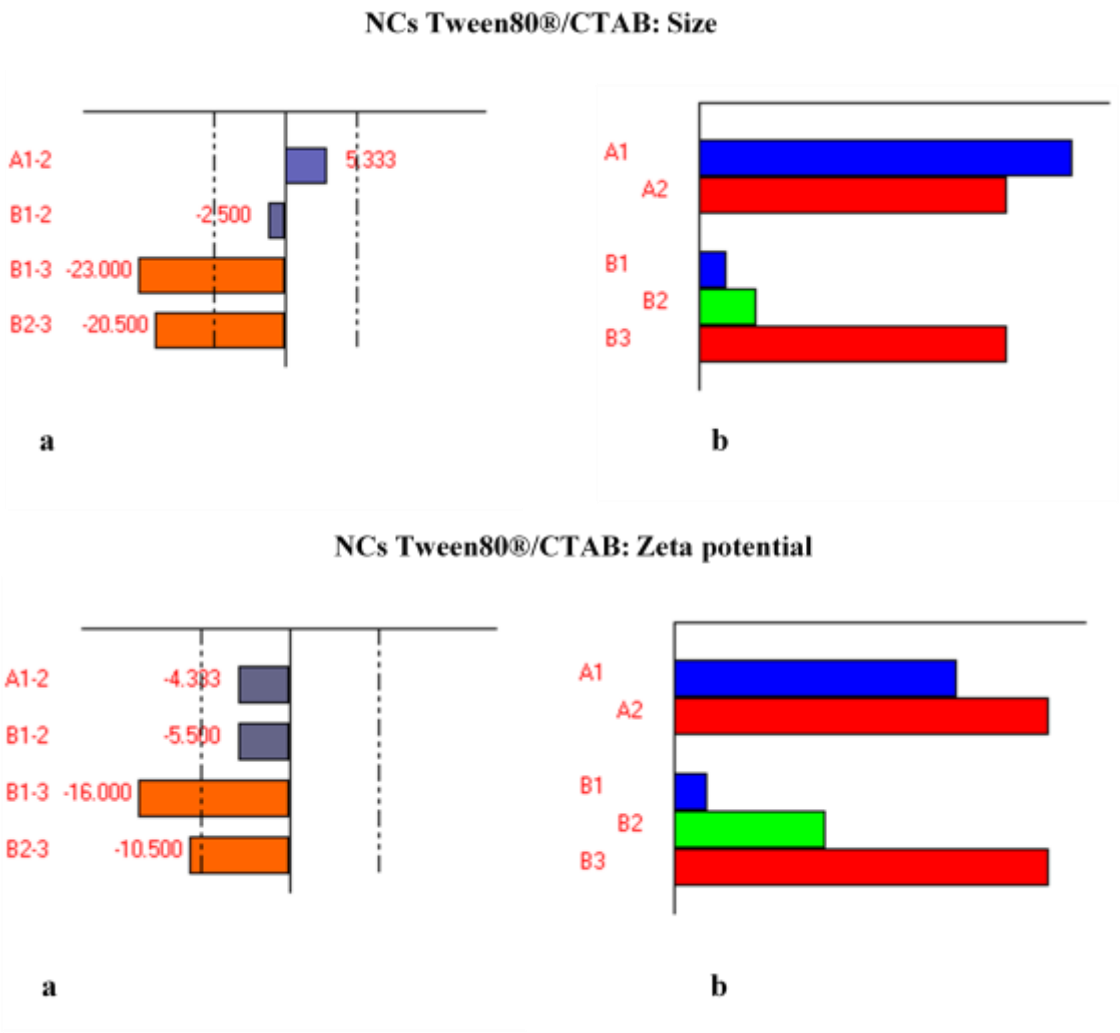

Figure 12: *NCs Tween80®/CTAB.* ***(a)*** *Graphic analysis of effects: A1 coefficient relative to the change of level of the factor U1 (amount of polymer); B1–B3 coefficients relative to the change of levels of the factor U2 (amount of cationic surfactan).* ***(b)*** *Response trend due to the different factor levels.*

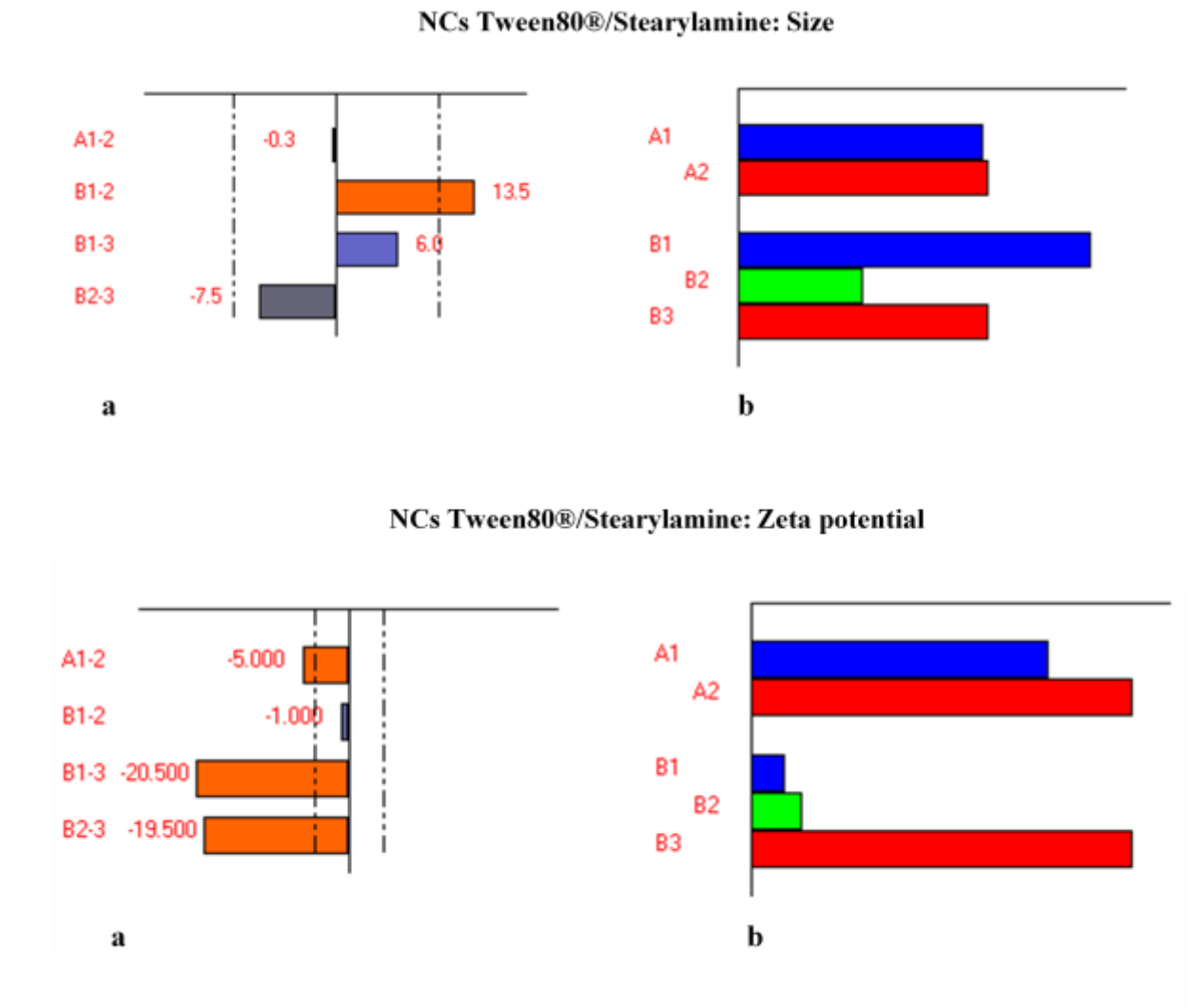

Figure 13: *NCs Tween80®/Stearylamine.* ***(a)*** *Graphic analysis of effects: A1 coefficient relative to the change of level of the factor U1 (amount of polymer); B1–B3 coefficients relative to the change of levels of the factor U2 (amount of cationic surfactan).* ***(b)*** *Response trend due to the different factor levels.*

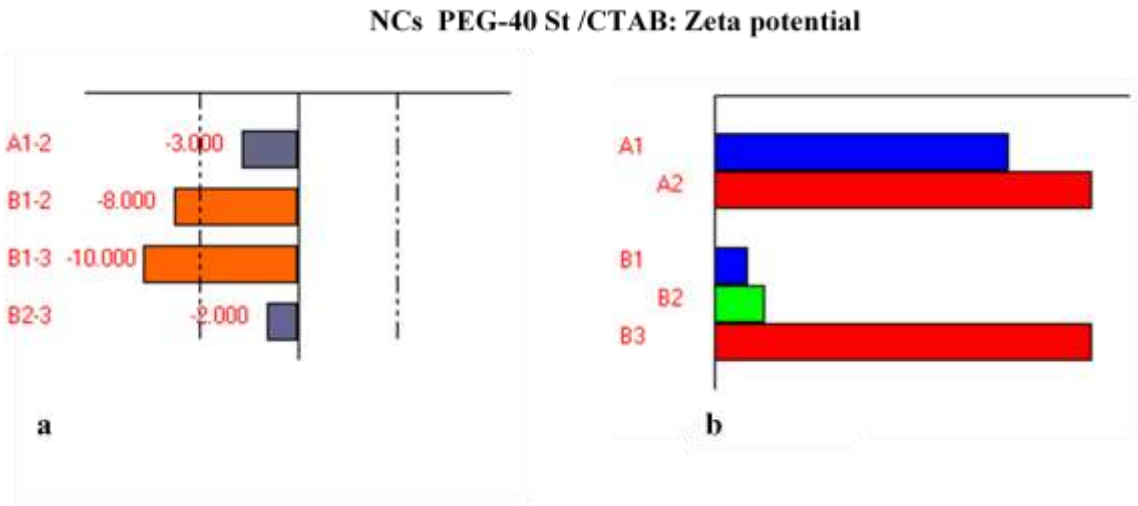

Figure 14: *NCs PEG40-St/CTAB nanocapsules* ***(a)*** *Graphic analysis of effects: A1 coefficient relative to the change of level of the factor U1 (amount of polymer); B1–B3 coefficients relative to the change of levels of the factor U2 (amount of cationic surfactan).* ***(b)*** *Response trend due to the different factor levels.*

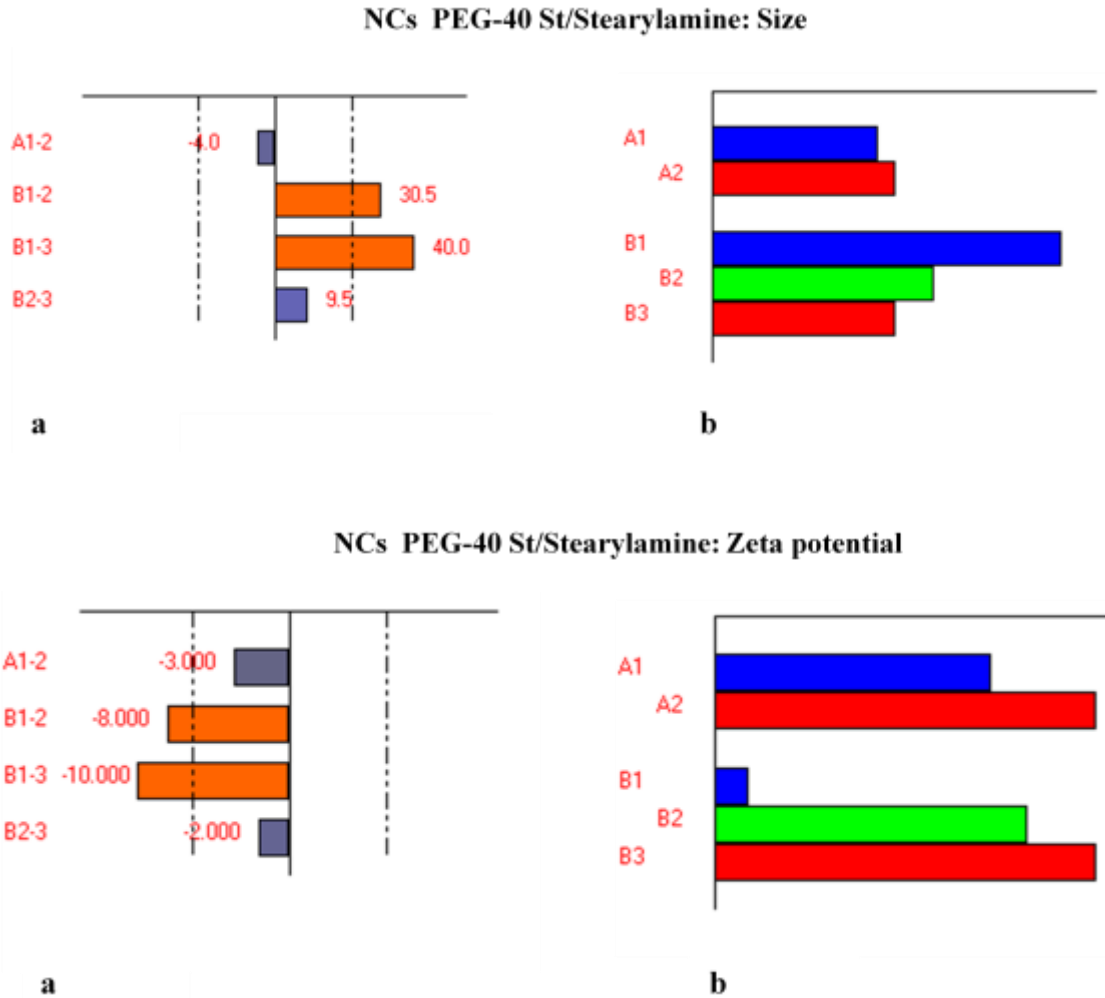

Figure 15: *PEG40-St/stearylamine nanocapsules.* ***(a)*** *Graphic analysis of effects: A1 coefficient relative to the change of level of the factor U1 (amount of polymer); B1–B3 coefficients relative to*

the change of levels of the factor U2 (amount of cationic surfactan). ***(b)*** *Response trend due to the different factor levels.*

In the case of nanocapsules of Tween80® and CTAB (figure 12) we can observe that the effect of two level of factor U_1 on the considered responses (size and zeta potential) is not statistically important. In contrast, the change in level of the other factor (amount of cationic surfactant) was statistically significant, and the results indicated that for minimizing size an amount of 0.3 mg should be used. The results indicate that for maximizing zeta potential values an amount of 0.9 mg of CTAB should be used. The change of P.I values wasn't statistically significative.

In the case of nanocapsules of PEG40-Stearate and CTAB (figure 14) we observed that the change of size wasn't statistically significative (data not showed). The effect of the factor U_1 wasn't statistically significative. In contrast for maximizing zeta potential values an amount of 0.9 mg should be used.

With regard to the nanocapsules of Tween80® and stearylamine (Figure 13) the graphic analysis of the effects showed that the amount of PGA on size is not statistically important. The change in level of the second factor (amount of cationic surfactant) was statistically significant, and the results indicated that for minimizing size an amount of 0.5 mg should be used. In addition for maximizing zeta potential values an amount of 0.9 mg of stearylamine should be used. Also the amount of PGA was important and to maximizing zeta potential value an amount of 2 mg/ml should be used. The change of P.I values wasn't statistically significative.

In the case of nanocapsules of PEG40-stearate and stearylamine (figure 15) we observe that for minimizing size an amount of 0.9 mg of stearylamine is necessary. In addition for maximizing zeta potential values an amount of 0.9 mg of stearylamine should be used as well. The change of P.I values wasn't statistically significative. We can also observe a slight difference between B_2 and B_3 coefficients relative to the change of levels of the factor U2 (amount of cationic surfactant) in both size and zeta potential.

In conclusion the results obtained underlined that the **amount of polymer** was statistically important only in one case (size of NCs of Tween80® and stearylamine). In general increasing the amount of polymer we didn't observe any significative change in size, zeta potential or P.I. It can be reasonably hypothesized that the polymeric coating of nanoemulsion is complete with PGA concentration of 1 mg/ml.

In the case of NCs Tween80®/CTAB and NCs PEG40-Stearate/CTAB for maximizing zeta potential values an amount of 0.9 mg of **CTAB** should be used. The presence of bigger amount of cationic surfactant promote the electrostatic interaction with the chain of polymer, this can explain the decreasing of zeta potential values. This amount of cationic surfactant was selected to get stable formulation by one step technique for further investigation.

In the case of **stearylamine** as cationic surfactant an amount of 0.5 mg was selected. This formulation optimizes the size for NCs of Tween80®/stearylamine and it has a very similar behavior to that obtained with 0.9 mg of cationic surfactant. Graphic analysis of the effect for NCs

of PEG40-stearate/stearylamine showed only slight differences between B_2 and B_3 coefficients in size and zeta potential so the reduced amount of cationic surfactant was priority. Nanocapsules obtained with selected amounts of polymer and cationic surfactant have been previously described on section 3.3.3.

3.4 CONCLUSIONS

In conclusion two different nanocapsules for doceaxel delivery were developed and fully characterized. The formulations were developed avoiding use of lecithin as surfactant and show good characteristics for parenteral delivery: have nanometric size (about 200 nm), low polydispersity and good values of zeta potential. A decrease in the amount of cationic surfactant used was possible in the case of stearylamine without any alteration in stability of NCs. Docetaxel, used as model drug, was incorporated in the formulations without modification in their properties. Encapsulation efficiency was between 40-50 %. The formulations selected showed good stability in phosphate buffer and in cell culture medium and preliminary cellular uptake studies support nanocapsules internalization. Further *in vitro* studies need to be performed in order to compare the toxicity of these new formulation with the nanocapsules previously developed and to show the advantage in reduction of cationic surfactant.

3.5 REFERENCES

Addelman S., et al., Orthogonal main-effect plans for asymmetrical factorial experiments, Technometrics. 1962. 4: p. 21–46.

Broudiscou A., et al., Genetic algorithm as a tool for selection of D-optimal design, Chem. Intell. Lab. Sys. 1996. 35: p. 105–116.

Calvo P., et al., Development of positively charged colloidal drug carriers: Chitosan-coated polyester nanocapsules and submicron- emulsions. Colloid & Polymer Science, 1997. 275(1): p. 46-53-53.

Couvreur P., et al., Nanocapsule technology: A review. Critical Reviews in Therapeutic Drug Carrier Systems, 2002. 19(2): p. 99-134.

Dash B.C., et al., The influence of size and charge of chitosan/polyglutamic acid hollow spheres on cellular internalization, viability and blood compatibility. Biomaterials, 2010. 31(32): p. 8188-8197.

Gabrielsson J., et al., Multivariate methods in pharmaceutical applications. J. Chemometrics. 2002. 16: p. 141–160.

Garcion E., et al., A new generation of anticancer, drug-loaded, colloidal vectors reverses multidrug resistance in glioma and reduces tumor progression in rats. Molecular Cancer Therapeutics, 2006. 5(7): p. 1710-1722.

Gelderblom H., et al., Cremophor EL: the drawbacks and advantages of vehicle selection for drug formulation. Eur. J. of Cancer, 2001. 37(13): p. 1590-1598.

Haass N. K., et al., The mitogen-activated protein/extracellular signalregulated kinase kinase inhibitor AZD6244 (ARRY-142886) induces growth arrest in melanoma cells and tumor regression when combined with docetaxel. Clin. Cancer Res. 2008. 14: p. 230–239.

Han H.D., et al., Enhanced circulation time and antitumor activity of doxorubicin by comb-like polymer-incorporated liposomes. J Control Rel. 2007. 120: p. 161–168.

Kajiwara E., et al., Long-circulating liposome-encapsulated ganciclovir enhances the efficacy of HSV-TK suicide gene therapy. J Control Rel. 2007. 120: p. 104–110.

Lee, S.H., et al., Rapid and sensitive determination of paclitaxel in mouse plasma by high-performance liquid chromatography. Journal of Chromatography B-Analytical Technologies in the Biomedical and Life Sciences, 1999. 724(2): p. 357-363.

Lewis G.A. et al., Pharmaceutical Experimental Design, Marcel Dekker, New York, 1999.

Lozano M. V., et al., Polyarginine nanocapsules: a new platform for intracellular drug delivery. Submitted.

Lozano M.V., et al., Highly Efficient System To Deliver Taxanes into Tumor Cells: Docetaxel-Loaded Chitosan Oligomer Colloidal Carriers. Biomacromolecules, 2008. 9(8): p. 2186-2193.

Lunstedt T., et al., Experimental design and optimization. Chem. Intell. Lab. Sys. 1998. 42: p. 3–40.

Mathieu D., et al., Criblage et e´tude des facteurs, LPRAI SARL, Marseille, France, 1996.

Mathieu D., et al., NEMRODW, LPRAI sarl, Marseille, France, 2000.

Mora-Huertas C.E., et al., Polymer-based nanocapsules for drug delivery. International Journal of Pharmaceutics, 2010. 385(1–2): p. 113-142.

Park J.H., et al., Polymeric nanomedicine for cancer therapy. Progress in Polymer Science, 2008. 33(1): p. 113-137.

Ramadan A., et al., Oral fondaparinux: use of lipid nanocapsules as nanocarriers and in vivo pharmacokinetic study. International Journal of Nanomedicine, 2011. 6 : p. 2941-2951.

Saloustros E., et al., Docetaxel in the treatment of advanced non-small-cell lung cancer. Expert Rev. Anticancer Ther. 2008. 8: p. 1207–1222.

Saloustros E., et al., Paclitaxel and docetaxel in the treatment of breast cancer. Expert Opin. Pharmacother. 2008. 9: p. 2603–2616.

Schwartz J.B., et al., Optimization techniques in pharmaceutical formulation and processing in: G.S. Banker, C.T. Rhodes (Eds.), Modern Pharmaceuticsthird ed., Marcel Dekker, New York. 1997. p. 727–752.

Teixeira, M., et al., Development and characterization of PLGA nanospheres and nanocapsules containing xanthone and 3-methoxyxanthone. European Journal of Pharmaceutics and Biopharmaceutics, 2005. 59(3): p. 491-500.

Vlachy N., et al., Determining the cytotoxicity of catanionic surfactant mixtures on HeLa cells. Colloids and Surfaces B: Biointerfaces, 2009. 70 (2): p. 278-280.

CHAPTER 4

Liposomes for dihydroartemisinin delivery to cancer cells: development, characterization and *in vitro* studies

This work was carried out in collaboration with MARCELLA CORONNELLO[1]

[1]*Department of Pharmacology, University of Florence, Florence, Italy.*

4.1 INTRODUCTION

Poor solubility of a chemical entity is a major obstacle affecting its drugability (Fahr, 2007). It is estimated that more than 40% of the new chemical entities generated in drug discovery programs are poorly soluble (Lipinski, 2001). With growing interest in the role of modern pharmaceutics in early stage of drug discovery and development, rationale design of drug delivery systems for poorly soluble drugs has been widely explored, such as emulsions (Bansal, 2008; Chen, 2008), solid lipid nanoparticles (Hanafy, 2007; Ye, 2008), micelles, and liposomes (Pastorino, 2003; Harvey, 2007). Dihydroartemisinin (DHA), a semi-synthetic derivative of artemisinin, is isolated from *Artemisia annua*. Artemisinin and its derivatives are well known as a treatment for malaria (Klayman, 1985), but more recent studies have revealed that it also has a preferentially cytotoxic effect on cancer cells, including leukemia cells, fibrosarcoma cells, ovarian cells, breast cancer cells and cervical cancer cells (Lu, 2009; Kim, 2006; Colm, 2010). Moreover, some studies have indicated that artemisinin derivatives have anti-cancer activities *in vitro* and *in vivo*. The fact that dihydroartemisinin induces cytotoxicity and apoptosis in cancerous cells has been reported by several groups. Lai and others treated molt-4 lymphoblastoid cells with dihydroartemisinin and showed that their survival was less than 50% after incubation (Efferth, 2002). However, DHA has poor water-solubility and low bioavailability for oral administration due to slow drug dissolution (Gabriëls, 2004). Furthermore, the half-life of DHA is very short (34–90 min) (Batty, 1996). It has been demonstrated that intravenous delivery of DHA results in the highest availability to body as compared to all other routes and can lead to quick eradication of the malarial infection (Li, 1998). Therefore, the development of the new formulation of DHA that enables quick availability to the body is in great need. Our work was focused on development and characterization of conventional and stealth liposomes for dihydroartemisinin delivery to cancer cells.

To further advance biomedical application, it is important to characterize the interactions between liposomes and blood components, particularly with serum proteins that play an important role in the stability and properties of liposomes in blood e.g. in their circulation lifetimes (Panagi, 1999; Chonn, 1992). The amount of serum proteins associated on the liposomes used was inversely related to their circulation half-lives (Chonn, 1992). The serum proteins associated onto the surface of liposomes systematically administered have been suggested to be one of the most important factors to determine their *in vivo* fate (Drummond, 1999; Cattel, 2003). The amount of blood protein associated with liposomes in the circulation dramatically affects liposome clearance behaviour *in vivo* (Chonn, 1992). Specific bounded proteins can have a direct effect on particle internalization and biodistribution. Certain proteins allow macrophages of the reticulo endothelial system (RES) to more easily recognize nanoparticles (Owens, 2006). On the other hand, dysopsonins such as albumin are said to promote prolonged circulation times in the blood (Goppert, 2005; Moghimi, 1993; Ogawara, 2004). It has been found that proteins partially penetrate (Juliano, 1971; Sabin, 2009) and modify the lipid bilayer (Lis, 1976; Hoekstra, 1979) when they are in contact with the membrane surface. This protein penetration into the liposomal membrane can change the properties of the bilayer with drastic consequences in their use as drug delivery systems

(Sabin, 2009). Increase in the rate of efflux of different liposomal contents in contact with serum albumin has been reported (Sweet, 1969,1970; Zborowski, 1977), but the role of albumin in phospholipid transfer, leading to loss of bilayer integrity and release of liposomal contents, is controversial. Near-physiological concentration (30 mg/mL) albumin dissolved more then 50% of liposomes (Michnik, 1997).

The addition of PEG can add protein/opsonization resistance properties by preventing interactions between the particle surface and the plasma proteins (Owens, 2006; Jeon, 1991). Often water-soluble polymers like polyethylene glycol (PEG) are attached to the surface of long-circulating liposomes to reduce adhesion of opsonic plasma proteins that would otherwise induce recognition and rapid removal from the circulation by macrophages in the liver and spleen (Woodle, 1994; Oku, 1994; Aggarwal, 2009). Using this approach, PEG-coated long-circulating liposomes can remain in the circulation with a half-life as long as 50 hours (Gabizon, 1994; Hong, 2001).

In this work, conventional and stealth liposomes were designed for the delivery of dihydroartemisinin. Loaded DHA liposomes were prepared and studied physicochemically. Their capacity to encapsulate the drug and the stability of the formulations in storage condition and *in vitro* in presence of albumin were evaluated. Flow cytometry analysis was used also for this aim and like alternative technique for rapid size determination of liposomes.

4.2 MATERIALS AND METHODS

4.2.1 Materials

All the solvents used were HPLC grade from Merck (Darmstadt, Germany); 85% formic acid was provided by Carlo Erba (Milan, Italy). Water was purified by a Milli-Q_{plus} system from Millipore (Milford, MA). Dihydroartemisinin (DHA) was provided by Sigma-Tau (Pomezia, Roma). PEG 2000 (18:0/18:0) was purchased from Spectra2000 srl (Rome, Italy). Egg phosphatidylcholine (Phospholipon90G, P90G) was gently provided from Natterman Phospholipids, GmbH, Hermersberg, Rhineland-Palatinate, Germany. Cholesterol was analytical grade from Aldrich (Milan, Italy). Dihydroartemisinin reference standard (ST3105, batch no. C005641) was kindly provided by Sigma-Tau (Pomezia, Rome, Italy). NBD-PE (N-(7-nitrobenz-2-oxa-1,3-diazol-4-yl)-1,2-dihexadecanoyl-snglycero-3-phosphoethanolamine, triethylammonium salt; λ_{ex}= 463 nm; λ_{em}= 536 nm) were purchased from Molecular Probes, Invitrogen, Breda, The Netherlands.

4.2.2 Preparation of conventional and PEGylated liposomes

Conventional and PEGylated liposomes were prepared according to the film hydration method (Bangham, 1965), according to the optimised molar ratios reported in Table 1**.**

Constituent	L-C-DHA	L-P-DHA
P90G	5	5
Cholesterol	0.6	0.6
PE 18:0/18:0 PEG 2000	-	0.25
DHA	2	2

***Table 1**: Molar ratios between the constituents of dihydroartemisinin-loaded conventional liposomes (L-C-DHA) and dihydroartemisinin-loaded PEGylated liposomes (L-P-DHA).*

Briefly, in the case of loaded conventional liposomes P90G, cholesterol and DHA were dissolved in dichloromethane. The organic solvent were vacuum evaporated and the dry lipid film was hydrated by addition of phosphate buffered saline solution. The dispersion was stirred with a mechanical stirrer for 30 minutes in a waterbath at the constant temperature of 38°C. In order to reduce the dimensions of the vesicles from MLV to LUV, a sonication probe was used at power delivery of 50 % for different intervals of time (5'-15' with pulsed duty cycle of 5 s on and 2 s off) with sample in ice bath to overcome lipid degradation. In order to obtain loaded PEGylated liposomes, PE 18:0/18:0 PEG 2000 was weighted together with P90G, cholesterol and DHA and then the vesicles were prepared as describe above. Fluorescent liposomes were prepared by the addition of the fluorescence label NBD-PE at the concentration of 1% mol of the total lipid concentration. NBD-PE's stock solution had a concentration of 1 mg/mL in $CHCl_3$ and it could be saved in freezer.

4.2.3 Characterization of liposomes

Liposomes size, polydispersity and zeta potential were measured by photon correlation spectroscopy. For these measurements, 20 µL of each liposomal dispersion was diluted 100-folds with aqueous solution. Measurements were carried out at the setted temperature of +25°C using a Zetasizer® Nano ZS3600 (Malvern Instruments, Malvern, UK). The morphological characterization of the systems was performed using the transmission electron microscopy technique (TEM, CM12 Philips, Netherlands). Samples were stained with 2% (w/v) phosphotungstic acid solution and placed on copper grids with Formvar films for viewing by TEM.

The encapsulation efficiency (EE) is defined as the percentual amount of drug entrapped in the vesicles in relation to the total amount of drug present during the vesicle formation and entrapment procedure. Free DHA was removed by means of dialysis. Liposomal formulation was transferred in a dialysis bag. This dialysis bag was stirred in 2 L of PBS at room temperature for 2 hours. The aqueous medium was refreshed once. The content of DHA into the liposomes was quantified by HPLC/DAD analysis using DHA as external standard.

Dihydroartemisinin loaded concentration was assayed by HPLC/DAD analysis performed HP 1100 Liquid Chromatograph (Agilent Technologies, Palo Alto, CA, USA) equipped with a HP 1040

Diode Array Detector (DAD), an automatic injector, an autosampler and a column oven and managed by a HP 9000 workstation (Agilent Technologies, Palo Alto, CA, USA). The UV-Vis spectra were recorded between 220–500 nm and the chromatographic profiles was registered at 210 nm. Separations were performed on a reversed phase column Luna C18 (250 x 4.6 mm, 5 µm, Phenomenex) maintained at 27°C. The eluents were H_2O at pH 3.2 by formic acid (A) and acetonitrile (B). The multi-step linear gradient applied is described on Table 2. The injection volume was 20 µl. The content of fluorescent probes into the liposomes was quantified by HPLC with fluorometric detection. Detector was set to excitation and emission of 460 nm and 535 nm respectively. In order to quantified the amount of fluorescence, a calibration curve was prepared using increasing amount of not dialyzed distrupted liposomes. The formulations were stored at +4°C and physicochemical characterisation was carried out according to the techniques described above. All the measurements were performed in triplicate.

Time (min)	Eluent A (%)	Eluent B (%)
0.10	50	50
15	50	50
20	0	100
23	0	100
28	50	50

.

Table 2: *HPLC method for dihydroartemisinin quantification.*

4.2.4 Stability studies

4.2.4.1 Stability in storage condition

Stability of dihydroartemisinin-loaded vesicles dispersion was studied over 20 days. Vesicles dispersions were kept at 4±1°C and at fixed time intervals they were assayed for their physical and chemical stability. Physical stability was checked by monitoring of size and polidispersity in time. Chemical stability was checked by quantification of drug content after disruption of purified vesicles by HPLC-DAD analysis.

4.2.4.2 Stability in presence of albumin

I. Flow cytometry for rapid size determination

Flow cytometry analysis

Flow cytometry was performed using a FACSCanto II (Becton and Dickinson, Mountain View, CA, USA) equipped with three air-cooled lasers at 488 and 633 nm. Side scatter outcome was set to logarithmic and detected at a scattering angle of 90° with a threshold set on FL-1 (set to logarithmic amplification) to exclude side scatter values from non-fluorescent particulate matter. Flow rates and/or dilutions were chosen such that less than 2000 events/s were recorded to prevent coincidence. For each measurement a total number of 10000 events were recorded. Results were analyzed by software WinMDI 2.9.

FACS data processing

For calibration, histograms of SSC values were plotted and the geometric means of each peak corresponding to a bead size were derived. Bead sizes (y) and geometric means of SSC values (x) were then plotted in Graphpad Prism and fitted with non linear regression using: $y=a+bx^c$ as described previously (Vorauer-Uhl, 2000).

Calibration curves by labeled beads

The size distribution of the liposomes was determined by correlating the side scattered signals of the vesicles and the side scattered signals of the calibration beads. For the calibration of the size distribution, fluorescence labeled latex beads FluoSpheres Size Kit #2, carboxylate-modified microspheres of 0.1-0.2-0.5-0.7-1.0–, yellow-green fluorescent (505/515) were used. Diameters of the fluorescent beads were confirmed by Dynamic Light Scattering (100, 200, 500, 700 and 1000 nm bead). The standard beads were analized by FACS and a calibration curve based on measurements of the labeled beads was calculated.

II. Incubation with albumin and FACS analysis

Conventional and PEGylated liposomes loaded with DHA were incubated with a solution of albumin (40 mg/mL in PBS) at the body temperature in a shaking waterbath to mimic the *in vivo* condition. They were labeled with NBD-PE 1% mol and analysed by FACS experiment. 200 µL of fluorescent liposomes were exposed to 2.2 mL of albumin solution (40 mg/mL). This volume of albumin was choosen because for *in vivo* mouse studies, the total blood volume of a mouse of approx. 25 grams is 2 mL, which equals approx 1.1 ml of serum (55% of 2 mL) and the maximum injection volume of 100 µL is used. Fluorescent liposomes were sampled (150 µL) at 20, 40, 60, 90 and 120 minutes. Conventional and PEGylated DHA-liposomes were diluted $4x10^3$ times in PBS. Conventional and PEGylated DHA-liposomes after incubation with albumin were diluted $4x10^2$ times in PBS. They were subsequently analyzed by FACS for particle size and number of fluorescent events. The experiment and the measurements were repeated in triplo.

4.2.5 Cell lines

The MCF-7 human breast cancer cell line was obtained from the American Type Culture Collection (Rockville, MD). This line was grown in Dulbecco's modified Eagle medium-high glucose (DMEM) (GIBCO, European Division, San Giuliano Milanese, MI, Italy), supplemented with 10% FBS, 1% L-glutamine (Euroclone Company, Celbio s.r.l Italy). Cells were maintained at 37ºC in a humidified atmosphere with 5% CO_2. The culture medium was changed every two days for approximately 5-6 days until cells reached approximately 80-90% confluence.

4.2.6 Sulforhodamine B cytotoxicity assay

This assay is based on a method described by Skehan et al. (Skehan, 1990) for measuring cellular protein content. Briefly, MCF-7 cells were seeded onto Greiner 96-well microplates (International pbi, Milan, Italy). After 24 h, culture medium was replaced with fresh medium and either liposomes formulation at final drug concentrations varying from 1µM to 1000 µM or medium (controls) was added. After 72 hours of incubation a 96-well microplate was processed by using the sulforhodamine B (SRB) method to determine cell growth inhibition. Cells were fixed, air-dried, and stained for 30 min with 0.4% SRB (Sulforhodamine B) (Sigma–Aldrich, St. Louis, MO, USA) dissolved in 1% acetic acid. At the end of the staining period, SRB was removed and protein-bound dye was extracted with 10 mM unbuffered Tris base (Hidroxymethylaminomethan, pH 10.5, Merk, Germany) for 10 min on a shaker. Optical density was read in a computer-interfaced, 96-well microplate reader (Bio-Rad Laboratories, Milano, Italy) at 540 nm.

4.2.7 Cellular uptake of liposomes by flow cytometry analysis

Flow cytometry analysis was conducted on conventional and PEGylated liposomes labeled with NBD-PE 1% mol and on no labeled liposomes (negative controls). Fluorescent liposomes were fully characterized as previously described. Cells (10^5/ml) were treated for 1h with blank liposomes, and conventional or PEGylated liposomes incapsulating NBD-PE (400 µM). After incubation at 37ºC, cells were washed twice with PBS and dissociated with 0.05% trypsin/EDTA. After a centrifugation step at 1200 rpm for 5 min at 4ºC, supernatants were discarded and cell pellets were washed with cold PBS. Cells were then resuspended in 1 ml of cold PBS and kept on ice in the dark. Analyses were performed using the flow cytometer FACS Canto (Becton Dickinson, San Jose, CA, USA). The autofluorescence of cell line was determined and a total of 20000 events were recorded.

4.2.8 Fluorescence microscopy analysis

MCF-7 cells were seeded (2 x 10^4 cells/well) onto 2-well chamber slides and cultured overnight prior to the experiment. Cells were washed with PBS and 400 µM NBD-PE labeled liposomes in serum-free medium was added. After 1 hour, unbound liposomes were removed and the cells were

washed with PBS. The cells were either fixed with EtOH for 10 minutes before visualization. Fluorescence microscopy analysis was performed with a Leica TCS-SP confocal laser scanning microscope equipped with a 488 nm Argon, 568 nm Krypton and 647 nm HeNe laser.

4.3 RESULTS AND DISCUSSION

4.3.1 Characterization of liposomes

Conventional and PEGylated liposomes were prepared according to the film hydration method as previously described and dimensions of the vesicles were reduced from MLV to LUV by sonication. Sonication time was affected the liposomal particle size and P.I. as reported in Table 3. By increasing the sonication time from 5 min to 15 min, the particle size decreases from 218 nm to 111 nm in conventional liposomes loaded with DHA. Only five minutes of sonication were necessary to decrease P.I and size of PEGylated liposomes respectively to 0.19 and 99 nm.

Formulation	Sonication time (min)	Size (nm)	P.I.
L-C-DHA	0	218 ± 3	0.29
	5’	181 ± 2	0.33
	10’	125 ± 2	0.27
	15’	111 ± 7	0.28
L-P-DHA	0	112 ± 1	0.31
	5’	99 ± 9	0.19

***Table 3**: Optimization of sonication time during liposomes preparation. L-C-DHA: dihydroartemisinin-loaded conventional liposomes; L-P-DHA: dihydroartemisinin-loaded PEGylated liposomes. Data were shown as mean ± S.D. (n=3).*

All liposomal dispersions were analyzed in terms of size (nm), polydispersity (P.I.) and zeta potential by photon correlation spectroscopy. The correlation coefficient is superior to 0.9 that means that the signal to noise ratio is good (noise is 10%). The mean diameters of all the artemisinin-based vesicles was ≤200 nm and resulted suitable for the parenteral administration. The measurements performed three-times for each formulation were nicely reproducible. ζ-potential is around -32 mV for conventional liposomes and -25 mV for PEGylated liposomes. This change is a first indication of the presence of PEG shielding liposomes as observed before for other nanocarriers (Garcia-Fuentes, 2004). The DHA loading efficiencies were about 71% and 69% for both conventional liposomes and PEGylated liposomes, respectively, evaluated by HPLC/DAD analysis (Table 4). DHA loading efficiency for L-P-DHA was slightly lower than in the case of L-C-DHA. This fact could be related to the smaller size of PEGylated liposomes which decreases the bilayer capacity of solubilising lipophilic drugs (Isacchi, 2012).

The morphological appearance of the systems was observed by transmission electron microscopy (Figure 1). Both formulations had a round shape and results were in good agreement with the ones obtained from dynamic light scattering analyses. In particular stealth liposomes exhibit a rounded shape and corona, which might be attributed to the PEG polymer shell (Figure 1D, E, F).

Formulation	Size (nm)	P.I.	ζ potential (mV)	Encapsulation efficiency (%)
L-C-DHA	111±7	0.28	-32.7±5.4	71±8.8
L-P-DHA	99±9	0.19	-25±8	69±5.5

Table 4: *Size, polydispersity index (P.I.), ζ-potential and encapsulation efficiency of L-C-DHA: dihydroartemisinin-loaded conventional liposomes and L-P-DHA: dihydroartemisinin-loaded PEGylated liposomes. Data were shown as mean ± S.D. (n=3).*

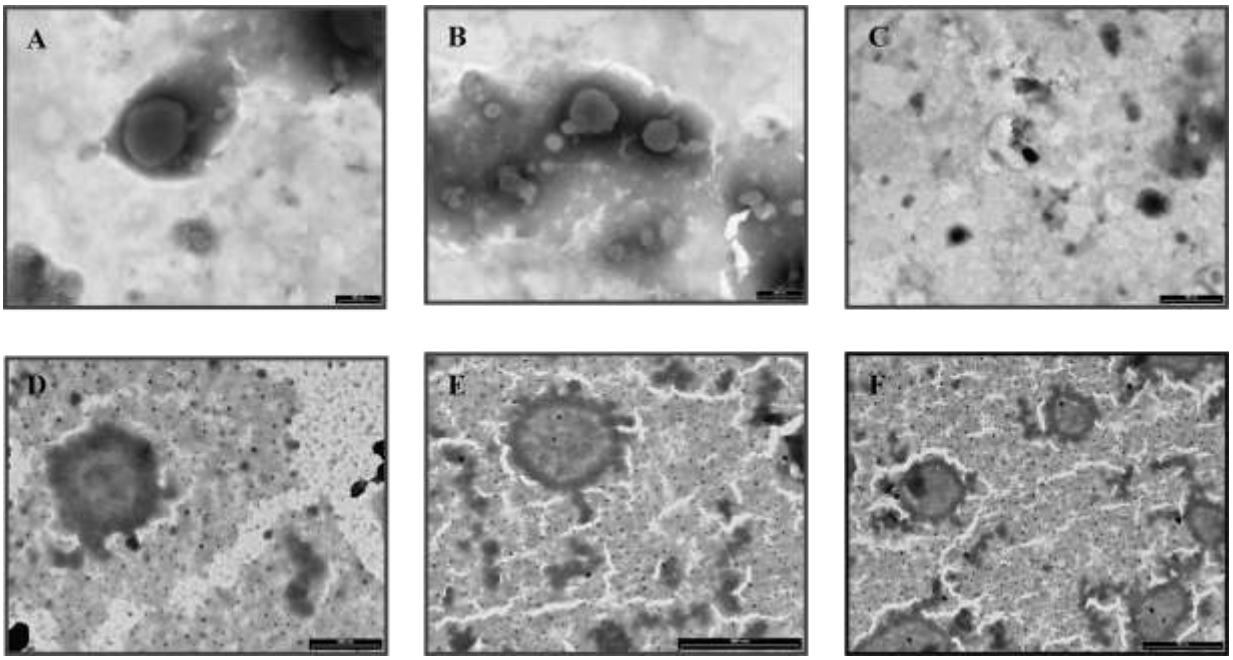

Figure 1*: TEM images revealing shape, structure, and sizes of conventional* ***(A, B, C)*** *and PEGylated* ***(D, E, F)*** *liposomes encapsulating dihydroartemisinin.*

4.3.2 Stability in drug storage conditions

Stability of dihydroartemisinin-loaded conventional and PEGylated vesicles was studied over 20 days. Physical stability was checked by monitoring of size and zeta potential in time, by DLS measurements. There was no modification on the particle size neither on the zeta potential of the liposomes, which maintained their original values throughout the study (Figure 2). Furthermore,

polydispersity of all the liposomal formulations was stable over time (data not showed). That means that no vesicle size alterations occurred over the whole period. Moreover, chemical stability was checked by quantification of drug content after disruption of purified vesicles. As described in the experimental section, the content of dihydroartemisinin into the liposomes was quantified by HPLC/DAD analysis. We found that dihydroartemisinin maintained a residual percentage of 82% and 77% after 20 days respectively in conventional and PEGylated liposomes (Figure 3).

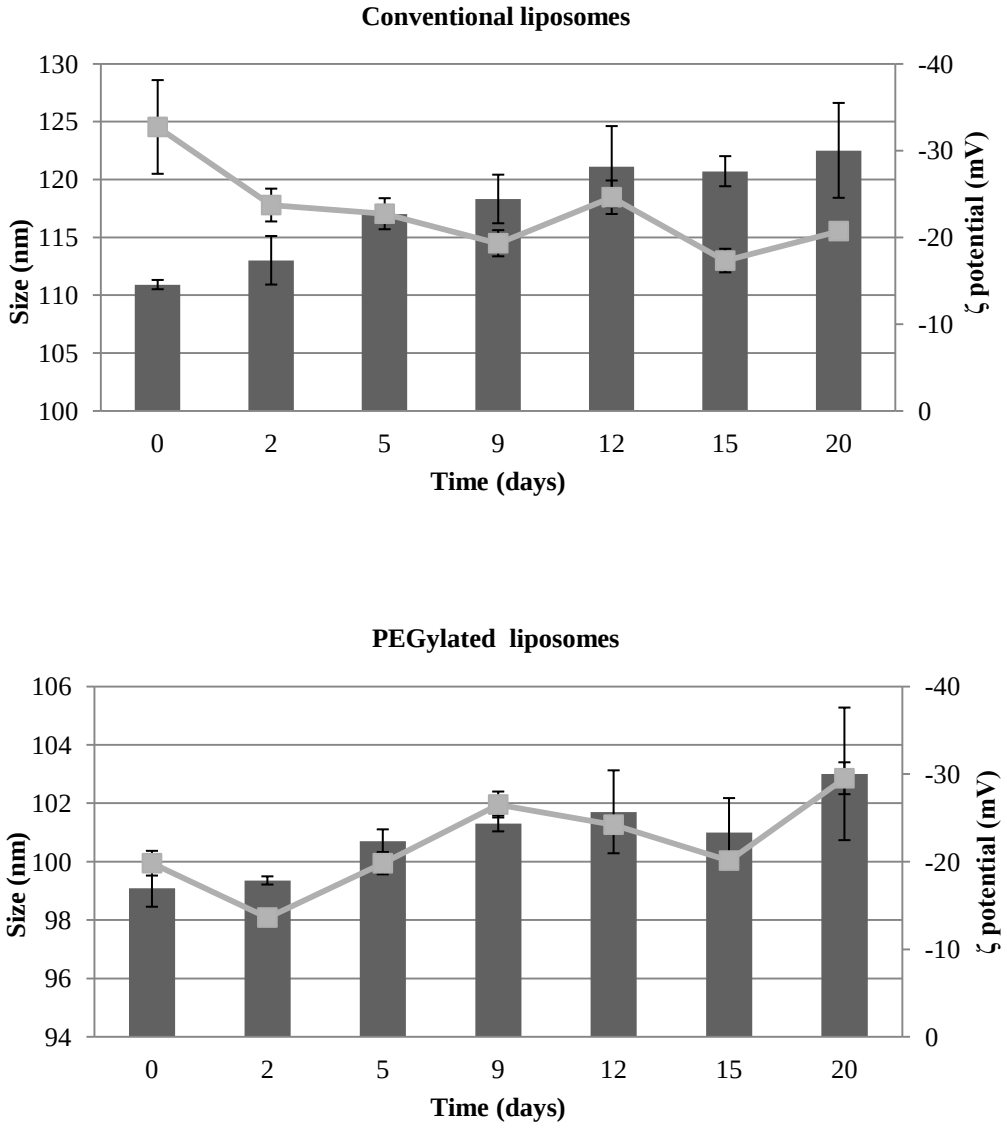

***Figure 2**: Particle size and zeta potential evolution of conventional DHA-liposomes and PEGylated DHA-liposomes at storage conditions (20 days, 4°C). (Mean ± S.D.; n=3).*

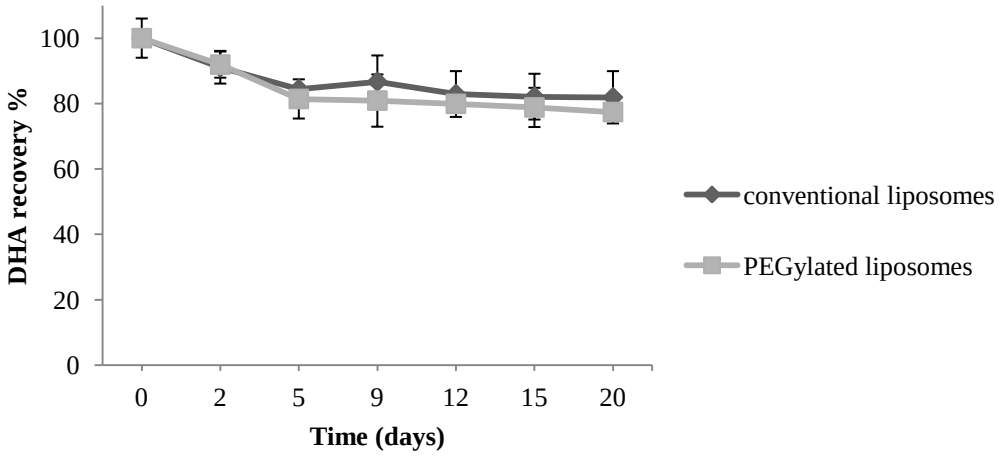

Figure 3: *Chemical stability of conventional and PEGylated DHA liposomes in terms of DHA content (Mean ± S.D; n=3).*

4.3.3 Characterization of fluorescent liposomes

Liposomes were prepared as previously described and NBD-PE (1 mol%) was added during lipidic film preparation; the resulting liposomes, containing NBD-PE only in the outer monolayer, were fully characterized as reported in Table 5. The fluorescent probe with lipophilic characteristics was efficiently encapsulated (80-85%) without altering the original structure of liposomes. Size of conventional and stealth DHA-fluorescent liposomes were slightly higher than DHA-liposomes but in any case under 200 nm; this fact could be related to the presence of both compound (DHA and NBD-PE) in the bilayer. Fluorescent liposomes obtained were used to investigate cellular uptake and stability in presence of albumin.

Formulation	Size (nm)	P.I.	ζ potential (mV)	Encapsulation efficiency (%)
L-C-DHA-F	198±2	0.35	-13.4±5	85±2.3
L-P-DHA-F	116±5	0.24	-12.4±1	80±5.2

Table 5: *Size, polydispersity index (P.I.), ζ-potential and encapsulation efficiency of L-C-DHA-F: dihydroartemisinin-loaded fluorescent conventional liposomes and L-P-DHA-F: dihydroartemisinin-loaded fluorescent PEGylated liposomes. Data were shown as mean ± S.D. (n=3).*

4.3.4 Cell uptake of conventional and PEGylated liposomes

Fluorescence microscopy study allowed evaluating the intracellular fate of liposomes themselves and of their encapsulated material as a function of time and in various cell lines. Fluorescence microscopy is frequently associated with Fluorescence Activated Cell Sorting (FACS) to provide

quantitative results related to the uptake of nanocarriers in cells. FACS produces simultaneously multiple optical measurements on individual cells at high rates. Herein, FACS study was conducted on MCF-7 cell lines to compare the internalization of conventional and stealth liposomes.

I) Fluorescence microscopy: Fluorescence microscopy showed that the dye localization inside the cell was in the cytoplasm without staining the nucleus (Figure 4). Moreover we can observe a stronger localization in the case of conventional liposomes. Although the application of PEG molecules has provided enhanced stability and relatively long circulation time for improved therapeutic effects, the steric hindrance of PEG molecules interfered with the cellular uptake of the drug systems (Raucher, 2001).

II) Flow cytometry analysis: To investigate the cellular uptake of prepared liposomes and to confirm results obtained by fluorescence microscopy, we measured fluorescence levels accumulated in MCF-7 cells by using flow cytometry. Each group was treated respectively with conventional and stealth fluorescent liposomes for 1 hour. As shown in Figure 5 the mean fluorescence intensity from conventional liposomes was 7.5 fold higher than that of stealth liposomes. Data confirm the possibility that hydrophilic steric barrier of PEG molecules reduce cellular uptake and the reduction of the cell-repellent property in conventional liposomes may have induced the affinity to cells, thereby resulting in higher cellular uptake (Raucher, 2001).

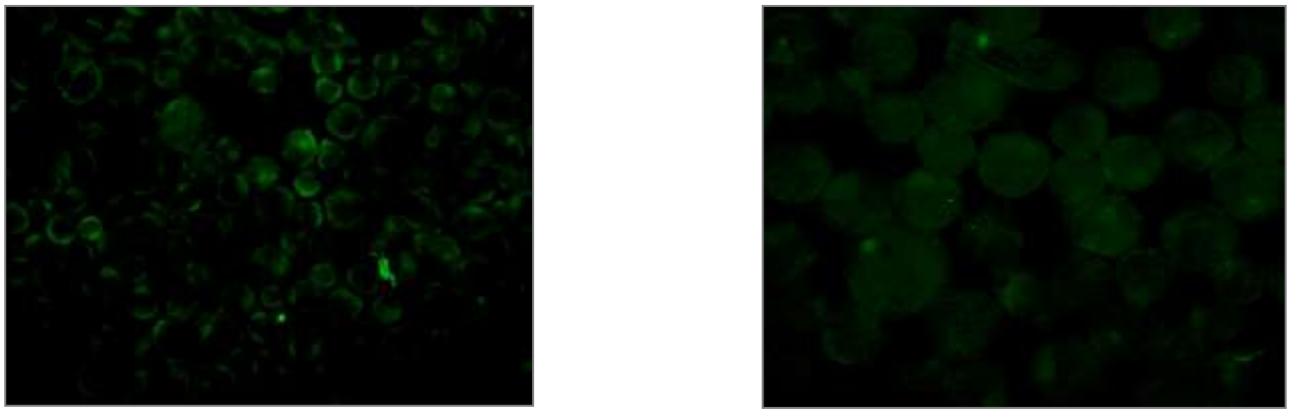

Figure 4: *Fluorescence microscopy image of MCF7 cells treated with fluorescent liposomes after 1h of incubation. On the left, the image corresponds to cells treated with fluorescent conventional liposomes. On the right the image corresponds to cells treated with fluorescent stealth liposomes.*

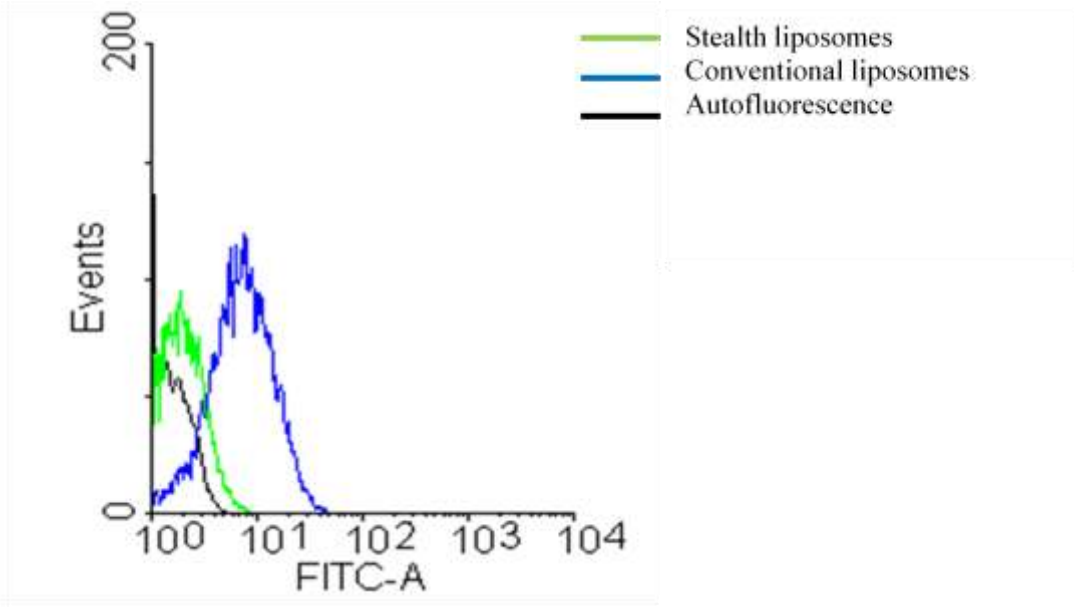

Figure 5: *Cellular uptake of liposomes detected by a flow cytometry assay: (black) control, (blue) conventional liposomes, (green) PEG-liposomes. The control corresponds to cells incubated in culture media without liposomes. Cells incubated with conventional or stealth empty liposomes showed values of fluorescence comparable with autofluorescence (data not showed).*

4.3.5 Stability in presence of albumin

4.3.5.1 Flow cytometry for rapid size determination

One of the essential quality parameters of liposome formulations is the mean size and size distribution of liposome vesicles. In particular, applications in therapeutic treatment and *in vivo* diagnostics require safe and well-defined products. The specification of liposome size ranges is therefore important. Methods currently available to measure particle size do not allow reliable measurements in the presence of small particulate contaminations present in biological fluids (e.g. serum) (Hsu, 2008). Serum is a complex fluid containing (among other) serum albumin, lipoproteins (HDL & LDL), immuno-, γ- and macrogobulins, and oleic acid. This heterogeneous nature can give rise to significant background signals, whereas sizing techniques based on conventional light scattering require minimum levels of background noise for generation of accurate results. With imaging techniques such as electron microscopy and atomic force microscopy individual particles can be studied, however, these techniques are laborious and have poor statistical power. Imaging is particularly valuable to obtain information regarding particle morphology, but the risk of artefacts must be taken into account. In this case we have used a method already reported (Gaal, 2009) based on flow cytometry that allows high-resolution size distribution analysis directly in biological in the submicron range. Flow cytometry is a well established technique that integrates light scattering and fluorescence measurements to gather information regarding size, shape, morphology of cells and presence and intensity of diverse fluorescent signals (indicative of molecular expression based on immunocytochemistry). Flow cytometry was originally developed as a tool to study cells, which have typical sizes of 2–120 μm (with a majority being 10–20 μm).

Recently this technique was exploited to study submicron matter, including unilamellar synthetic vesicles (Fuller, 1996), liposomes (Vorauer-Uhl, 2000) and viral particles (Hercher, 1979; Steen, 2004). Each single particle is measured in a continuous flow system, which is in contrast to the well-established light scattering systems, where a suspension is measured in a closed containment. By FACS, the detection of particles may be performed at an angle of 10° forward scatter and at 90° side scatter (Vorauer-Uhl, 2000). For a representative measurement, 10000 particles per sample were analyzed (Vorauer-Uhl K, 2000).

4.3.5.2 Calculation of the size ranges

The correlation between mean diameter of the latex beads and their side scatter signals was determined according to equation $y = a+bx^c$. Based on this equation, the side scatter signals of different samples may be classified in several relative size ranges to allow for better comparability between different samples. The results are represented either in frequency curves or in histogram form.

4.3.5.3 Size determination of nanoparticles with flow cytometry

First, we examined whether side scattering (SSC) values measured by flow cytometry could be correlated to sizes within the range of 100–1000 nm using fluorescently labelled polystyrene beads of distinct sizes. Sizes of the beads used for calibration were analyzed by Dynamic Light Scattering as shown in Table 6.

Beads (nm)	***Experimental beads values***	
	Size (nm)	**P.I.**
100	99.98±1.6	0.025±0.012
200	185±0.8	0.099±0.020
500	518±8.2	0.078±0.039
700	748±20	0.038±0.004
1000	1038±18	0.123±0.008

Table 6: *Diameters of fluorescein-labelled calibration beads as determined by dynamic light scattering (100–1000 nm).*

In the case of flow cytometry, scattering intensities detected at 90° were recorded for each batch of the calibration beads. Flow cytometry parameter settings were adjusted such that background noise is negligible and detected fluorescence and SSC are within scale. Flow speed and dilution of beads were adjusted until <2000 events/s and they were recorded in order to prevent coincidence (simultaneous detection of >1 particle). Geometric mean of SSC-H values and diameters were plotted and a calibration curve was fitted according to the equation (1) (Vorauer-Uhl, 2000):

$y = a+bx^c$ (1)

resulting in an R^2=0.9706 (Figure 6 B). As a second step we applied the method to a conventional liposome sample labeled with the fluorescent probe NBD-PE. Conversion of the geometric mean of SSC-H (that had a value of 125) to size using equation (1) gives an average diameter of 234 nm comparable with Z-average found by DLS (198±2 nm).

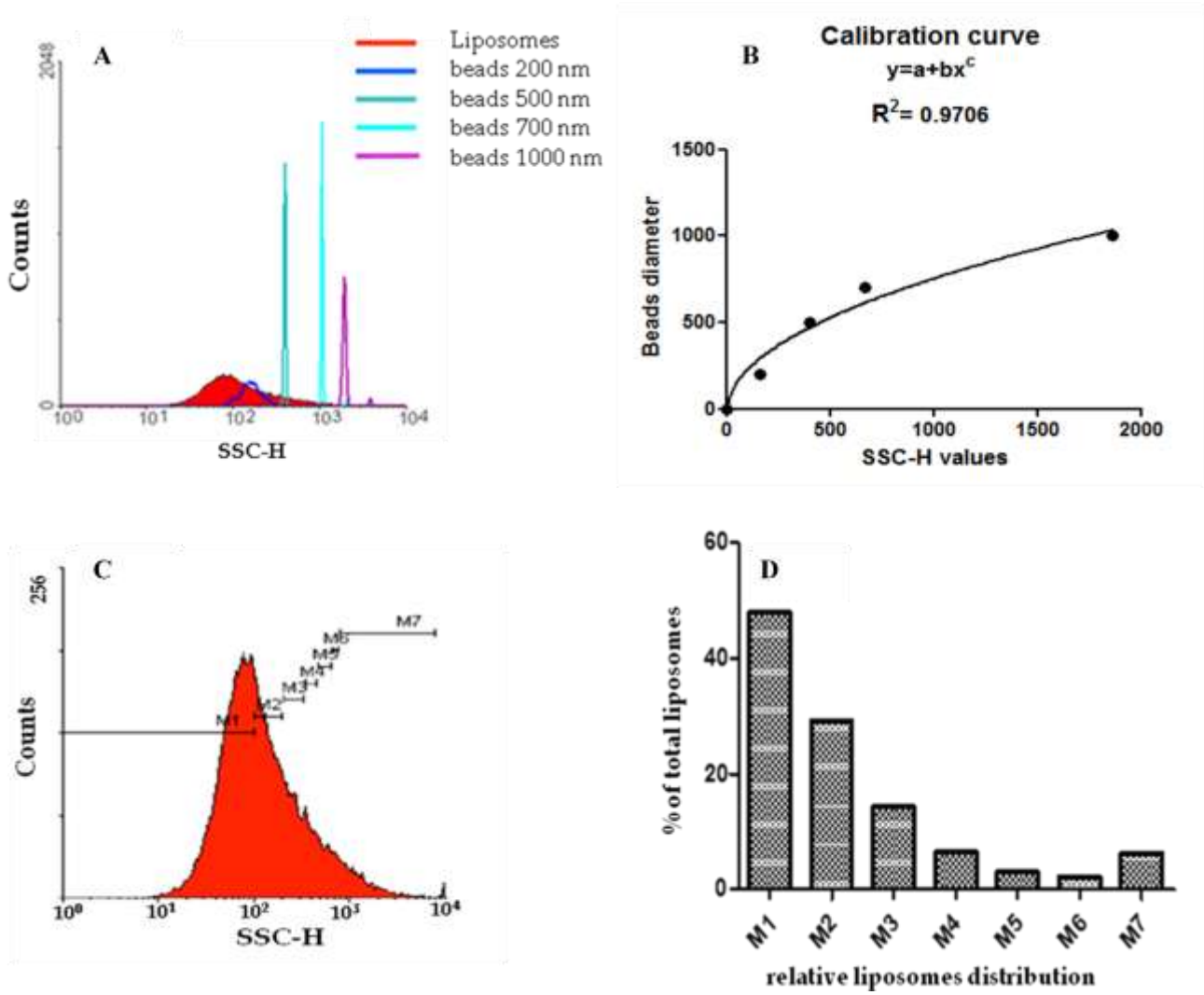

***Figure 6**: Determination of liposome distribution by FCM. Histograms of the side scatter values of the five chosen calibration bead classes. Latex beads (100–1000 nm) **(A)**. By correlating the geometric mean side scatter values with the corresponding standard beads, the calibration curve with the equation $y = a+bx^c$ (a=20.32; b=25.56; c=0.4940) **(B)**. To estimate the size distribution of a real liposome sample, the recorded side scatter values are subdivided into several size classes **(C)**. The calculated percentage distribution is illustrated in histogram form **(D)**.*

Figure 6 C shows the side scatter histogram of our liposome suspension. By subdividing the bead side scatter values into several size classes, according to Table 7, corresponding with the calibrated size ranges, the distribution of a liposome suspension may be described. The percentage of liposomes can be calculated for each class, as shown in Figure 7 D. Calculation based on defined classes was used when dealing with polydisperse liposome suspensions because gives a more

realistic image of the actual distribution. Characterizing vesicle populations by relative size classes was in good agreement with the result obtained by FACS as described in Table 7. In the case of homogeneous narrow distributed vesicle populations, a mean diameter is calculated only based on the geometric mean of the side scatter signal. The method used can be applied with liposomal formulations and it is valid within the nanoscale range, with a lower limit around 100 nm. Below this size, calibration is complicated due to insufficient sensitivity of the SSC detectors currently used in flow cytometry equipment. An important advantage of the method here presented compared to existing nanoparticle sizing methods such as dynamic light scattering is the potential to measure nanoscale particles in the presence of other particulate, matter which is often present in biological fluids. By adding fluorescence intensity as an inclusion criterion, this method can easily distinguish particles of interest from equally sized background noise. A disadvantage of introducing fluorescence measurements in particle size determination is the inherent requirement for sample labeling in fact the presence of fluorescence labels may influence particle characteristics. In our case fluorescent liposomes showed similar characteristics to conventional or stealth DHA liposomes so the effect of the fluorescent label is expected to be small. In conclusion flow cytometry can be used as alternative technique for size distribution evaluation of liposomes.

Size classes	SSC-H values	Mean diameter (nm)	Liposomes distribution by FACS (%)	Liposomes distribution by DLS (%)
M1	≤100	≤233	48.77	45.8
M2	100-200	233-334	25.31	24.9
M3	200-350	334-449	10.87	7.5
M4	350-500	449-528	4.80	6.5
M5	500-650	528-606	4.02	5.3
M6	650-800	606-679	1.70	4.1
M7	>800	>679	5.70	5.8

Table 7: *Percentage distribution of conventional fluorescent liposomes obtained by FACS and by DLS.*

4.3.5.4 Stability studies in presence of albumin

The stability of the liposomal formulations in presence of blood protein (albumin at physiological concentration) was evaluated by FACS analysis using fluorescent liposomes. Liposomes were labelled with NBD-PE 1% mol and the incubation with albumin was monitored at different time points measuring number of fluorescent events by FACS analysis. This kind of fluorescent label is lipophilic and it forms the bilayer together with the other lipid so we expected a decreasing of fluorescent events during 30 seconds if the vesicles were disrupted due to the interaction with

albumin. Number of events analyzed by flow cytometer doesn't decrease in time, it confirm that vesicles remain stable and intact also in presence of albumin in both formulation (Figure 7). This result was expected for stealth liposomes but not for the conventional formulation. Presence of DHA in the lipidic bilayer could stabilize vescicles.

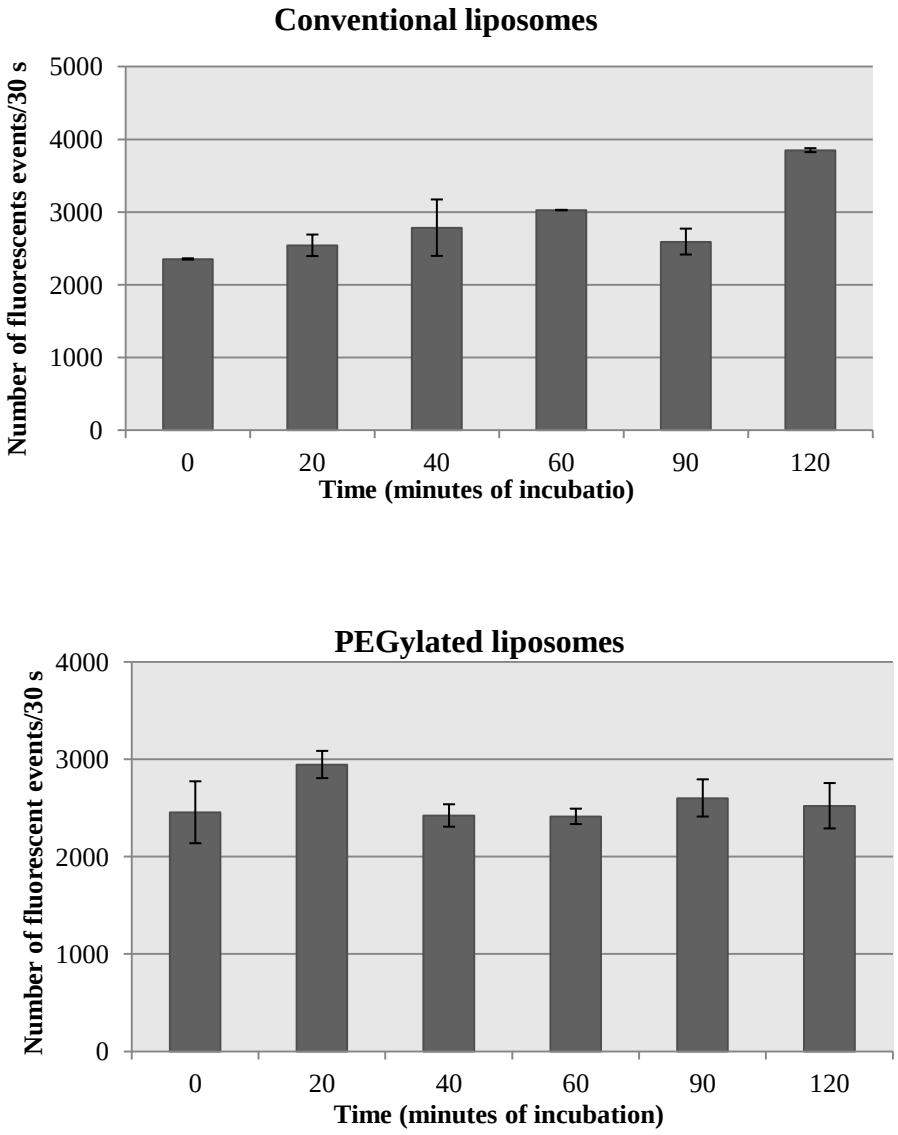

Figure 7: *Number of fluorescent events registered by flow cytometer for conventional and PEGylated liposomes after 2 hours of incubation with albumin.*

4.3.5.5 Evaluation of size in presence of albumin

The dot plots represent the SCC-A (indicative of size) against FITC-A (fluorescence intensity of the particles). The size of conventional and stealth DHA liposomes are respectively around 200 and 100 nm, according with the DLS measurements. Size is not affected in presence of albumin. The vesicles remain stable and intact for 2 hours. Conversion of the geometric mean of SSC-H (that had

a value of 125 for conventional liposomes and 19.86 for stealth liposomes) to size using equation (1) gives an average diameter of 234 nm and 93 nm respectively for conventional and stealth liposomes.

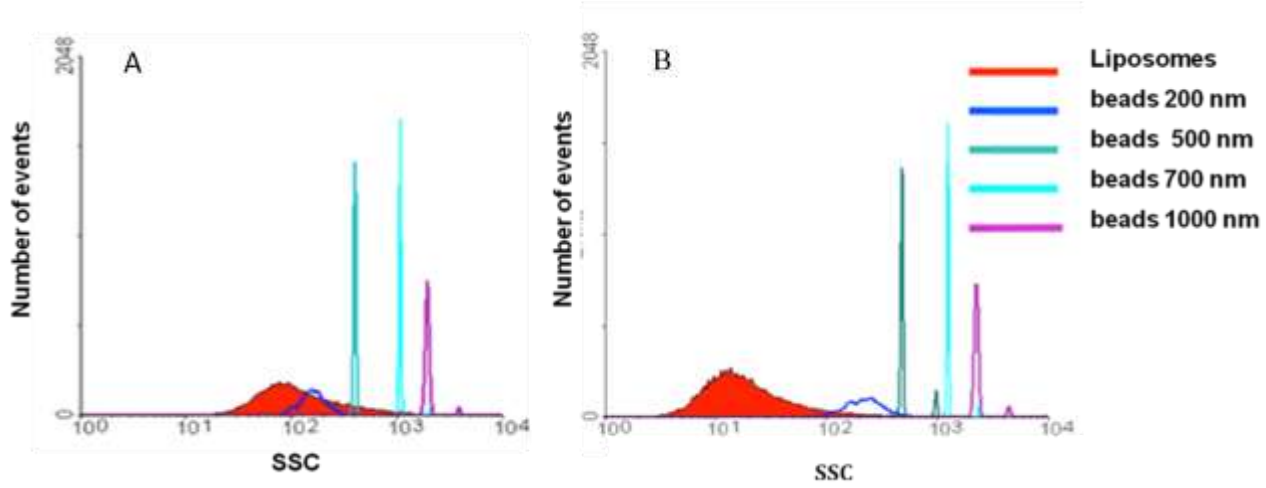

Figure 8: *SSC signals of conventional* ***(A)*** *and PEGylated* ***(B)*** *fluorescents liposomes, after incubation with albumin, overlapped to the signal of fluorescents beads.*

4.3.6 Cytotoxicity of DHA conventional and stealth liposomes

The cytotoxicity of DHA and its relative liposomal formulations was measured in the breast cancer cell line MCF-7. Unloaded liposomes were evaluated as well to ensure the absence of toxicity of the empty vehicle. As shown in Figure 9, they don't exhibit toxicity since more than 90% of cell viability was measured for all cell lines after 72 h exposure even at the highest concentration. Encapsulated DHA was less efficient than free DHA for both formulations but conventional liposomes showed higher toxicity (1,6-fold drop in IC_{50}) to that of stealth liposomes. The higher cytotoxicity of conventional liposomes (IC_{50}=48.2 μM) compared with stealth liposomes (IC_{50}= 77 μM) is consistent with the notion that pegylated liposomes might not interact directly with the tumor cells (Figure 10; Table 8).

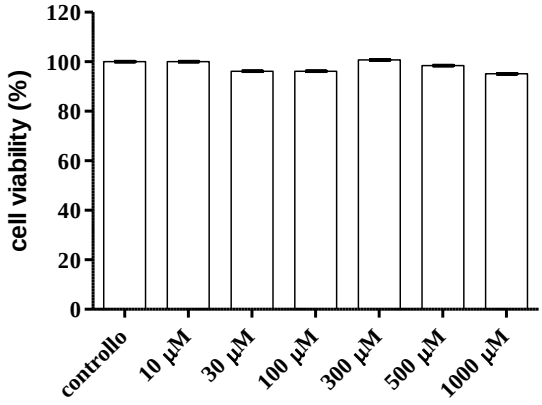

Figure 9: *Cell viability data from sulforhodamine B cytotoxicity assay to evaluate potential cytotoxic effects of empty liposomes in MCF-7 cancer cell line. After 72 h, no toxic effect of empty liposomes was evident.*

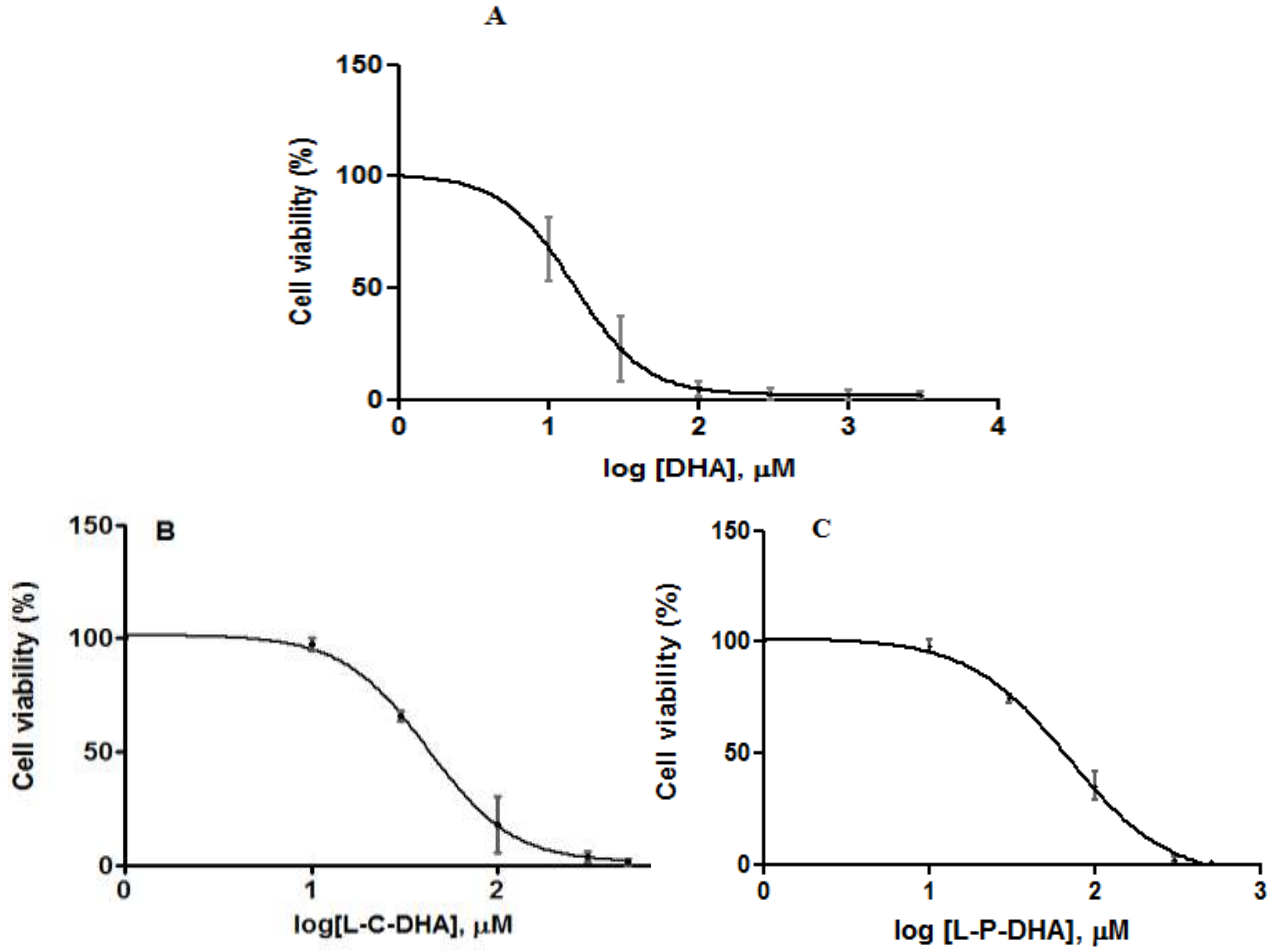

Figure 10: *In vitro cytotoxicity of* ***(A)*** *free DHA,* ***(B)*** *dihydroartemisinin-loaded conventional liposomes and* ***(C)*** *dihydroartemisinin-loaded PEGylated liposomes on MCF-7 breast cancer cells as a function of log (drug concentration). Data are expressed as percentage of cellular viability as evaluated by sulforhodamine B test. Results are the mean of three different experiments ±standard deviation.*

Samples	IC_{50} (μM)
DHA	12.1±0.6
L-C-DHA	48.2±7.5
L-P-DHA	77±7

***Table 8**: Free and encapsulated DHA antiproliferative activities. IC_{50} (mean of three separate experiments±SD) was defined as the drug concentration that inhibits cell growth by 50% compared to untreated cells. Values represent data extrapolated from curves A, B and C (Figure 10).*

Although it is difficult to extrapolate from *in vitro* data *in vivo* results for a therapeutic success, it is expected that this liposomal formulations could be of clinical interest. It is important to note that liposomal DHA and free DHA have very difference kinetic properties, both in terms of *in vitro* cellular uptake, which is diffusion driven for free drug and enocytosis/fusion for liposomes, both *in vivo* plasma residence time, which is determined by the mechanism of clearance. Due to this differences, direct comparison of IC_{50} values for liposomal DHA and free DHA using equal exposure time in a cytotoxicity assay is not always realistic, since the comparison would have no relevance to *in vivo* therapeutic efficacy. In our case for example free DHA was the most efficient in breast cancer cell line, but since this compound has been reported to be rapidly metabolized *in vivo* following i.v. injection, the advantage of DHA-liposomes results from the preserved biological activity of the encapsulated drug. However, it is possible to carry out *in vitro* comparisons among the various liposomal formulations. In this case our data suggest that the mechanism of cellular entry is an important determinant for cytotoxicity; for PEGylated liposomes the low cytotoxicity on MCF-7 cells could be attributed to low cellular uptake for the presence of the hydrophilic steric barrier of PEG molecules that reduce the process of endocytosis.

4.3.7 Time course experiments

The cytotoxicity of DHA and its relative liposomal formulations was evaluated during a time course experiment in the same cell line MCF-7. We can observe that IC_{50} values of free drug are constant during all the time considering that the permeation is driven by diffusion and it is complete after the first hours of incubation. In conventional and PEGylated liposomes we can observe higher IC_{50} values after 24 hours of incubation and a decrease of IC_{50} values after 48 hours of incubation. The results confirm that after cellular uptake the release from vescicles is a modified release during time.

TIME (h)	DHA IC_{50} (µM)	L-C-DHAIC5_{50} (µM)	L-P-DHAIC_{50} (µM)
24	19.1±0.3	96.4±3.3	155.1±7.1
48	16.2±5.2	56.0±-0.5	59.8±5.1
72	12.1±0.6	48.2±7.5	77±7
96	14.1±1.6	45.0±1.0	81.1±3.4
120	14.4±0.0	50.7± 47.7	85.4±7.6

Table 9*: Free and encapsulated DHA antiproliferative activities evaluate during time (24-120 hours). Mean of three separate experiments ± SD.*

4.4 CONCLUSIONS

The two liposome formulations developed represent a successful attempt to incorporate dihydroartemisinin in liposomes. They have proper physical characteristics as drug carrier for parental administration in terms of particle size, polydispersity, encapsulation efficacy and ζ-potential. Liposomes provide an appropriate solvent for the drugs and because of their well known biocompatibility and tolerability (Allen, 1991) can overcome toxic and irritating effects of standard DHA vehicles like DMSO sometimes used for i.p. or i.v. administration in animal models. Liposome provide also stabilising system for their storage, during a substancial time after production, and in presence of blood protein. Finally, the preliminary results obtained with liposomal formulations encourage further evaluation of their antitumor activity in appropriate animal models. In fact DHA was confirmed to be a compound cytotoxic in cancerous cells and could be considered as a molecule of interest *in vivo* thank to an appropriate delivery system able to protect the drug from its fast metabolism occurring after i.v. administration (half life 45 minutes). Moreover, such a delivery system should lead to a decrease of the administered doses and to diminish their frequency, while preserving DHA antitumor activity.

4.5 REFERENCES

Aggarwal P., et al., Nanoparticle interaction with plasma proteins as it relates to particle biodistribution, biocompatibility and therapeutic efficacy. Advanced Drug Delivery Reviews. 2009, 61: 428-437.

Allen T.M., et al., Liposomes containing synthetic lipid derivatives of poly(ethylene glycol) show prolonged circulation half-lives in vivo. Biochimica et Biophysica Acta (BBA)-Biomembranes. 1991, 1066, 1: 29–36.

Bangham AD., et al., Diffusion of univalent ions across the lamellae of swollen phospholipids. J. Mol. Biol. 1965, 13: 238-252.

Bansal T., et al., Solid self-nanoemulsifying delivery systems as a platform technology for formulation of poorly soluble drugs. Crit Rev Ther Drug Carrier Syst 2008, 25:63–116.

Batty KT., et al., Selective highperformance liquid chromatographic determination of artesunate and α- and β dihydroartemisinin in patients with falciparum malaria. Journal of Chromatography 1996, B 677: 345–350.

Cattel et al., From conventional to stealth liposomes. A new frontier in cancer chemotherapy. Tumori 2003, 89: 237-249.

Chen Y., et al., Selfmicroemulsifying drug delivery system (SMEDDS) of vinpocetine: formulation development and in vivo assessment. Biol Pharm Bull 2008, 31:118–125.

Chonn A., et al., Association of blood proteins with large unilamellar liposomes in vivo: Relation to circulation lifetimes. J Biol Chem 1992, 267:18759–18765.

Colm M., et al., Effect of artemisinin derivatives on apoptosis and cell cycle in prostate cancer cells. Anticancer Drugs 2010, 21: 423–432.

Drummond S., et al., Temporal differences in the appearance of NEP-B78 and an LBR-like protein during Xenopus nuclear envelope reassembly reflect the ordered recruitment of functionally discrete vesicle types. J. Cell Biol 1999, 144: 225-240.

Efferth T., et al., Activity of drugs from traditional Chinese medicine towards sensitive and MDRI- or MRPI-overexpressing multidrug-resistant human CCRF-CEM leukemia cells. Blood Cells Mol. Dis. 2002, 28: 160–168.

Fahr A., et al., Drug delivery strategies for poorly water-soluble drugs. Expert Opin Drug Deliv 2007, 4:403–416.

Fuller R., et al., Characterizing submicron vesicles with wavelength resolved fluorescence in flow cytometry. Cytometry 1996, 25: 144–155.

Gaal et al., Flow cytometry for rapid size determination and sorting of nucleic acid containing nanoparticles in biological fluids. J Control Release. 2010, 141(3):11.

Gabizon A., et al., The role of surface charge and hydrophilic groups on liposome clearance in vivo. Biochim. Biophys. Acta. 1992, 1103: 94 –100.

Gabriëls M., et al., Design of a dissolution system for the evaluation of the release rate characteristics of artemether and dihydroartemisinin from tablets. International Journal of Pharmaceutics 2004, 274: 245–260.

Garcia-Fuentes M., et al., Application of NMR Spectroscopy to the Characterization of PEG-Stabilized Lipid Nanoparticles. Langmuir, 2004. 20(20): 8839-8845.

Goppert et al., Adsorption kinetics of plasma proteins on solid lipid nanoparticles for drug targeting. Int J Pharm, 2005, 302: 172–86.

Hanafy A., et al., Pharmacokinetic evaluation of oral fenofibrate nanosuspensions and SLN in comparison to conventional suspensions of micronized drug. Adv Drug Deliv Rev 2007, 59:419–426.

Harvey RD., et al., The effect of electrolyte on the encapsulation efficiency of vesicles formed by the nonionic surfactant, 2C18E12. J Colloid Interface Sci 2007, 315:648–661.

Hercher M., et al., Detection and discrimination of individual viruses by flow cytometry. J. Histochem. Cytochem. 1979, 27: 350–352.

Hoekstra D., et al., Biochim. Biophys. Acta. 1979, 551: 109–121.

Hong R.l.,et al., Phase I and pharmacokinetic study of a stable, polyethylene-glycolated liposomal doxorubicin in patients with solid tumors: the relation between pharmacokinetic property and toxicity. Cancer. 2001, 91: 1826–33.

Hsu Y., et al., Effects of size and topology of DNA molecules on intracellular delivery with non-viral gene carriers. BMC Biotechnol. 2008, 8, 23.

Isacchi et al., Artemisinin and artemisini plus curcumin liposomal formulation: enhanced antimalarial efficacy against Plasmodium berghei-infected mice. Europ J Pharm 2012, 80 (3): 528-534.

Jeon S.I., et al., Protein surface interactions in the presence of polyethylene oxide. 1. Simplified theory. J. Colloid Interface Sci. 1991, 142: 149–158.

Juliano R., et al., Synergistic effects of a membrane protein (spectrin) and Ca2+ on the permeability of phospholipid vesicles. Biochim. Biophys. Acta 1971, 241: 894—905.

Kim SJ., et al., Dihydroartemisinin enhances radiosensitivity of human glioma cells in vitro. Cancer. Res. Clin. Oncol. 2006, 132: 129–135.

Klayman DL., et al., Qinghaosu (artemisinin): an antimalarial drug from china. Science 1985, 228: 1049–1055.

Law S., et al., The electrokinetic behavior of liposomes adsorbed with bovine serum albumin. Int. J. Pharm. 1988, 43: 257–260.

Li G., et al., Pharmacokinetics and bioavailability of dihydroartemisinin, arteether, artemether, artesunic acid and artelinic acid in rats. Journal of Pharmacy and Pharmacology 1998, 50: 173–182.

Lipinski CA., et al., Experimental and computational approaches to estimate solubility and permeability in drug discovery and development settings. Adv Drug Deliv Rev 2001, 46:3–26.

Lis L.J., et al., Biochim. Biophys. Acta. 1976, 436: 513–522.

Lu Y., et al., Dihydroartemisinin (DHA) induces caspase-3-dependent apoptosis in human lung denocarcinoma ASTC a-1 cells, J. Biomed. Sci. 2009, 16: 1–15.

Michnik A., et al., Destabilisation of liposomes by bovine serum albumin; Sepharose 2B-Cl experiment. Chromatographia. 1997, 45: 155 – 157.

Moghimi S., et al., Enhanced hepatic clearance of intravenously administered sterically stabilized microspheres in zymosan-stimulated rats. J Leukoc Biol 1993, 54:513–517.

Ogawara K., et al., Pre-coating with serum albumin reduces receptor-mediated hep- atic disposition of polystyrene nanosphere: implications for rational design of nanoparticles. J. Control. Release 2004, 100: 451–455.

Oku N., et al., Long-circulating liposomes. Crit Rev Ther Drug Carrier Syst.1994, 11: 231–70.

Owens D., et al., Opsonization, biodistribution, and pharmacokinetics of polymeric nanoparticles. Int. J. Pharm. 2006, 307: 93–102.

Panagi Z., et al., In vitro binding of HSA, IgG, and HDL on liposomes of different composition and its correlation with the BLOOD/RES ratio of liposomes. International Journal of Pharmaceutics 1999, 176: 203-207.

Pastorino F., et al., Vascular damage and anti-angiogenic effects of tumor vessel-targeted liposomal chemotherapy. Cancer Res 2003, 63:7400–7409.

Raucher et al., Enhanced uptake of a thermally responsive polypeptide by tumor cells in response to its hyperthermia-mediated phase transition. Cancer Res. 2001, 61(19):7163-70.

Sabín J., et al., Interactions between DMPC Liposomes and the Serum Blood Proteins HSA and IgG. J. Phys. Chem. B. 2009, 113: 1655–1661.

Skehan P., et al., New colorimetric cytotoxicity assay for anticancer-drug screening. J Natl Cancer Inst 1990, 82:1107– 1112.

Steen HB., et al., Flow cytometer for measurement of the light scattering of viral and other submicroscopic particles. Cytometry A 2004, 57: 94–99.

Sweet C., et al., Biochim. Biophys. Acta. 1969, 173: 94–103.

Sweet C., et al., Biochim. Biophys. Acta.1960, 219: 253.

Vorauer-Uhl K., et al., Determination of liposome size distribution by flow cytometry. Cytometry 2000, 38: 166–171.

Woodle M.C., et al., Sterically stabilized liposomes: physical and biological properties. J Drug Target 2. 1994. 397–403.

Ye J., et al., Injectable actarit-loaded solid lipid nanoparticles as passive targeting therapeutic agents for rheumatoid arthritis. Int J Pharm 2008, 352:273–279.

Zborowski J., et al., Biochim. Biophys. Acta. 1977, 497: 183.

CONCLUSIONS

CONCLUSIONS

The study developed demonstrated the usefulness of nanoparticulate technology to enhance the therapeutic effectiveness of natural and semi-synthetic compounds.

Curcumin loaded solid lipid nanoparticles have been developed by homogenization and ultrasound technique; they showed good features for oral administration with size around 200 nm and mean encapsulation efficiency values of 80%. Parallel artificial membrane permeability assay (PAMPA) showed a considerable increasing in curcumin permeation by SLNs. SLNs offer a promising delivery system for enhancing the oral absorption of poorly soluble drugs like curcumin.

Two different polymeric nanocapsules were developed avoiding use of lecithin as surfactant; they showed good characteristics for parenteral delivery of docetaxel: have nanometric size (about 200 nm), low polydispersity and good values of zeta potential. Formulations selected showed good stability in phosphate buffer and in cell culture medium and preliminary cellular uptake studies support nanocapsules internalization. Nanocapsules developed showed positive features for further *in vitro* and *in vivo investigations.*

Conventional and PEGylated liposomes represented a successful attempt to delivery of dihydroartemisinin. They have proper physical characteristics as drug carrier for parental administration in terms of particle size, polydispersity, encapsulation efficacy and ζ-potential. Liposomes provide an appropriate solvent for the drugs and a stabilising system for their storage and in presence of blood protein. Results obtained with liposomal formulations encourage further evaluation of their antitumor activity in appropriate animal models.

ANNEX I

Different separation methods of polymethoxylated flavonoids and artemisinin from *Artemisia annua* L. acetone extract and development of artemisinin liposomes for active targeting

This work was carried out in collaboration with PATRICIA TIMOTEO[1], GIORGIA ROS[1], CRISTIAAN WESSELS[1]

[1]*Department of Pharmaceutical Sciences, University of Florence, Florence, Italy.*

1. INTRODUCTION

Artemisia annua L. (Asteraceae) is an annual herbaceous plant well known in the traditional Chinese medicine, used as a remedy for chills and fevers for over 2000 years. *A.annua* is the only (commercial) source of the sesquiterpene lactone artemisinin. It also contains characteristic compounds such as: flavonoids, coumarins, triterpenoids, steroids, phenolics, purines, lipids and aliphatic compounds and monoterpenoids from different plant parts (Bhakuni, 2001). Polymethoxyflavonoids and artemisinin are among the most promising natural products for antimalarial and anticancer purposes.

Artemisinin has been an effective drug against malaria, even against the chloroquine and quinine-resistant *Plasmodium falciparum*. More recent studies have shown that artemisinin has a positive effect against tumor growth of several types of tumors, including: breast cancer, human leukemia, colon cancer, and small–cell lung carcinomas (Efferth, 2001). It contains an endoperoxide group that reacts with ferrous iron Fe^{2+}, to generate short lived radical species, which are linked to its antiparasitic and anticancer activity. Although synthesis of artemisinin is possible, it is not a reliable source for production due to the low yields and high production costs because of its complex structure. Therefore extraction from the plant remains the most economical and reliable resource (Baraldi, 2008).

Other studies have show that the efficacy of the *A. annua* plant itself derives from a synergistic effect and that it is a combination of constituents in the plant which can produce the total antiplasmodial and anticancer activity. Several polymethoxylated flavonoids, such as: artemetin, the constitutional isomers casticin and chrysosplenetin, chrysosplenol-D and cirsilineol may contribute to the *in vitro* activity of artemisinin (Elford, 1987; Liu, 1992; Phillipson, 1999). Flavonoids can serve as artemisinin's synergists by reacting with iron and converting Fe^{3+} to Fe^{2+} (Tsao, 2004), which is important in the bioactivity of artemisinin leading to the release of short-lived toxic free radicals that may be part of its antimalarial and anticancer mode of action (Efferth, 2004). By combining antioxidant flavonoids, tannins, phenolic acids, and coumarins with artemisinin to treat malaria and cancer, as well as to prevent the latter, could be an interesting consideration for prophylactic or therapeutic reasons (Ferreira, 2010). On the other hand, it has been reported that flavonoids themselves can prevent DNA mutation that can appear in oncogenes or tumor suppressor genes. Thereby preventing cancer initiation or progression (Nijveldt, 2001). The modes of action of flavonoids for anticancer activity vary considerably on different cell lines. Mostly having an inhibitory effect on cell growth, proliferation and signal transduction by inhibiting various kinase proteins or inducing apoptosis and arresting the cell cycle (Ferreira, 2010).

The first part of our work was focused on artemisinin and polymethoxylated flavonoids isolation from *Artemisia annua* L. acetone extract with the comparison of three separation methods: Sephadex LH-20, silica gel column chromatography and flash chromatography.

In the second part of the work preliminary results about development and characterization of transferrin (Tf) conjugated liposomes for artemisinin delivery to cancer cells are reported. The

knowledge of Tf-Receptor-over-expression in tumour tissues had led to a focused targeting of Tf-R in anticancer therapy (Maruyama, 1998) and subsequently to a number of small drugs (e.g. adriamycin) and colloidal carrier systems (e.g. liposomes and nanoparticles) linked to Tf (Wagner, 1994; Tros, 2002). Considering that the cytotoxic effect of artemisinin is specific to cancer cells, because Tf-receptors are highly expressed on the surfaces of tumour cells and iron content is higher than in normal cells (Moore, 1995; Efferth, 2004), the aim of our work was to develop a nanocarrier which can enhance the selectivity to tumour cells due to the presence of transferrin and enhance the activity of artemisinin by interaction with iron.

2. MATERIALS AND METHODS

2.1 Isolation

2.1.1 Plant material

A crude *Artemisia annua* L. acetone extract was kindly provided by Centro Tecnológico Agroalimentario Extremadura (CTAEX, Badajoz, Spain, 2006).

2.1.2 Chemicals

All the solvents used for extraction, chromatography methods and HPLC analysis (n-heptane, EtOAc, CH_2Cl_2, MeOH, EtOH, cyclohexane, acetone and CH_3CN) were HPLC grade, provided by Sigma Aldrich (Steinheim, Germany); formic acid 85% was provided by Carlo Elba (Milan, Italy). The water was purified by a Milli-Q_{plus} system (Milford, MA, USA). Different standards were used, in order to make the calibration curves: artemisinin standard (98% purity) (Sigma Aldrich, 07529BJ, Steinheim, Germany), casticin standard (99,7% purity) (MADAUS, Lot: 810715/F/MADAUS, Colone, Germany) narigenina (90% purity)(EXTRASYNTHESE, Lotto 97060217, 69730 Genay, France), scopoletin (99% purity) (SIGMA, Lotto: 37F02891, Steinheim, Germania). The chemicals used in the spray reagents: 2-Aminoethylborinate (Sigma Aldrich, D9754-25G, Steinheim, Germany) and polyethylene glycol 4000 (PEG 4000) (Sigma Aldrich, Steinheim, Germany) were used to reveal the TLC plates.

2.1.3 Liquid-liquid extraction

The *Artemisia annua* L. acetone extract (51.4 g) was dissolved in 500 mL of MeOH, and sonicated for 30 minutes, to create a homogenous solution, and defatted at room temperature with n-heptane (500 mL, three times). 500 mL of H_2O was added to the remaining MeOH phase and extracted with dichloromethane (DM) (1.0 L, three times). The same procedure was repeated using EtOAc instead of DM. All fractions were concentrated to complete dryness, using a rotary evaporator system.

2.1.4 Size exclusion chromatography

A separation was performed on Sephadex LH-20 (GE Healthcare Bio-Sciences, AB, Uppsala, Sweden). An amount of the dried DM fraction was re-suspended in MeOH and applied over Sephadex LH-20 (30 cm × 4.6 cm). Different elution systems were tested: MeOH (100%); MeOH: H_2O (90:10); EtOAc : MeOH (70:30) and MeOH:DM (50:50). The fractions were followed by TLC, HPLC-DAD-MS analyses and the fractions concerning the casticin/chrysosplenetin were analyzed by ^{1}H NMR for monitoring the separation of the pair of isomers.

2.1.5 Sample preparation for silica gel and flash chromatography

The extract (25 g) was suspended in 200 ml of acetone and mixed with 113.4 g of Silica gel 100 (Art. 10184, grain size 0.063 – 0.200 mm, 70 – 230 mesh ATM, Merck, Darmstadt, Germany). The acetone was then evaporated in order to form a dry powder and submitted to open column and flash chromatography.

2.1.6 Silica gel chromatography

The dry powder was applied on a normal phase silica gel column (30 cm x 4.6 cm), a mobile phase gradient was used, with solvent of increasing polarity: cyclohexane 100%, cyclohexane/DM (50:50, 30:70, 15:85, 5:95), DM 100%, DM/EtOAC (95:5, 90:10, 85:15, 75:25), in a volume of 280 ml. HPLC-DAD-MS analysis was performed to quantify and qualify the fractions and ^{1}H NMR analyses were done for monitoring the eventual separation of the isomers casticin and chrysosplenetin.

2.1.7 Flash chromatographic system

For a more rapid separation method, a flash chromatographic system was used. The Combi Flash system (Combi Flash® Rf, Teledyne ISCO Inc., St. Lincoln, NE, USA) was programmed with a method composed of two parts, both parts using a mobile phase with gradient of increasing polarity. **Part I** (artemisinin isolation): 5 min. 100% cyclohexane, 5 min. 50:50 cyclohexane/DM, 5 min. 30:70 cyclohexane/DM, 10 min. 100% DM. Flow rate: 15 ml/min. **Part II** (polymethoxylated flavonoids separation): 5 min 100% DM, 10 min. 5:95 EtAC/DM, 20 min. 10:90 EtAC/ CH_2Cl_2, 20 min. 15:85 EtAC/ CH_2Cl_2, 10 min. 25:75 EtAC/DM. Flow rate: 10 ml/min. The chromatography runs were carried out, using a prepacked Silica column stationary phase (RediSep Rf High performance GOLD, 24 gram HP Silica, Lot: 191316001W, Teledyne ISCO, St. Lincoln, NE, USA).

2.1.8 Thin layer chromatography

Thin layer chromatography (TLC) method was performed, for qualitative purpose, in order to follow the separation of the compounds in the fractions, after the preparative chromatography methods. Normal phase TLC plates (Silica gel 60 F_{254}, Merck, Darmstadt, Germany), a mobile phase of DM/MeOH (95:5) and a spray reagents, with a mixture of 1% 2-Aminoethylborinate in MeOH and 5% Polyethylglycol 4000 in EtOH were used to reveal the TLC plates.

2.1.9 HPLC-DAD-ESI-MS analysis

The HPLC-DAD-ESI-MS analyses were performed using a HP1100 Liquid Chromatograph system (Agilent Technologies, Palo Alto, CA, USA), equipped with a HP1040 diode-array Detector (DAD), automatic injector, auto sampler and a column oven, managed by a HP9000 workstation (Agilent Technologies, Palo Alto, CA, USA). The UV-Vis spectra were recorded between 200–600 nm. The HPLC system was interfaced with a HP1100 MSD API-electro spray (Agilent Technologies, Palo Alto, CA, USA). The interface geometry, with an orthogonal position of the nebulizer with respect to the capillary inlet, allowed the use of analytical conditions similar to those of HPLC-DAD analysis. Mass spectrometry operating conditions were optimized in order to achieve maximum sensitivity values: gas temperature 350 °C at a flow rate of 10 ml/min, nebulizer pressure of 30 psi, quadruple temperature 30 °C, and capillary voltage 3500 V. A full scan spectra from m/z 100–800 in the positive ion mode were obtained with scan time of 1 s. The fragmentor was set at 80. The column used was a reversed-phase column, Luna C18(2), size 250 × 4.6 mm, particle size 4.98 μm, pore diameter 97 Å (Phenomenex, Part. No. 00G-4252-E0, Batch No. 5291-50, St. Torrence, CA, USA), maintained at 26°C. The used eluents were: (A) acidified water (pH 3.2) with formic acid, (B) acetonitrile as reported in Table1.

Time	Eluent A (%)	Eluent B (%)	Flow (ml/min.)
0.10	50.0	50.0	1.0
15.00	50.0	50.0	1.0
20.00	0.0	100.0	1.0
23.00	0.0	100.0	1.0
28.00	50.0	50.0	1.0

Table 1: *Method used for HPLC analysis*

2.1.10 HPLC sample preparation

5 mg of the dried defatted acetone extracts and fractions were accurately weighed and suspended in 1 ml of CH_3CN. The suspensions (5 mg/ml) were sonicated for 20 minutes and centrifuged for 5 minutes (14000 rpm) before HPLC analysis. Fractions eluted by the three chromatography methods were adjusted to a final concentration of 1 mg/ml. The analyses were done in triplicates.

2.1.11 Calibration curves and quantitative analysis

To evaluate the content of constituents, a HPLC analysis was performed using a method described in the literature (Bilia, 2006), adapted to our experimental necessities. In particular four standards were used, to quantify artemisinin, scopoletin and the main polymethoxylated flavonoids presents in the acetone extract of *A. annua*. For artemisinin calibration, HPLC injection volumes in a range from 5 to 30 µl of artemisinin standard (C=0.052 mg/ml) were performed and the peak areas were recorded by MS instrument. For calibration of polymethoxyflavones, HPLC injection volumes in a range from 5 to 40 µl of casticin standard (0.212 mg/ml) were performed (the chromatograms were recorded at 280 nm). For scopoletin quantification, HPLC injection volumes in a range from 5 to 30 µl of scopoletin standard (C=0.234 mg/ml) were performed (the chromatograms were recorded at 330 nm) and for quantification of the naringenin methoxylated derivatives, naringenin standard was used (C=0.226 mg/ml), with HPLC injection volumes in a range from 5 to 30 µl. Linear regression was performed to establish the calibration curves. The analyses were done in duplicates (RSD were ≤ 0.02). All data obtained by HPLC was inserted into a Spreadsheet (Microsoft® Office Excel 2007™) and calculated by interpolation of the peak areas, with respect to the initial concentration and injection volume used.

2.1.12 NMR analysis

Final control analysis of purity and identification of the isolated compounds were performed with HPLC-DAD-ESI-MS and NMR. The ^{1}H NMR spectra were recorded in CD_3Cl and DMSO-d_6 on a Bruker DRX-400 instrument at 295 K (Bruker AG, Ultrashield™ NMR Magnet System, 400Mhz/54 nm, Fällanden, Zwitzerland).

2.2 Transferrin conjugated liposomes: preparation and characterization

2.2.1 Materials

All the solvents used were HPLC grade from Merck (Darmstadt, Germany); 85% formic acid was provided by Carlo Erba (Milan, Italy). Water was purified by a Milli-Q_{plus} system from Millipore (Milford, MA). Artemisinin (ART) was isolated as described in section 3.1. PEG 2000 (18:0/18:0) was purchased from Spectra2000 srl (Rome, Italy). Egg phosphatidylcholine (Phospholipon90G, P90G) was gently provided from Natterman Phospholipids, GmbH, Hermersberg, Rhineland-Palatinate, Germany. Cholesterol was analytical grade from Aldrich (Milan, Italy). 1,2-distearoyl-sn-glycero-3-phosphoethanolamine-*N*-[carboxy(polyethylene glycol) 2000] DSPE-PEG_{2000}-COOH was purchased from Avanti Polar Lipids (Alabaster, AL). *N*-(3-dimethylaminopropyl)-*N*'-ethylcarbodiimide hydrochloride (EDC), sulpho-N-hydroxysuccinimide (S-NHS), human holo-transferrin, Sepharose CL-4B, bicinchoninic acid (BCA) kit for protein determination were from Sigma Aldrich (Seelze, Germany).

2.2.2 Liposomes preparation

Multilamellar vesicles were prepared according to the film hydration method from Phospholipon® 90 G, cholesterol and DSPE-PEG_{2000}-COOH (6:3:0.6 molar ratio). Briefly, a mixture of phosphpolipid and cholesterol in CH_2Cl_2 was dried to a thin lipid film in a rotary evaporator (Büchi, Essen, Germany) and loaded with artemisinin (2 mg/ml). Lipids were re-suspended in an appropriate amount of 400 mM citrate/5 mM phosphate buffer (pH 4) resulting in a final lipid concentration of 10 mg lipid/ml corresponding buffer. After vortexing for 30 minutes at 38°C an extruder was used to reduce vesicle size from MLVs to LUVs and to increase size distribution homogeneity. Unilamellar liposomes were obtained by extruding the resulting multilamellar vescicles trough 400 nm, 200 nm and 100 nm polycarbonate membranes using a Liposofast Basic device (Avestin, Mannheim, Germany).

2.2.3 Coupling of transferrin to the liposomes

Small unilamellar liposomes obtained were conjugated to transferrin like previously described by Anabousi (Anabousi, 2005). The lipids were re-suspended in an appropriate amount of citrate/phosphate buffer. Then, 1 ml of PBS (pH 7.4) and 360 ml of both EDC (0.25 M in H_2O) and S-NHS (0.25 M in H_2O) were added per 10 mmol of lipid. The mixture was allowed to incubate for 10 min at room temperature, before adjusting to pH 7.5 with 1 M of NaOH. 125 mg Tf/mmol of phospholipid was added and gently stirred for 8 h at 4ºC. Unbound protein was removed by passing the liposome suspension through a Sepharose CL-4B gel column (Ishida, 2001).

2.2.4 Protein assay and Tf-binding efficacy

The average amount of transferrin conjugated to the liposomes was quantified as described by Derycke et al. (Derycke, 2002). One hundred microlitres of liposome suspension were added to 400 µl of methanol. The mixture was vortexed and centrifuged (10 s at 9000x*g*). Then, 200 µl of chloroform were added and the sample was vortexed and centrifuged again (10 s at 9000x*g*). For phase separation, 300 µl of water were added and the sample was vortexed again and centrifuged for 1 min at 9000x*g*. The upper phase was carefully removed and discarded. Three hundred microlitres of methanol were added to the chloroform phase and the interphase with the precipitated protein. The sample was mixed and centrifuged to pellet the protein (2 min at 9000x*g*). The supernatant was removed and the protein pellet was dried under a stream of air. The pellet was then dissolved in 20 µl of PBS (pH 7.4) and the concentration was determined with a bicinchonic acid (BCA) protein assay using albumin as standard protein. The coupling efficiency was calculated as µg Tf/µmol phospolipid.

2.2.5 Liposomes characterization

Size and polydispersity index (P.I.) of liposomes were determined by dynamic light scattering (DLS).Vesicle formation and morphology of liposomes were observed by transmission electron microscopy (TEM) after negative staining with phosphotungstic acid 1% w/v. Free ART was removed by means of dialysis and encapsulation efficacy was evaluated by HPLC-DAD/ESI/MS by method described in section 2.1.9, using artemisinin as external standard. For determination of liposomes stability size, P.I. and encapsulation efficiency of prepared liposomes were monitored during their storage at 4ºC for twenty days.

3. RESULTS AND DISCUSSION

3.1 Polymethoxylated flavonoids and artemisinin isolation

3.1.1 Liquid-liquid extraction

In an attempt to separate the most abundant polymethoxylated flavonoids (PMFs) found in the *A.annua* acetone extract, the techniques of Sephadex LH-20, silica gel column chromatography and flash chromatography were applied. Row extract was suspended in MeOH (for final concentration of 100 mg/ml) and defatted with n-heptane. In order to isolate the PMFs, the extract was further partitioned with CH_2Cl_2 or EtOAc and H_2O was added to enhance the partitioning and isolate more polar compounds. Analyses showed that the CH_2Cl_2 fraction had the highest content of polymethoxylated flavonoids and artemisinin so this method was selected as the best one.
HPLC-DAD-ESI-MS analysis showed that minimal loss of PMFs occurred during this treatment (total experimental setup is visible in Figure 1). The result can be seen in Table 1, where a percentual comparison between raw extract and defatted extract is showed.

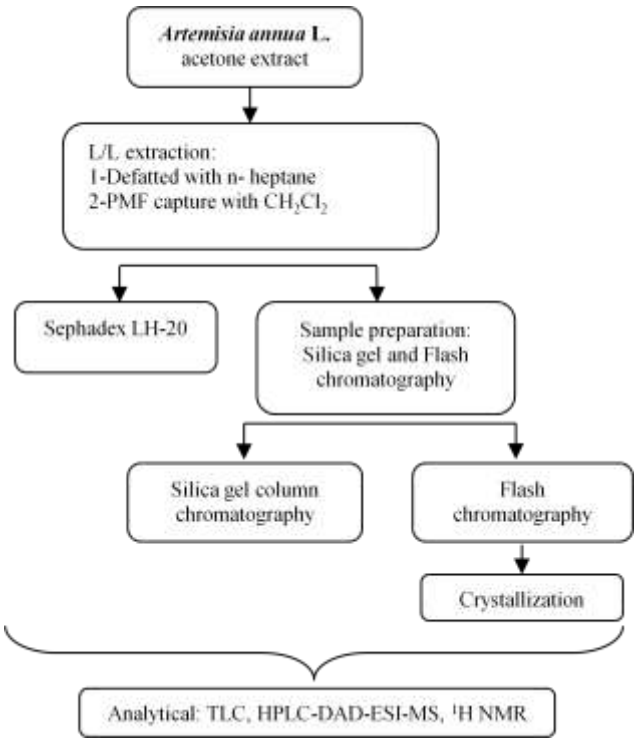

Figure 1: *Flowchart of entire experiment.*

Compunds	Total acetone extract		Defatted acetone extract	
	(mg/g)	%	(mg/g)	%
Eupatin	15.81±0.32	1.6	27.15±0.08	2.7±0.01
Casticin/Chrysosplenetin	13.84±0.18	1.4	23.74±0.04	2.4
Artemetin	0.74±0.02	0.01	1.20	0.1
5-hydroxy-3,6,7,4'-tetramethoxyflavone	1.21±0.01	0.1	1.95±0.02	0.2
Total flavonoids	31.14±0.061	3.1±0.01	54.04±0.23	5.4

Table 1: *Table of contents of A. annua extract. Yields of PMFs in the raw extract and defatted extract are reported.*

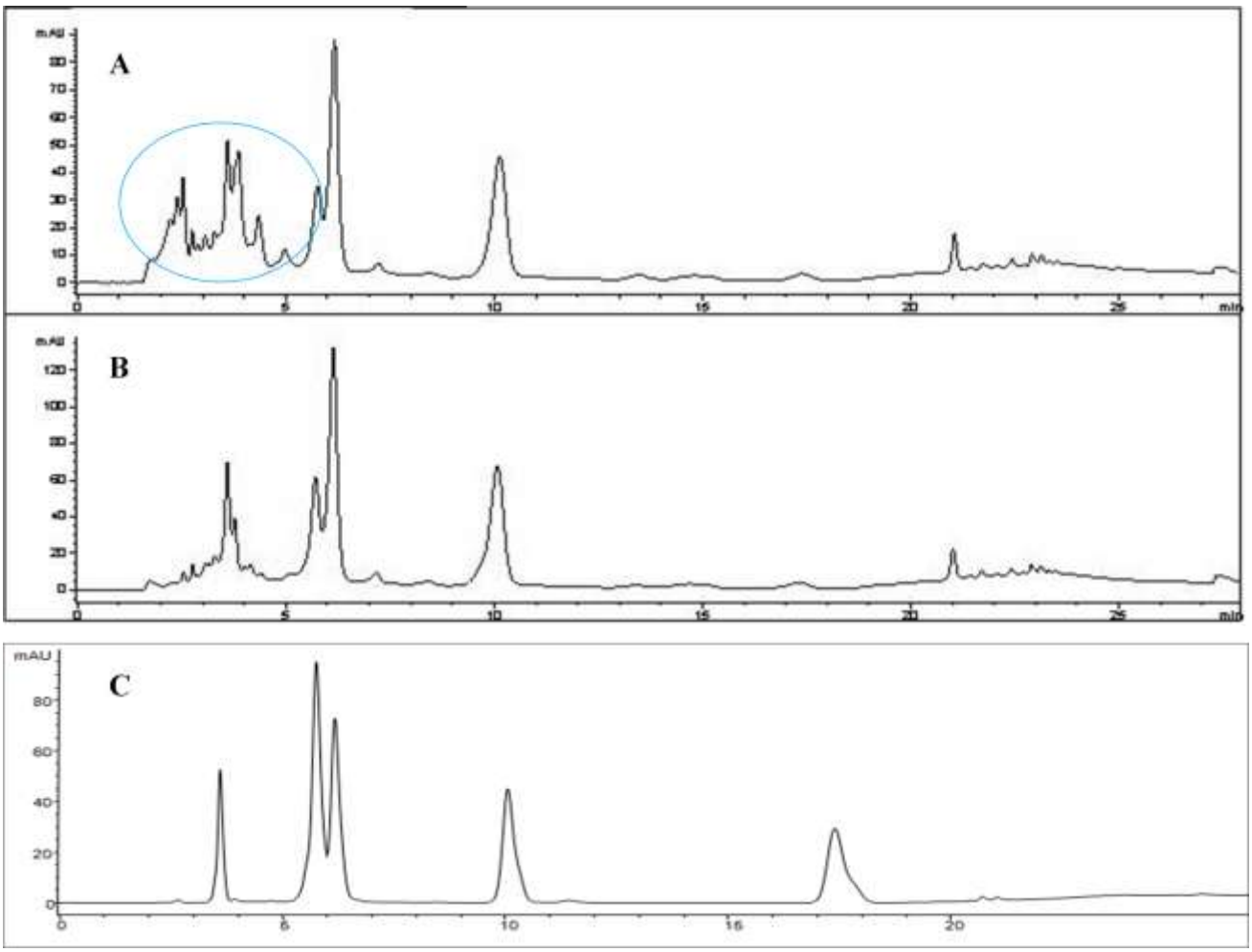

Figure 2: *HPLC-DAD chromatograms at 280 nm, with* ***(A)*** *total raw extract and* ***(B)*** *defatted total extract. Clearly visible is that the defatted extract is removed from more polar compounds, wich enhances separation and purification afterwar.* ***(C)*** *Standard compounds. 1: scopoletin, t_r= 3.5 min; 2: esperetin, t_r= 6.05 min; 3: eupatin, t_r= 6.1 min; 4: casticin/ chrysosplenetin, t_r=10.1 min; 5: artemetin, t_r= 17.3 min; 6: 5-hydroxy-3,6,7,4'-tetramethoxyflavone, t_r: 21 min; 7: artemisinin (no uv absorption) t_r =23.7.*

As reported in Figure 2 the defatted total extract, used for the different types of chromatography, showed the presence of different flavonoids: scopoletin, esperetin, eupatin, the isomers casticin and chrysosplenetin, artemetin and 5-hydroxy-3,6,7,4'-tetramethoxyflavone and artemisinin that was identified by HPLC-ESI-MS analysis because of the lack of UV absorption. Peaks characterization was carried out comparing results obtained by HPLC-DAD-ESI-MS with results of relative standards and with literature data.

3.1.2 Investigated separation methods

The first method (**size exclusion chromatography**) gave the poorest results, as, independently of the elution system, the main flavonoids were not separated an eluted together with other constituents, i.e. hydroxy coumarins, chlorogenic acid with its analogues. The compounds eluted in the following order: artemisinin, a non-identified flavonoid (later identified, when better separated

by flash chromatography) eluted with artemetin, scopoletin, casticin/chrysosplenetin, eupatin eluted all together. Therefore, an increased number of successive columns were needed in order to get better purities of the PMF's, however the isomers casticin and chrysosplenetin always eluted together.

Application of **silica gel column chromatography** increased the separation of PMFs, but was also unable to separate the isomers, even when combined with further silica gel or Sephadex LH-20 column chromatographies of the fraction containing the pair of isomers. Preparation of the extract allow to obtain a sample suitable for both the silica gel column and the pre-column of the flash chromatography system. 25 g of the defatted extract was suspended in an excess of acetone and mixed with a minimum possible of silica gel powder (113.4g) in order to enhance the extract concentration in the mixture. Acetone was then evaporated leaving a homogeneus dark green sample powder.

Flash chromatography showed to be the most efficient method among the three applied methods for the extract considered, due to the real-time detection (UV light optimum absorptions were set at 280 and 350 nm) of the PMFs. It enables to better separate the fractions, including the isomers casticin and chrysosplenetin, which were the most problematic to separate especially with the others two open column chromatographic methods (Figure 3 and 4). The purity of the compounds of interest, obtained from the tested chromatographic methods were evidenced by monitoring the fractions with: TLC, HPLC-DAD-ESI-MS.

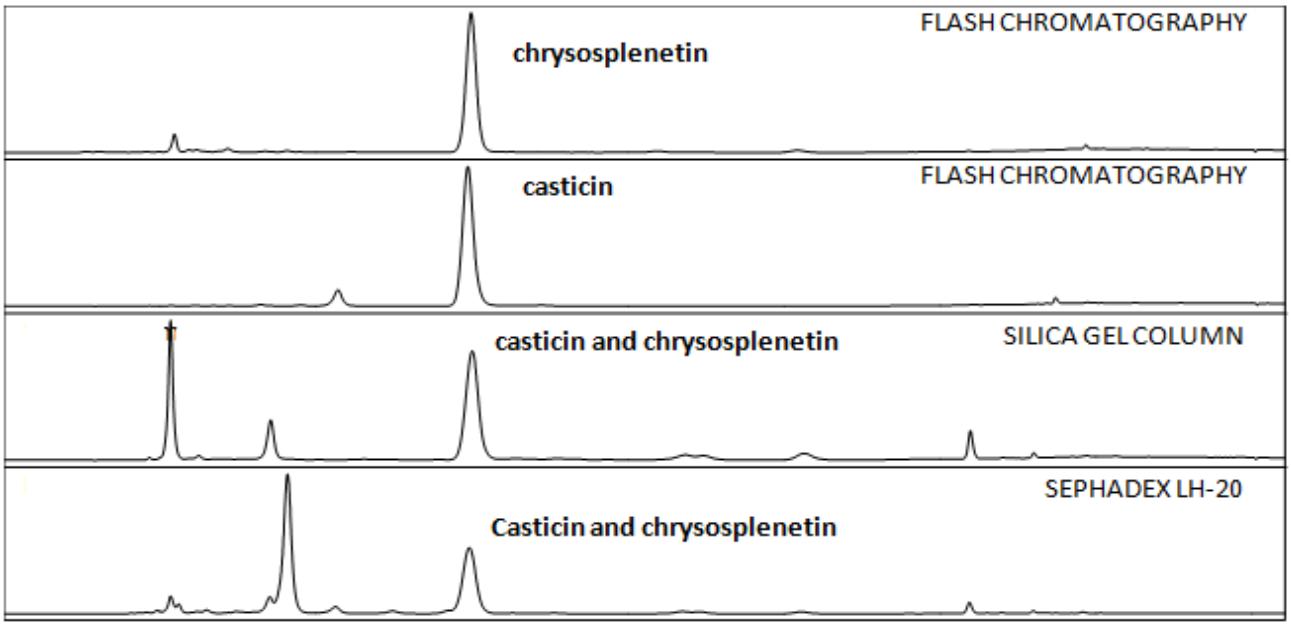

Figure 3: *Chromatograms at 280 nm of the isomers casticin and chrysosplenetin from A. annua L. acetone extract, obtained after fractionation using the three different chromatographic methods.*

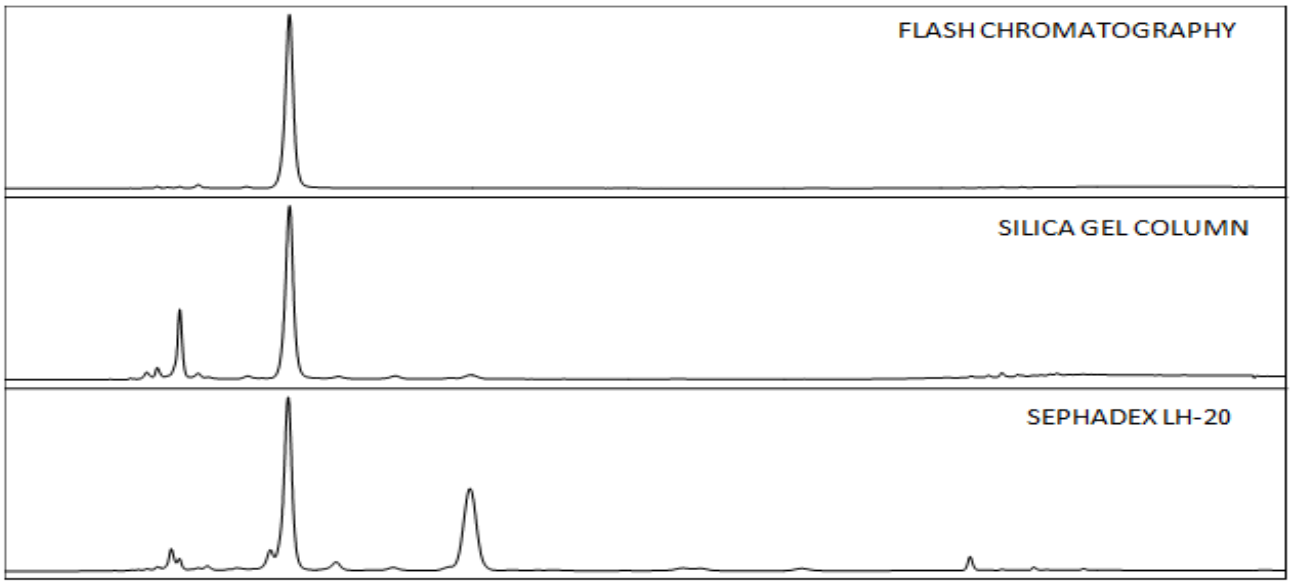

Figure 4: *Chromatograms at 280 nm of eupatin from A. annua L. acetone extract, obtained after fractionation using the three different chromatographic methods.*

3.1.3 Optimization of flash chromatography method

After establishing that the chromatographic methods, such as size exclusion chromatography (SEC) and silica gel normal phase column chromatography were not adequate enough to separate the PMFs (Table 2) presents in the acetone extract of *A. annua* (in particular casticin /chrysosplenetin) further enhancement of the flash chromatography method was performed.

Fine-tuning of the solvents gradient and flow rate was needed, until complete separation of the main PMFs (casticin, chrysosplenetin and eupatin) was achieved by adapting the mobile phase and the flow parameters with those used during the silica gel open column chromatography. For comparison purposes, the sample powder (previously prepared for both silica open column and flash chromatography) was loaded, however in minor quantity (4.4 g of sample powder containing 0.795 g of extract) due to the capacity of the precolumn (up to 5 g, for dry samples only) available for the experiment.

	R_1	R_2	R_3	R_4	R_5	R_6	R_7	R_8	MW
Casticin	$-OCH_3$	$-OCH_3$	-OH	$-OCH_3$	$-OCH_3$	-OH	$-OCH_3$	-H	374
Artemetin	$-OCH_3$	$-OCH_3$	-OH	$-OCH_3$	$-OCH_3$	$-OCH_3$	$-OCH_3$	$-OCH_3$	388
Chrysosplenetin	$-OCH_3$	$-OCH_3$	-OH	$-OCH_3$	-OH	$-OCH_3$	$-OCH_3$	-H	374
5-hydroxy-5,6,7,4'-tetramethoxyflavone	$-OCH_3$	$-OCH_3$	$-OCH_3$	$-OCH_3$	-OH	-OH	$-OCH_3$	-H	358
Eupatin	$-OCH_3$	$-OCH_3$	-OH	-OH	$-OCH_3$	-OH	$-OCH_3$	-H	360

Table 2: *Chemical structures of main PMFs found in A. annua.*

3.1.4 Isolation by flash chromatogaphy method

The fractions, containing the PMFs , collected automatically by the instrument, were analyzed by TLC and identified by HPLC-DAD-ESI-MS means, using standards when available. Flash chromatography method allowed the separation of six compounds (Figure 5), eluted in the following order: artemisinin (a sesquiterpene lactone), 5-hydroxy-3,4',6,7-tetramethoxyflavone and artemetin (5-hydroxy-3,3',4',6,7-tetramethoxyflavone), found both in very small quantities, scopoletin (7-hydroxy-6-methoxycoumarin), which, in a small amount, eluted together with the flavonol chrysosplenetin (4',5-dihydroxy-3,3',6,7-tetramethoxyflavone), the isomer casticin (3',5-dihydroxy-3,4',6,7-tetramethoxyflavone) and finally eupatin (3,3',5-trihydroxy-4',6,7-trimethoxyflavone). The effective separation of chrysosplenetin and casticin, were confirmed by ^{1}H NMR (Figure 6). The identification of the compound **5-hydroxy-3,4',6,7-tetramethoxyflavone** was possible by comparing the obtained results with literature data (Sy, 1998) : UV λ_{max}= 336 and 272 nm; ESI-MS: $[M + H]^+$= 359 m/z (100%); ^{1}H NMR ($CDCl_3$) δ 3.88 (3H, s, 3-OCH_3), δ 3.90 (3H, s, 4'-OCH_3), δ 3.93 (6H s, 6-OCH_3), δ 3.97 (3H, s, 7-OCH_3), δ 6.52 (1H, s, H-8), δ 7.05 [2H, d, (8Hz), H-3' and H-5'], δ 8.09 [2H, d, (8 Hz), H-2'and H-6']; δ 12.15 (1H, s, 5-OH).

3.1.5 Cristallization and characterization of isolated compounds

The main compounds isolated (artemisinin, chrysosplenetin, casticin and eupatin) were submitted to crystallization using different solvents according to their polarity, which were the following: EtOH for crystallizing **artemisinin** (acquiring a purity of 96% confirmed by ESI-MS using the artemisinin standard as external standard); EtOAc for crystallizing **chrysosplenetin** to obtain a purity of 84,54% and the following spectral data: UV λ_{max}: 257, 270 and 350 nm ; ESI-MS: $[M + H]^+$= 375 m/z (100%); ^{1}H NMR ($CDCl_3$) δ 3.87 (3H, s, 3-OCH_3), δ 3.94 (3H, s, 6-OCH_3), δ 3.98 (6H s, 7-OCH_3), δ 4.00 (3H, s, 3'-OCH_3), δ 6.02 (1H, s, 4'-OH), δ 6.52 [1H, s, H-8], δ 7.07 [1H, d, (7.96 Hz), H-5'], δ 7.68 [1H, dd (1.96 Hz e 8.3Hz), H-6'], δ 7.73 [1H, d, (1.72 Hz), H-2']. These results were in accordance with literature data available for this compound (Sy, 1998). The same solvent (EtOAc) also used to crystallize **casticin** to obtain a purity of 85.42% and a spectral data of: UV λ_{max}: 257, 270 and 350 nm; ESI-MS: $[M + H]^+$= 375 m/z (100%); ^{1}H NMR ($CDCl_3$) δ 3.89 (3H, s, 4'-OCH_3), δ 3.95 (3H, s, 7-OCH_3), δ 3.98 (6H s, 3-OCH_3), δ 4.01 (3H, s, 6-OCH_3), δ 5.71 (1H, s, 3'-OH), δ 6.52 [1H, s, H-8], δ 6.99 [1H, d, (8.52 Hz), H-5'], δ 7.70 [1H, d (1.96 Hz), H-2'], δ 7.75 [1H, dd, (2.4 e 8 Hz), H-6']. These results were consistent with the previously published data for this compound (Mesaik, 2009). MeOH was used for crystallizing **eupatin**, to resulting in a purity of 97.61% and the following spectral data was obtained: UV λ_{max}: 258, 270 and 350 nm; ESI-MS: $[M + H]^+$= 361 m/z (100%); ^{1}H NMR ($CDCl_3$) δ 3.80 (3H, s, 6-OCH_3), δ 3.88 (3H, s, 7-OCH_3), δ 3.99 (6H s, 4'-OCH_3), δ 6.80 (1H, s, 8-H), δ 7.01 [1H, d, (8.4 Hz), H-5'], δ 7.61 [1H, dd (2 e 8.42 Hz), H-6'], δ 7.73 [1H, d, (2.4 Hz), H-2'], also in agreement with literature data available for the compound (Sy, 1998).

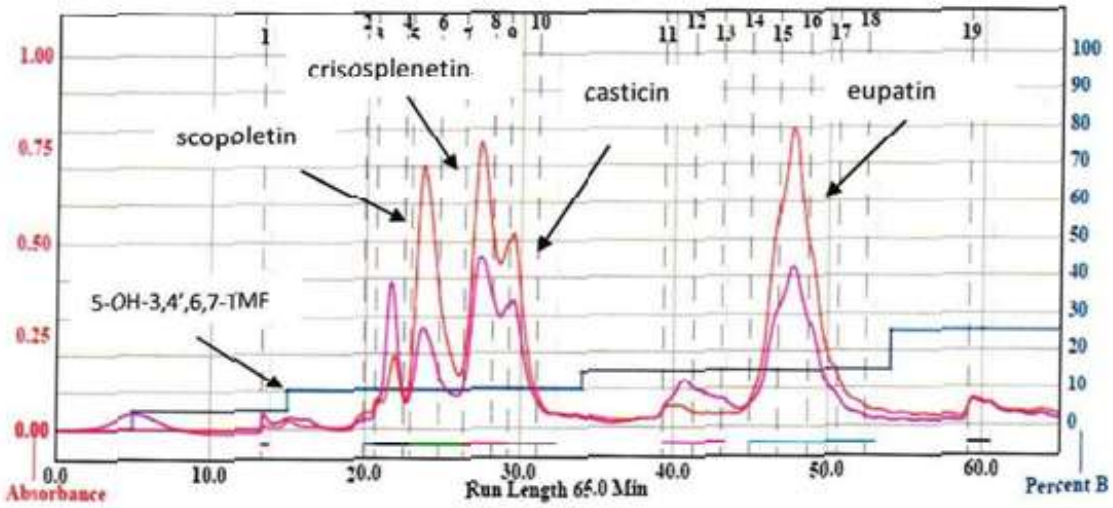

Figure 5: *Chromatograms at 280 and 350 nm obtained by flash chromatography.*

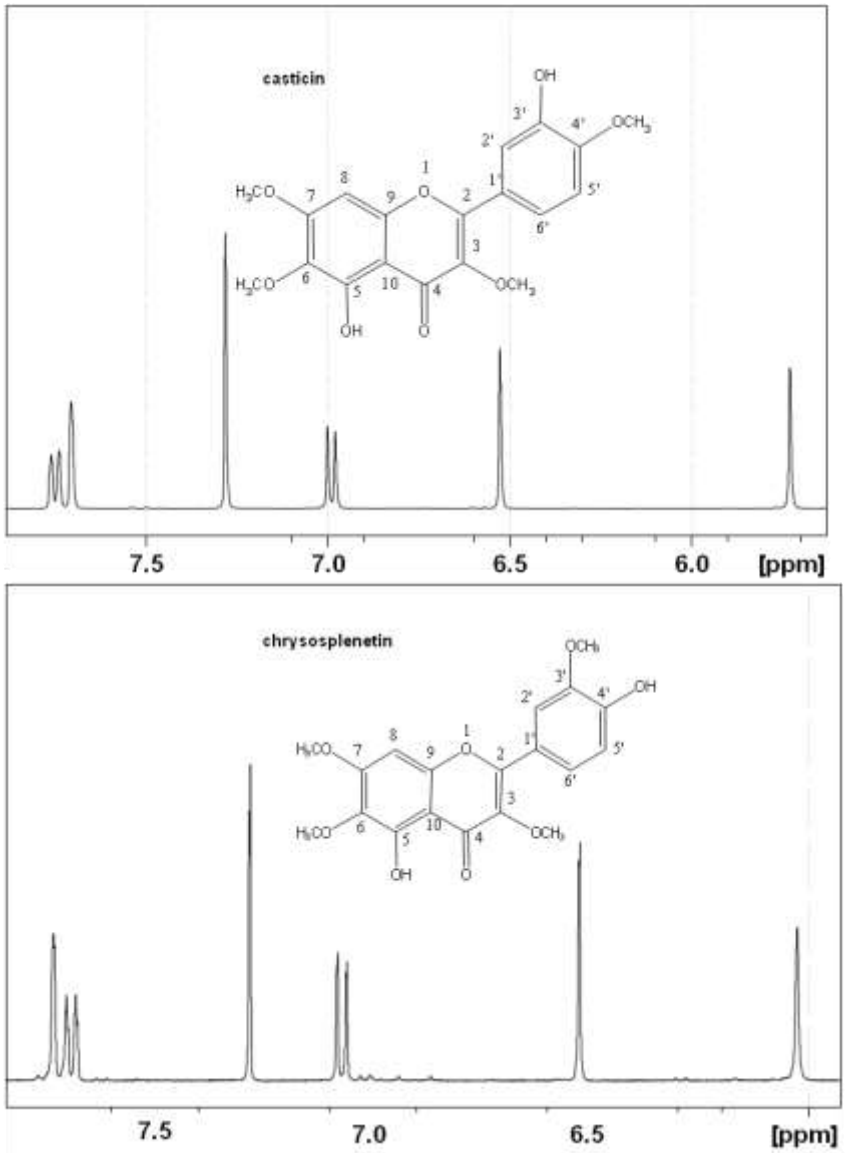

Figure 6: *^{1}H NMR spectra of casticin and chrysosplenetin compounds in $CDCl_3$ (400 MHz).*

3.1.6 Comparison of separation methods

Characteristics of the different isolation methods are reported on Table 3. The displayed results are percentual recoveries from the defatted extract. Although it seems that the differences in recovery are similar between the used chromatographic methods, the separation of the PMFs was most efficiently observed with the silica gel open column and flash chromatography. But, the separation of casticin and chrysosplenetin was possible only with the flash chromatographic method (Figure, 7).

	Sephadex LH-20	**Silica gel Column**	**Flash Chromatography**
Time	High	High	Low
Amount of Solvents	Low	High	High
Cost	Low	High	High
Recovery of Flavonoids (%)	85.34[1]	75.02[1]	78.28[2]
Other compunds		Isolation of artemisinin	Isolation of artemisinin and scopoletin

(1) impossible isolation of isomers casticin and chrysosplenetin
(2) possible isolation of isomers casticin and chrysosplenetin

Table 3: *Comparison between different isolation methods.*

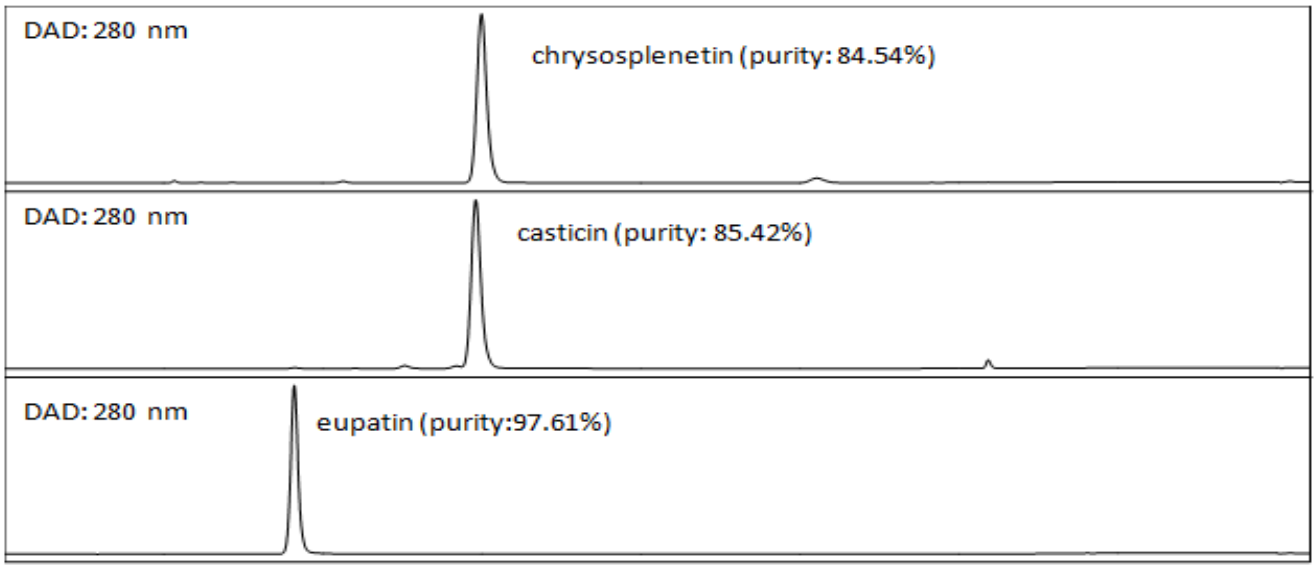

Figure 7: *Chromatograms of the main polymethoxyflavonoids from A. annua L. acetone extract obtained from flash chromatography, after crystallization.*

3.2 Transferrin conjugated liposomes for artemisinin delivery to cancer cells: preliminary results.

The high specificity of endocytic uptake of transferrin (Tf) by the transferrin receptor (TfR) has made it a subject of interest for targeted drug delivery. TfR-targeted drug conjugates can be delivered across epithelial barriers or accumulated in proliferating tissues (Widera, 2003). Liposomes have been used as vehicles for drug delivery because of their biocompatibility and the possibility to incorporate both water-soluble and hydrophobic materials (Torchilin, 2000). They received much attention as carrier systems for advanced drug delivery in the context of anticancer therapy (Shimizu, 2003). In general, formation of ligand–liposome-complexes should be simple, fast, efficient, reproducible and yield stable, non-toxic bonds. The biological properties of the ligands (i.e. target recognition and binding efficiency) should not be substantially altered and the drug loading efficiency and drug release rates of the vesicle should not be negatively affected. Lastly, the ligand targeted liposomes should be stabile and their circulation half-lives should be long enough to allow them to reach and interact with the target cells.

A particularly useful protein– liposome coupling procedure involves the covalent modification of functional groups of proteins using polyethylene glycol (PEG)-linked lipid residues (Bendas, 1997). A bond between free amino groups of the protein and carboxylic groups of the linker (DSPE-PEG_{2000}-COOH) is formed in the presence of a water-soluble carbodiimide (Figure 8). The method uses sulpho-N-hydroxysuccinimide (S-NHS) in addition to N-(3-dimethylaminopropyl)-N'-ethylcarbodiimide hydrochloride (EDC). S-NHS is a water-soluble analogue to NHS which is used to modify carboxyl groups to amine-reactive NHS-esters. This is accomplished by mixing the NHS with a carboxyl containing molecule and a dehydrating agent, EDC, which reacts with the carboxyl group first and forms an amine-reactive intermediate, an O-acylisourea.

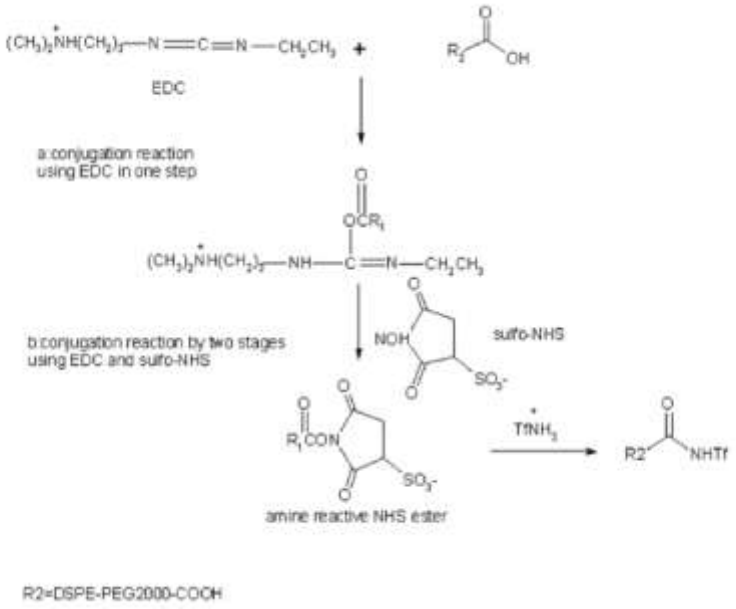

Figure 8: *Coupling reaction of transferrin to the surface of liposomes using DSPE-PEG_{2000}-COOH as linker lipid (Anabousi, 2005).*

3.2.1 Characterization of liposomes

In the present study Tf-coupled liposomes for artemisinin delivery have been developed; the physicochemical characterization and drug-loading parameters of formulation are summarized in Table 4. A good value of transferrin coupling efficiency (46,71 µg/µmol lipids) has been obtained. It can be seen from transmission electron microscopy (TEM) that liposomes were spherical and the size correlated well with the results of the laser diffraction particle size (Figure 9).

Formulation	Mean size (nm)	P.I	EE (%)
L-Tf	175.9±1	0.35	-
L-Tf-A	164.2±5	0.30	55

Table 4: *Size, polydispersity index (P.I.), and encapsulation efficiency of L-Tf: empty liposomes conjugated with transferrin and L-Tf-A: artemisinin loaded liposomes conjugated with transferrin.*

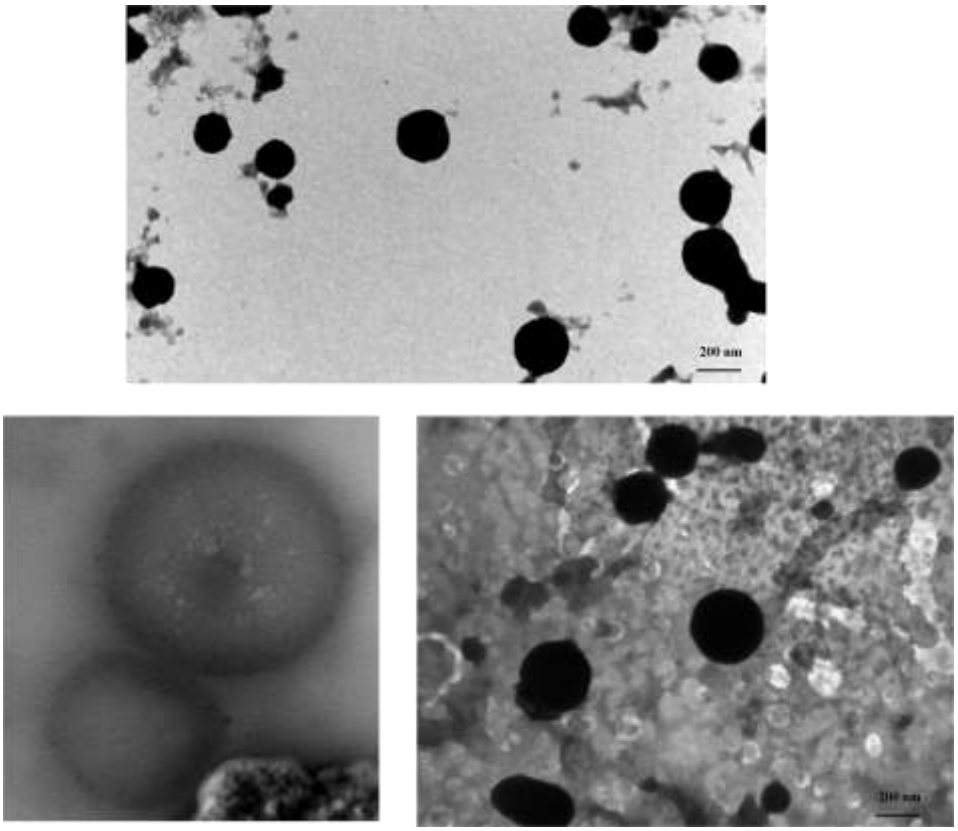

Figure 9: *TEM images revealing shape, structure, and sizes of transferrin conjugated liposomes loaded with artemisinin.*

3.2.2 Stability studies

Chemical and physical stability were checked within 20 days (Figure 10); vescicles were stable with a leakage of drug of 20% after 15 days; we can observe at the same time slightly increasing in size and P.I. values.

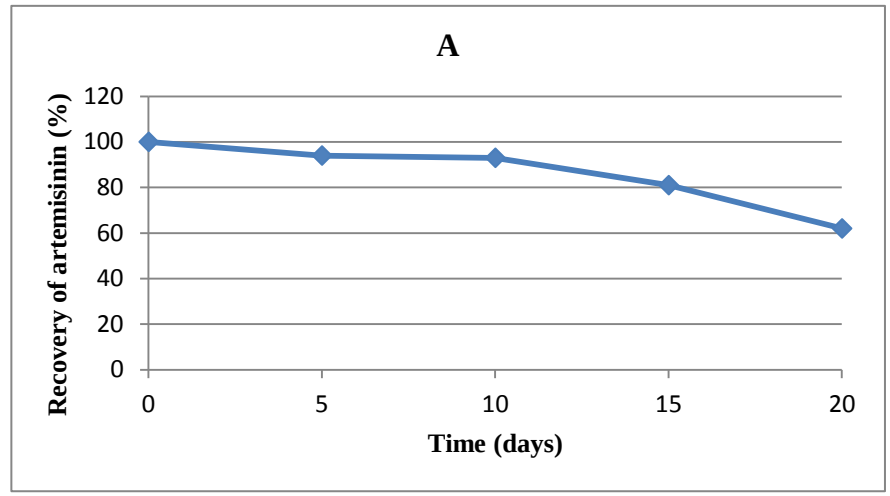

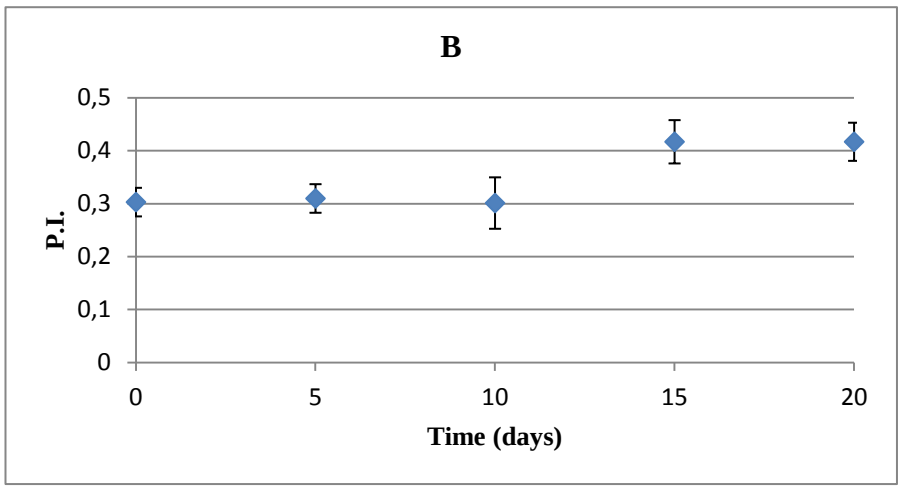

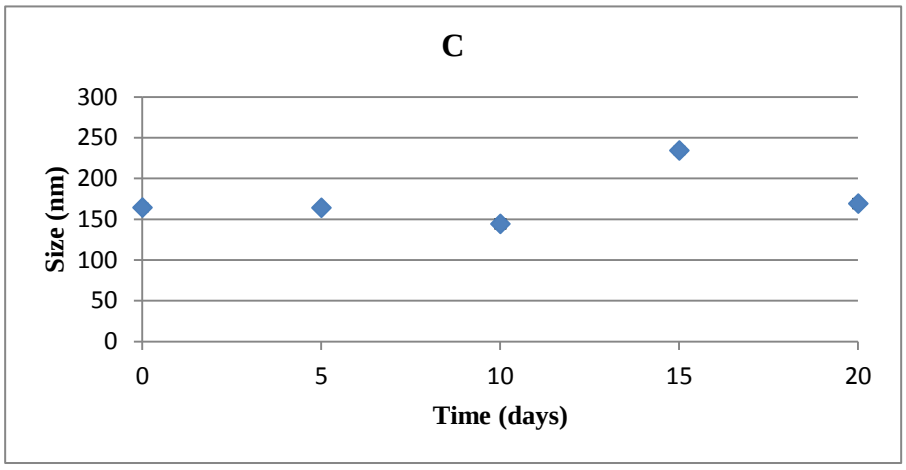

Figure 10: *Chemical* ***(A)*** *and physical* ***(B; C)*** *stability of transferrin conjugated liposomes loaded with artemisinin at storage conditions (20 days, 4°C).*

4. CONCLUSIONS

This work reports the comparison of three separation methods: Sephadex LH-20, silica gel column chromatography and flash chromatography. *Artemisia annua* acetone extract was first pretreated, using liquid/liquid extraction and after the compounds of interest were separated with the previous mentioned methods. The latter one has been proven to be the most convenient method for the separation of polymethoxylated flavonoids. The results showed that artemisinin and the main polymethoxylated flavonoids were well separated with silica gel column and flash chromatography methods, however the pair of isomers chrysosplenetin and casticin was only separated by flash chromatography. Followed by a standard crystallization method, using EtOH for artemisinin, MeOH for eupatin and EtOAc for both casticin and chrysosplenetin, the isolated compounds were better purified (purities ranged between 85-98%).

Flash chromatographic method resulted the most rapid and efficient way for separating polymethoxylated flavonoids and artemisinin. This method was a little bit more expensive than the other two chromatographic methods but it compensates drastically for time. Especially converted to industrial scale, when the applied solvents can be recycled, it promises to be an efficient methodology; price of Sephadex-LH 20 and time required for this method, makes it infeasible in this scale. In conclusion *Artemisia annua* is proven to be a valuable source of polymethoxylated flavonoids and artemisinin and flash chromatography demonstrated to be a rapid and reproducible technique for the isolation of these compounds, and could make them available for further purposes, such as anticancer activities.

The second part of our work was focused on the development of a nanocarrier for artemisinin delivery to cancer cells to improve its activity and selectivity. Iron content is higher in tumor cells (Shterman, 1991) than in normal cells making them more susceptible to artemisinin derivatives. The susceptibility of tumor cells to artemisinins can further be enhanced by the addition of transferrin or ferrus iron (Moore, 1995; Efferth, 2004). Active targeting of therapeutic drugs associated with nanocarrier is achieved by conjugated a cell-specific ligand at the surface of the carrier, thereby allowing a preferential accumulation of the drug in the target cell or tissue. This approach may be succesfull when the receptor for surface-bound ligands are expressed uniquely in diseases cells or if their expression is differentially higher in disease cells as compared to normal ones. It is the case of our target TfR overexpressed in several tumoral tissues. Human Tf has been previously used for this purpose because of its ability to deliver liposomes into the intracellular compartment through receptor-mediated endocytosis (Fonseca, 2005). The formulation developed and loaded with isolated artemisinin has proper physical characteristics as drug carrier for parental administration in terms of particle size, polydispersity, encapsulation efficacy. Further investigation and optimization of this formulation would be best addressed through *in vitro* experimentation.

5. REFERENCES

Anabousi S., et al., Assessing transferrin modification of liposomes by atomic force microscopy and transmission electron microscopy, European Journal of Pharmaceutics and Biopharmaceutics. 2005, 60 (2): 295-303.

Baraldi R., et al., Distribution of artemisinin and bioactive flavonoids from *Artemisia annua L.* during plant growth. Biochemical Systematics and Ecology. 2008, 36, 340-348.

Bendas G., et al., Targetability of novel immunoliposomes prepared by a new antibody conjugation technique, Int. J. Pharm. 1999, 181 (1), 79–93.

Bhakuni R.S., et al., Secondary metabolites of Artemisia annua and their biological activity. Curr. Sci. 2001, 80, 35-48.

Bila, A.R., et al., Simultaneous analysis of artemisinin and flavonoids of several extracts of *Artemisia annua* L. obtained from a commercial sample and a selected cultivar. Phytomedicine. 2006, 13, 487–493.

Deryke A.S., et al., Transferrin-mediated targeting of hypericin embedded in sterically stabilized PEG-liposomes, Int. J. Oncol. 2002, 20 (1): 181-187.

Efferth T., et al., Enhancement of cytotoxicity of artemisinin toward cancer cells by ferrous iron. Free Rad. Biol. Med. 2004, 37, 998–1009.

Efferth T., et al., The anti-malarial artesunate is also active against cancer. Int. J. Oncol. 2001, 18, 767–773.

Elford B.C., et al., Potentiation of the antimalarial activity of qinghaosu by methoxylated flavones. Trans. R. Soc. Trop. Med. Hyg. 1987, 81, 434–436.

Ferreira J.F., et al., Flavonoids from *Artemisia annua* L. as Antioxidants and Their Potential Synergism with Artemisinin against Malaria and Cancer. Molecules. 2010, 15, 3135–3170.

Fonseca C., et al., Targeting of sterically stabilized pH-sensitive liposomes to human T-leukaemia cells. Eur. J. Pharm. Biopharm. 2005, 59: 359-366.

Ishida O., et al., Liposomes bearing polyethyleneglycol-coupled transferrin with intracellular targeting property to the solid tumors in vivo. Pharm. Res. 2001, 18 (7), 1042–1048.

Liu K., et al., Antimalarial activity of Artemisia annua flavonoids from whole plants and cell cultures. Plant Cell Rep. 1992, 11, 637.

Maruyama K., et al., Possibility of active targeting to tumor tissues with liposomes. Adv. Drug Deliv. Rev. 1999, 40(1–2), 89–102.

Mesaik A.M., et al., Isolation and immunomodulatory properties of a flavonoid, casticin from Vitex agnus-castus. Phytother. Res. 2009, 29, 1516–1520.

Moore et al., Oral administration of dihydroartemisinin and ferrous sulfate retarded implanted fibrosarcoma growth in the rat. Cancer Lett. 1995, 98, 83–87.

Nijveldt R.J., et al., Flavonoids: a review of probable mechanisms of action and potential applications. Am. J. Clin. Nutr. 2001, 74, 418–425.

Phillipson J.D., New drugs from nature–it could be yew. Phytother. Res. 1999, 13, 2.

Shimizu K., et al., Stability and antitumor effects of all-trans retinoic acid-loaded liposomes contained sterylglucoside mixture. Int. J. Pharm. 2003, 258 (1–2), 45–53.

Shterman N., et al., Comparison of transferrin receptors, iron content and isoferritin profile in normal and malignant human breast cell lines. Pathobiology. 1991, 59: 19-25

Sy L., et al., Three Sesquiterpenes form Artemisia annua, Phyt. chem. 1998, 48, 7, 1207–1211.

Torchilin V.P., Drug targeting, Eur. J. Pharm. Sci. 11 (2) (2000) S81–S91.

Tros C., et al., Enhanced gene delivery in vitro and in vivo by improved transferrin-lipoplexes. Biochim. Biophys. Acta. 2002, 1561 (2), 209–221.

Tsao R., et al., Separation procedures for naturally occurring antioxidant phytochemicals. J. Chromat. 2004, B 812, 85–99.

Wagner E., et al., Delivery of drugs, proteins and genes into cells using transferrin as a ligand for receptor-mediated endocytosis. Adv. Drug Deliv. Rev. 1994, 14 (1), 113–135.

Widera A., et al., Mechanism of TfRmediated transcytosis and sorting in epithelial cells and applications toward drug delivery, Adv. Drug Deliv. Rev. 2003, 55 (11): 1439–1466.

ANNEX II

Microarray-based mRNA expression profiling of leukemia cells treated with the flavonoid casticin

This work was carried out in collaboration with TOLGA EICHHORN[2], ANASTASIA KARIOTI[1], ANNA RITA BILIA[1] and THOMAS EFFERTH[2]

[1]*Department of Pharmaceutical Sciences, University of Florence, Florence, Italy;*
[2]*Department of Pharmaceutical Biology, Institute of Pharmacy and Biochemistry, University of Mainz, Mainz, Germany*

1. INTRODUCTION

Leukemic diseases are a heterogeneous group of malignant diseases, some of which have a poor prognosis. Natural compounds are of considerable therapeutic interest for these tumors (Efferth, 2002). The search for anticancer agents with improved pharmacological features continues to be an important aspect for the discovery and development of novel therapeutic strategies. The huge structural diversity of natural compounds derived from plants, marine flora and microorganisms can serve as "lead" compounds for semi-synthetic derivatization and improvement of their therapeutic potential (Gordaliza, 2007).

As a starting point, the present study investigated the cytotoxic activity of 15 polyphenolic plant constituents belonging to different chemical classes, including flavonoids, phenylpropanoids, curcuminoids, catechins, and anthranoids. The rationale was to identify lead compounds with cytotoxic activity towards cancer cells. Polyphenols constitute one of the largest and ubiquitous groups of phytochemicals having a primary function to protect plants from photosynthetic stress, reactive oxygen species, and consumption by herbivores. Polyphenols are also present in large amounts in many vegetables and are thought to play a major role for health (Hounsome, 2008; Barnes, 2008; Gosh, 2009; McKay, 2011). Recently, a lower incidence of cancer in certain populations has been demonstrated to be related to the consumption of certain nutrients, and especially polyphenol-rich diets (Sporn, 2002). For this reason, there is an increasing interest using polyphenols as chemopreventive agents. This may be a promising approach aiming to reduce cancer-associated morbidity and mortality by delaying the process of carcinogenesis (Yang, 2001; Sing, 2009; Cui, 2009; Singh, 2010).

Polyphenols exert their anticancer activity not only by quenching the generation of reactive oxygen species and thereby protecting critical cellular targets (*i.e.*, DNA, proteins, lipids) from oxidative insult (Rafter, 2002; Potter, 1997; Roy, 2003). Their anticancer activity is also due to their interference with intracellular signaling pathways regulating proliferation, induction of apoptosis, and response to oxidative stress (Kong, 2001; Park, 2003; Loo, 2003; Heber, 2002). Among the investigated polyphenols, resveratrol has been shown to induce apoptotic cell death in HL60 human leukemia cells, but not in normal peripheral blood lymphocytes (Clement, 1998). Quercetin reduces cell proliferation, causes cell cycle arrest in the G0/G1 phase (Yoshida, 1992; Yoshida, 1990), the G2/M-phase (Koide, 1997; Choi, 2001) or the S-phase (Richter, 1999), and induces caspase-3 activity and apoptosis (Ritcher, 1999; Liesveld, 2003; Wang, 1999). Curcumin has anti-tumor activity in a variety of cell lines from solid tumors and leukemia *in vitro* as well as in animal tumor models (Duvoix, 2005). Ellagic acid causes G_0/G_1phase arrest, inhibition of proliferation, and induction of apoptosis (Narayanan, 1999; 2001). Epigallocatechin gallate induces internucleosomal DNA fragmentation in human epidermoid carcinoma cells, human carcinoma keratinocytes, human prostate carcinoma cells, mouse lymphoma cells, but not in normal human epidermal keratinocytes (Ahmad, 1997). The antitumor activity of other pholyphenols such as verbascoside, hypericin, pseudohypericin, and the novel constituents kaempferol-3-O-(2'',6''-di-*E*-p-coumaroyl)-β-

glucopyranoside or kaempferol-3-O-(3’’,4’’-diacetyl-2’’,6’’-di-*E*-p-coumaroyl)- β-glucopyranoside has not been investigated yet.

The multiple effects of flavonoids on gene regulation, cell proliferation and apoptosis in leukemia cells have recently been reviewed (Strissel, 2005). Matsui et al. (Matsui, 2005) demonstrated that six individual flavonoids, flavone, luteolin, apigenin, genistein, quercetin and fistein induced apoptosis in leukemia and lymphoma cell lines in a dose-dependent manner by disruption of mitochondrial membranes and activation of caspase-3.

Considering the growing interest in this field, a doxorubicin-sensitive acute T-lymphoblastic leukemia cell line (CCRF-CEM) and its multidrug-resistant subline (CEM/ADR5000) were used to evaluate the activity of 15 polyphenolic constituents derived from medicinal plant. Casticin was the most potent compound. To get insight into possible molecular modes of action, we performed microarray-based analyses to identify genes which are differentially regulated in treated cells compared to untreated controls.

2. MATERIALS AND METHODS

2.1 Plant Material

Fructus of *Vitex agnus-castus* (Verbenaceae) provided by Pierre Fabre (Pierre Fabre Laboratories, Boulogne, France) was used for the preparation of extract and the isolation procedures.

2.2 Polyphenols

Curcumin, epigallocatechin-3-gallate, silymarin, were purchased from Extrasynthese (Genay, France). The following compounds were isolated from plants as previously described: hypericin and pseudohypericin were isolated from *Hypericum perforatum* L. (Karioti, 2009a), rosmarinic acid and salvianolic acid B were isolated from *Salvia miltiorrhiza* (Wang, 2009), bergenin from *Ardisia crenata*, kaempferol-3-O-(2’’,6’’-di-*E*-p-coumaroyl)-β-glucopyranoside, kaempferol-3-O-(3’’,4’’-diacetyl-2’’,6’’-di-*E*-p-coumaroyl)-β-glucopyranoside, tiliroside and ellagic acid, were isolated from *Quercus ilex* (Karioti 2010; Karioti 2009b respect), oleuropein was isolated from *Olea europaea* (Karioti, 2006), verbascoside was isolated from *Lippia alba* (Timoteo, 2008), and casticin was isolated from the fruits of *Vitex agnus castus* L (Figure 1; Table1).

In brief, fruits of *Vitex agnus castus* L. (2 kg) were partially grounded and defatted with petroleum ether and exhaustively extracted with dichloromethane. The crude dichloromethane extract was partitioned with cyclohexane and MeOH (1:1) and the polar fraction was subsequently purified over Sephadex LH-20 column alternating between lipophilic (cyclohexane:CH_2Cl_2:MeOH, 7:4:1) and polar solvent systems (MeOH:H_2O, 90:10-70:30). The chemical structure of casticin was determined by combining the NMR and HPLC/DAD/MS data and by comparing its spectroscopic data with those reported in the literature (Han, 2007). Similarly, *Ardisia crenata* polar extract

containing bergenin (17%) and saponins was subjected to successive column chromatography over Sephadex LH-20 using polar mixtures of MeOH:H_2O 50:50 to give pure bergenin (purity > 98, checked by NMR and HPLC-DAD-MS).

2.3 Compound isolation and structure elucidation

^{1}H NMR spectra was recorded in CD_3OD on Bruker DRX-400 instrument at 295 K. Chemical shifts are given in parts per million (ppm) and were referenced to the solvent signals at 3.31 ppm for CD_3OD. The HPLC analyses were performed using a HP 1100 Liquid Chromatograph (Agilent Technologies, PaloAlto, CA, USA) equipped with a HP 1040 diode-array detector (DAD), an automatic injector, an auto sampler and a column oven and managed by a HP 9000 workstation (Agilent Technologies, Palo Alto, CA, USA). The HPLC system was interfaced with a HP 1100 MSD API electrospray (Agilent Technologies, Palo Alto, CA, USA). The interface geometry, with an orthogonal position of the nebulizer with respect to the capillary inlet, allowed the use of analytical conditions similar to those of HPLC-DAD analysis. Mass spectrometry operating conditions were optimized in order to achieve maximum sensitivity values: gas temperature 350ºC at a flow rate of 10 l/min, nebulizer pressure 30 psi, quadrupole temperature 30ºC, and capillary voltage 3500 V. Full scan spectra from m/z 100 to 800 in the positive-ion mode were obtained (scan time 1s). Separations were performed on a reversed phase column Purospher® Star RP-18, namely Hibar® Prepacked column RT (250×4.6 mm) with particle size 5 mm (Merck, Darmstadt, Germany). The eluents were A: water adjusted to pH 3.2 by formic acid; and B: acetonitrile. The mobile phase was isocratic using 50% A and 50% B for 15 min, following by gradient from 50% to 100% B in 5 min, at a flow rate of 1 mL/min. The system was operated with oven temperature at 26ºC; the injection volume was 20 µl. UV-VIS spectra between 210 and 350 nm, with a peak threshold of 0.1 mAu, were recorder; chromatograms were acquired at 280 nm for casticin. Column chromatography (CC) was carried out on a Sephadex LH-20 (Pharmacia). TLC: Merk silica gel 60 F_{254} (Art. 5554). Detection: UV-light, spray reagent (vanillin-H_2SO_4 on silica gel). All the solvents used for the extraction and HPLC analysis (MeOH, cyclohexane, dichloromethane, and acetonitrile) were HPLC grade from Merck (Darmstadt, Germany); 85% formic acid was provided by Carlo Erba (Milan, Italy). Water was purified using a Milli-Qplus system (Milford, MA, USA).

2.4 Cell lines

A drug-sensitive acute T-lymphoblastic leukemia cell line (CCRF-CEM) and its multidrug resistant subline (CEM/ADR5000) were used in XTT assay to evaluate the activity of the compounds. Human CCRF-CEM leukemia cells were maintained in RPMI-1640 (Invitrogen) supplemented with 10% FBS, antibiotics (1% of a 10,000 U/ml Penicillin G and 10 mg/ml Streptomycin), in a humidified 7% CO_2 atmosphere at 37ºC. Cells were passaged twice weekly. All experiments were done with cells in the logarithmic growth phase. The establishment of drug-resistant subline has been previously described (Kimmig, 1990). Drug-resistant CEM-ADR5000 cells were maintained

in the absence of drug and resistance was stabilized by treatment for one day every week with doxorubicin (5000 ng/ml). CEM/ADR5000 cells specifically over-express P-glycoprotein/*MDR1/ABCB1*, but none of the other resistance-related ATP-binding cassette (ABC) transporters (Efferth, 2003; Gillet, 2004). The cross-resistance profile of CEM/ADR5000 cells to established anti-cancer drugs and a panel of natural products has been previously published (Kimmig, 1990; Efferth, 2008).

2.5 XTT Assay

The cytotoxicity of compounds was determined by means of the Cell Proliferation Kit II (Roche Diagnostics, Mannheim, Germany). This test is based on the cleavage of the yellow 2,3-bis[2-methoxy-4-nitro-5-sulfophenyl]-2H-tetrazolium-5-carboxanilideinner salt (XTT) by ubiquitous dehydrogenases leading to the formation of an orange formazan dye (Scudiero, 1988). The amount of dye is commensurate to the number of metabolic active cells. Fresh stock solutions of each compound were prepared in DMSO or H_2O at a concentration of 100 mM. A dilution series ranging from 10^{-4} M to 10^{-9} M was prepared using RPMI medium to perform the XTT test. Cells were diluted to a final concentration of 1×10^5 cells/mL, and 100 µl of the cell suspension were sowed into the wells of a 96-well culture plate (Costar, Corning, USA). Marginal wells were filled with 100 µl of pure medium, in order to minimize effects of evaporation. Besides, wells filled with medium were required to determine the background absorbance caused by non metabolized XTT. A row of wells containing cells was left untreated, and another row of wells containing cells was treated with 1 µl of DMSO or H_2O. This served as solvent control. The other rows of wells containing cells were supplemented with different concentrations of compound. Each concentration was tested in at least two independent plates containing different batches of cells. After incubation for 72h with compounds at 37ºC, 5% CO_2 in humidified atmosphere, XTT reagent was freshly prepared and added to each well as specified by the manufacturer: XTT-labeling reagent and electron-coupling reagent were mixed in a ratio of 50:1, and 50 µl of this mixture were added to each well of the 96-well plate. The plates were incubated for about 6 h at 37ºC, 5% CO_2 in humidified atmosphere and read out after incubation. Quantification of cell cytotoxicity was performed in an ELISA plate reader (Bio-Rad, Munich, Germany) at 490 nm with a reference wavelength of 655 nm. Absorbance values at both wavelengths were subtracted. The cytotoxic effect of the treatment was determined as percentage of viability and compared to untreated cells (Konkimalla, 2010). The toxicity of compounds was determined by means of the formula:

Cell viability (%) = (Absorbance of sample cells/Absorbance of untreated cells) × 100

All *in vitro* experiments were carried out on two microplates with six parallel wells. All values are expressed as the mean ± SD of two independent experiments with each six-fold parallel measurements.

2.6 RNA isolation and analysis

Total RNA was isolated using the RNeasy Kit (Qiagen, Hamburg, Germany) according to the manufacturer's instructions. The quality of total RNA was checked by gel analysis using the total RNA Nano chip assay on an Agilent 2100 Bioanalyzer (Agilent Technologies GmbH, Berlin, Germany). Only samples with RNA index values greater than 8.5 were selected for expression profiling. RNA concentrations were determined using the NanoDrop spectrophotometer (NanoDrop Technologies, Wilmington, DE).

2.7 Probe labeling and Illumina Sentrix Bead Chip Array Hybridization

Biotin-labeled cRNA samples for hybridization on Illumina Human Sentrix-8 BeadChip arrays (Illumina, Inc.) were prepared according to Illumina's recommended sample labeling procedure based on the modified Eberwine protocol (Eberwine, 1992). In brief, 250 ng total RNA was used for complementary DNA (cDNA) synthesis, followed by an amplification/labeling step (*in vitro* transcription) to synthesize biotin-labeled cRNA according to the MessageAmp II aRNA Amplification kit (Ambion, Inc., Austin, TX). Biotin-16-UTP was purchased from Roche Applied Science, Penzberg, Germany. The cRNA was column purified according to TotalPrep RNA Amplification Kit, and eluted in 60 µl of water. Quality of cRNA was controlled using the RNA Nano Chip Assay on an Agilent 2100 Bioanalyzer and spectrophotometrically quantified (NanoDrop).
Hybridization with containing 19.730 genes per microarray was performed as previously described (Kimmig, 1990).

2.8 Scanning and data analysis

Microarray scanning was performed using a Beadstation array scanner, and the setting was adjusted to a scaling factor of 1 and PMT settings at 430. Data extraction was individually done for all beads, and outliers were removed, if median absolute deviations (MAD) were above 2.5. All remaining data points were used for calculation of the mean average signal of a sample. Standard deviations were calculated of all samples.
Data analysis was done by normalization of signals using the quantile normalization algorithm without background subtraction. Differentially regulated genes were defined by calculating the standard deviation differences of a given sample in one-by-one comparisons of samples or groups.
Genes were further filtered using Chipster software (http://chipster.csc.fi/) by discarding genes with a P-value lower than 0.05 and having a differential expression above one time of standard deviaton. The final set of filtered genes was analyzed using Ingenuity Pathway Analysis (http://www.ingenuity.com/) to identify affected networks of genes and pathways.

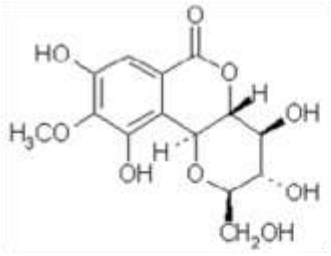

Bergenin

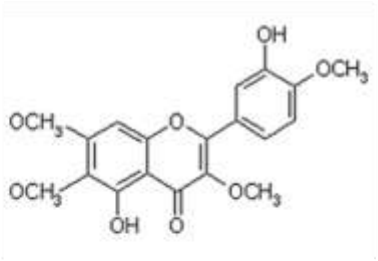

Casticin

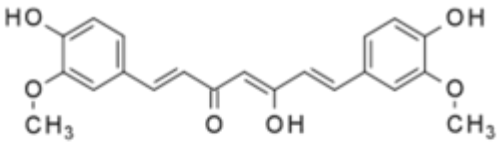

Curcumin

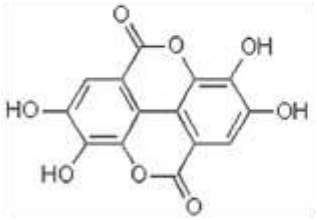

Ellagic acid

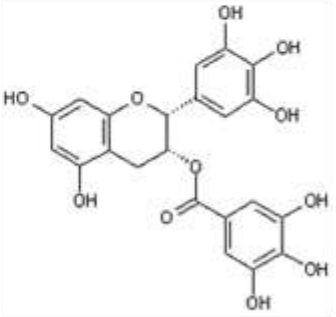

Epigallocatechine-3-gallate

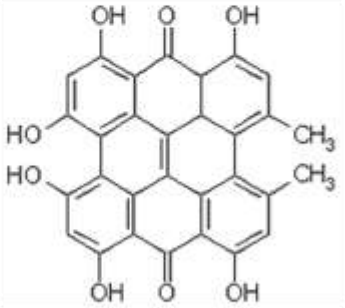

Hypericin

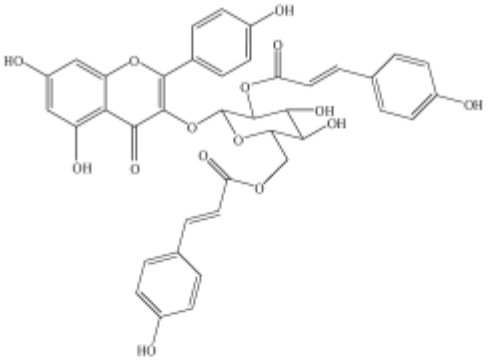

Kaempferol-3-O-(2'',6''-di-*E*-p-coumaroyl)-glucopyranoside

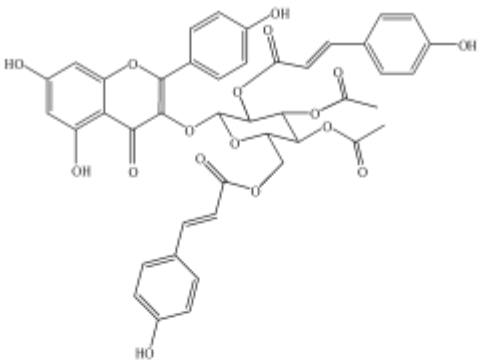

Kaempferol-3-O-(3,4-diacetyl-2,6-di-*E*-p-coumaroyl)-glucopyranoside

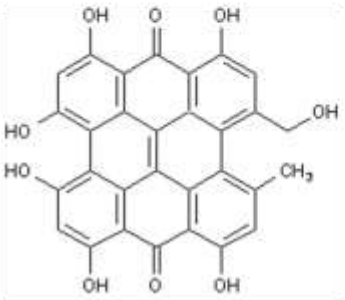

Pseudo-hypericin

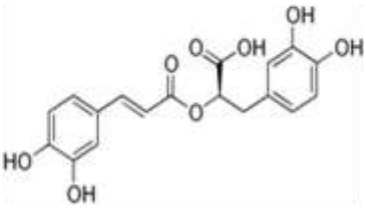

Rosmarinic acid

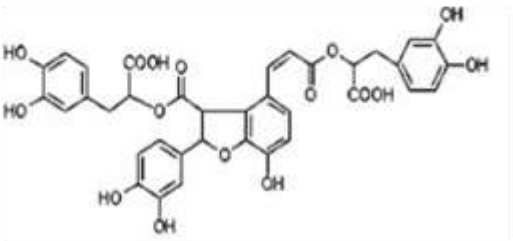

Salvianolic acid B

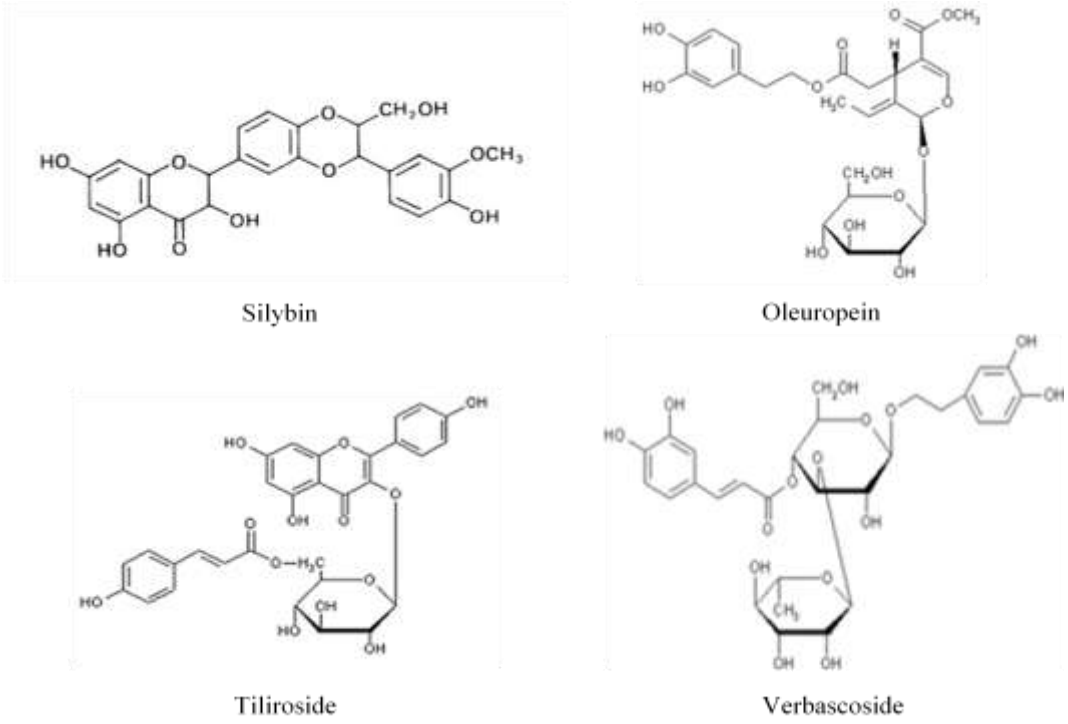

Figure 1: *Chemical structures of the compounds investigated*

3. RESULTS

3.1 Isolation of polyphenols

All polyphenols used in the present investigation were from commercial sources or isolated in our laboratory during previous projects (see Material and Methods) (Table 1). Casticin was isolated for the first time in the course of the present study. The presence of casticin was evidenced by monitoring of the fractions by thin layer chromatography. The casticin fraction was analyzed by NMR spectroscopy (^{1}H NMR) and HPLC-DAD-ESI-MS analyses (Figure 2A and 2B) and data were compared with those reported in the literature (Han, 2007). HPLC analyses indicated that casticin has a purity of 97% based on the peak area percent (Figures 2C).

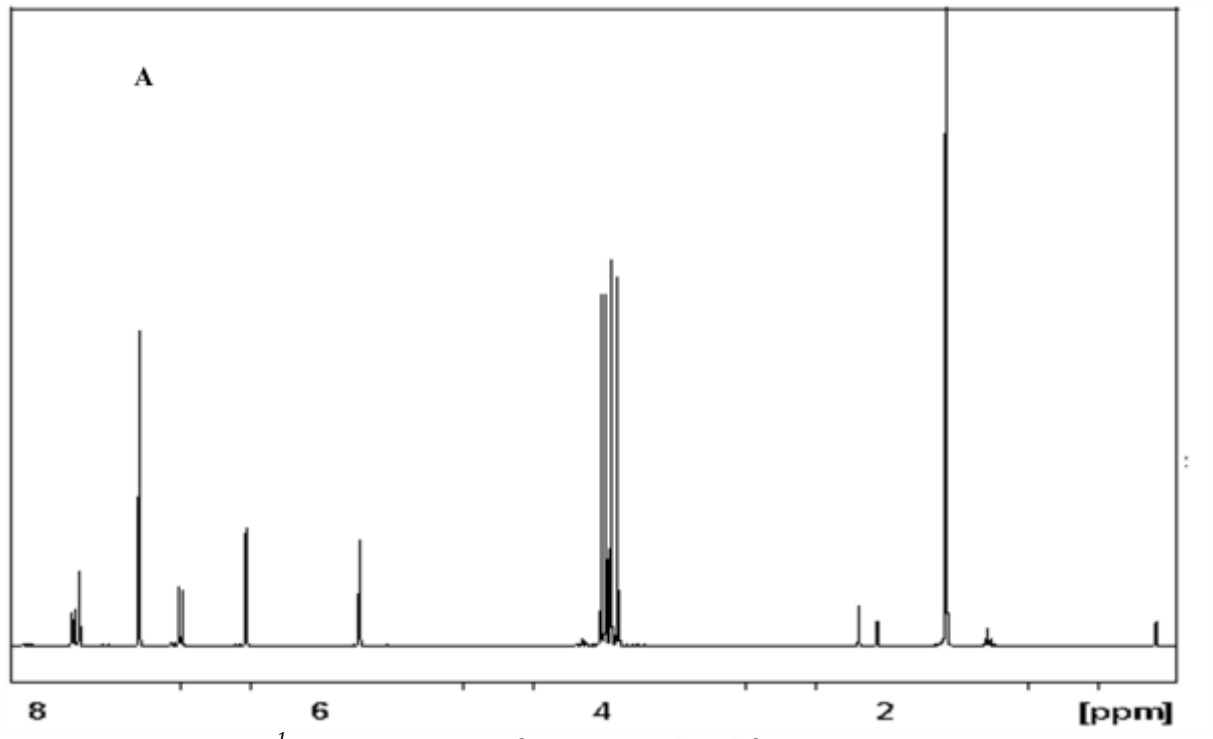

Figure 2A: *^{1}H NMR spectra of casticin isolated from Vitex agnus castus.*

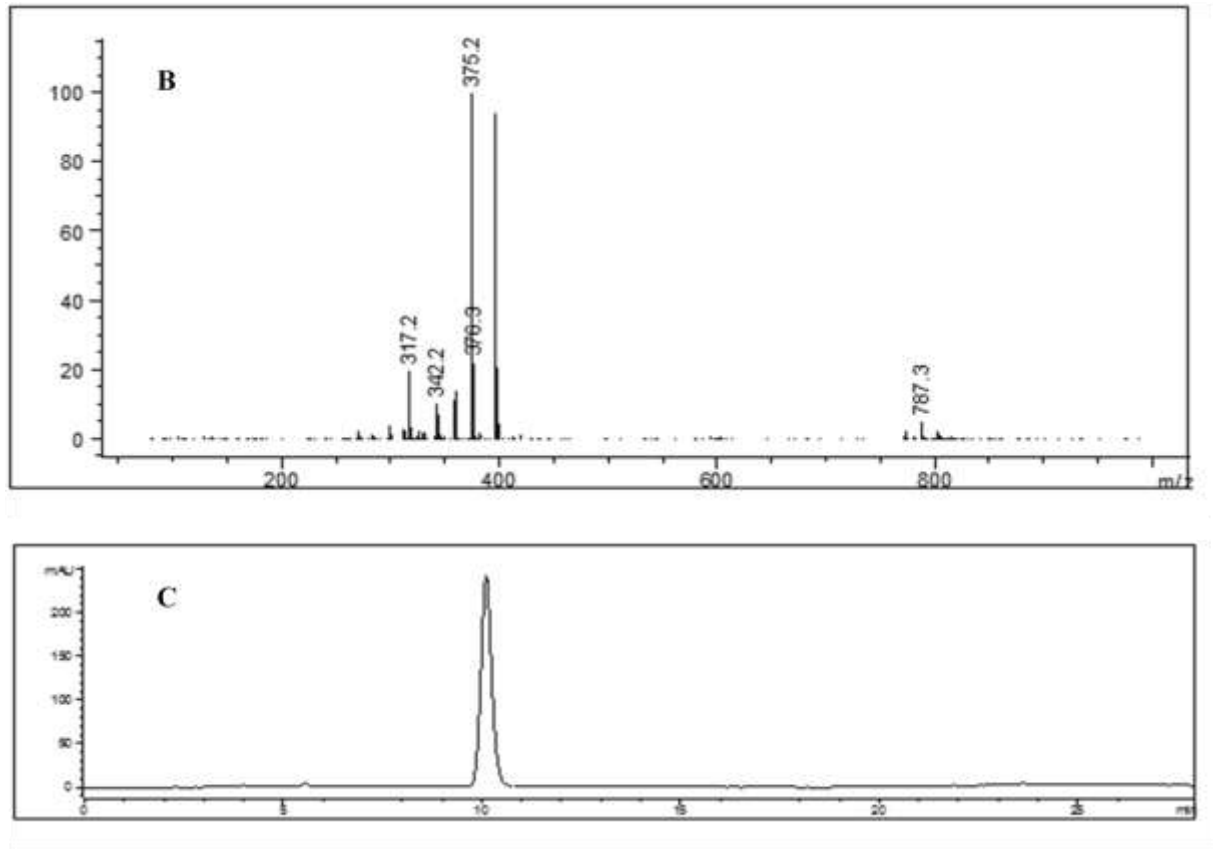

Figure 2B: *HPLC-ESI-MS and* ***2C:*** *HPLC-DAD chromatograms of casticin isolated from Vitex agnus castus.*

	MW	Purity	Medicinal plant of origin
Commercial Compounds			
Curcumin	368	≥ 98%	*Curcuma longa*
Epigallocatechin-3-gallate	458	≥ 98%	*Camellia sinensis*
Silybin (Silymarin)	482	_	*Silybum marianum*
Compounds isolated in house			
Bergenin	328	≥ 98%	*Ardisia crenata*
Casticin	374	≥ 98%	*Vitex agnus castus*
Ellagic acid	302	≥ 98%	*Quercus ilex*
Hypericin	504	≥ 98%	*Hypericum perforatum*
Kaempferol-3-O-(2'',6''-di-*E*-p-coumaroyl)-glucopyranoside	740	≥ 98%	*Quercus ilex*
Kaempferol-3-O-(3,4-diacetyl-2,6-di-*E*-p-coumaroyl)-glucopyranoside	824	≥ 98%	*Quercus ilex*
Oleuropein	540	≥ 98%	*Olea europaea*
Pseudo-hypericin	522	≥ 98%	*Hypericum perforatum*
Rosmarinic acid	360	≥ 98%	*Salvia miltiorrhiza*
Salvianolic acid B	718	≥ 98%	*Salvia miltiorrhiza*
Tiliroside	594	≥ 98%	*Quercus ilex*
Verbascoside	624	≥ 98%	*Lippia alba*

Table 1: *Phytochemical compounds and their plant origins.*

3.2 Cytotoxicity of phytochemicals toward sensitive and multidrug-resistant leukemia cells

The cytotoxicity of casticin has been determined towards wild-type CCRF-CEM leukemia cells and a multidrug-resistant subline thereof, CEM/ADR5000. For comparison, 14 other phytochemicals have been tested in these two cell lines. The IC_{50} values calculated from dose response curves are shown in Table 2. The phytochemicals most active towards CCRF-CEM cells were casticin, hypericin, and kaempferol-3-O-(3'',4''-diacetyl-2'',6''-di-*E-p*coumaroyl)-glucopyranoside. These compounds were tested in a multidrug-resistant subline of CCRF CEM, CEM/ADR5000. Of them, casticin had the lowest IC_{50} value for both cell lines. CEM/ADR5000 exhibited a low degree of cross-resistance towards casticin (1.57-fold). No or only weak cross-resistance was observed towards pseudo-hypericin, hypericin, oleuropein, verbascoside and kaempferol-3-O-(3'',4''-

diacetyl-2’’,6’’-di-*E*-*p*-coumaroyl)-β glucopyranoside (0.84-to 1.95-fold). CEM/ADR5000 exhibited a higher degree of cross-resistance towards curcumin (16.98-fold).

Compound	**CCRF-CEM (IC_{50})**	**CEM-ADR5000 (IC_{50})**	**Relative resistance***
Bergenin	Inactive	Inactive	-
Casticin	0.28±0.02 μM	0.44±0.17 μM	1.57
Curcumin	3.74±2.26 μM	63.50 μM	16.98
Ellagic acid	164.10±30.69 μM	Inactive	-
Epigallocatechin-3-gallate	16.04±1.56 μM	Inactive	-
Hypericin	1.52±0.23 μM	1.34±0.11 μM	0.88
Kaempferol-3-O-(2’’,6’’-di-E-p-coumaroyl)-glucopyranoside	57.43±22.75 μM	111.92±19.49 μM	1.95
Kaempferol-3-O-(3,4-diacetyl-2,6-di-E-p-coumaroyl)-glucopyranoside	2.15±0.37 μM	Inactive	-
Oleuropein	66.14±15.75 μM	70.05±1.30 μM	1.06
Pseudo-hypericin	12.14±5.10 μM	11.99±4.8 μM	0.99
Rosmarinic acid	80.95±15.97 μM	Inactive	-
Salvianolic acid B	Inactive	Inactive	-
Silymarin	68.12±16.33 μM	Inactive	-
Tiliroside	Inactive	Inactive	-
Verbascoside	97.27±3.65 μM	81.90±23.84 μM	0.84

Table 2: *50% inhibition concentration (IC_{50}) values (expressed as the mean±SD of two independent experiments each with six-fold determination) and relative resistance to natural compounds in CCRF-CEM cells and multidrug-resistant CEM/ADR5000 cells as determined by the XTT test. The IC_{50} values were calculated from dose-response curves using GraphPad Prism 5.0 (GraphPad Software Inc., San Diego, CA). *Relative resistance was calculated by dividing the IC_{50} of CCRF-CEM cells by the IC_{50} of CEM/ADR5000 cells.*

3.3 Differential gene expression in casticin-treated and untreated cells

The effect of casticin treatment on gene expression was determined by microarray-based mRNA hybridization. CCRF-CEM cells were treated with the IC_{50} dose of casticin (0.28 μM) for 24 or 72h or left untreated.

A total of 186 genes were up-regulated and 302 genes were down-regulated upon treatment for 24 h compared to untreated cells. After 72h treatment, 219 genes were up- and 72 genes down-regulated. In order to further analyze the molecular modes of action of casticin, we performed a signaling pathway analysis by means of the Ingenuity Pathway Analysis software. The most prominent functional groups of genes differentially regulated upon casticin treatment for 24 h ($p<0.05$) were

those involved in drug metabolism, lipid metabolism, small molecule biochemistry, and cell cycle (Figure 3A). Treatment of CCRF-CEM cells for 72 h affected genes involved in cell cycle, cellular assembly and organization, DNA replication and repair as well as cell death (Figure 3B). As a next step, we asked whether these genes from diverse functional classes act independently or whether they act together beyond the constraints of "canonical" pathways in a concerted manner after casticin challenge. For this reason, we built dynamic network analyses using the differentially regulated genes. As shown in Figure 4, specific pathways of interacting genes appeared after casticin treatment. A specific molecular network with a connection to cell death and cellular growth and proliferation was determined in CCRF-CEM cells treated for 24 h with casticin (Figure 4A). A comparable molecular network related to cellular growth and proliferation was identified in CCRF-CEM cells after 72 h treatment with casticin (Figure 4B). Interestingly, both networks were related to the same cellular regulators, *i.e.*, NFKB, p38MAPK, histones H3 or H4, and FSH, indicating importing functions for the activity of casticin in CCRF-CEM cells.

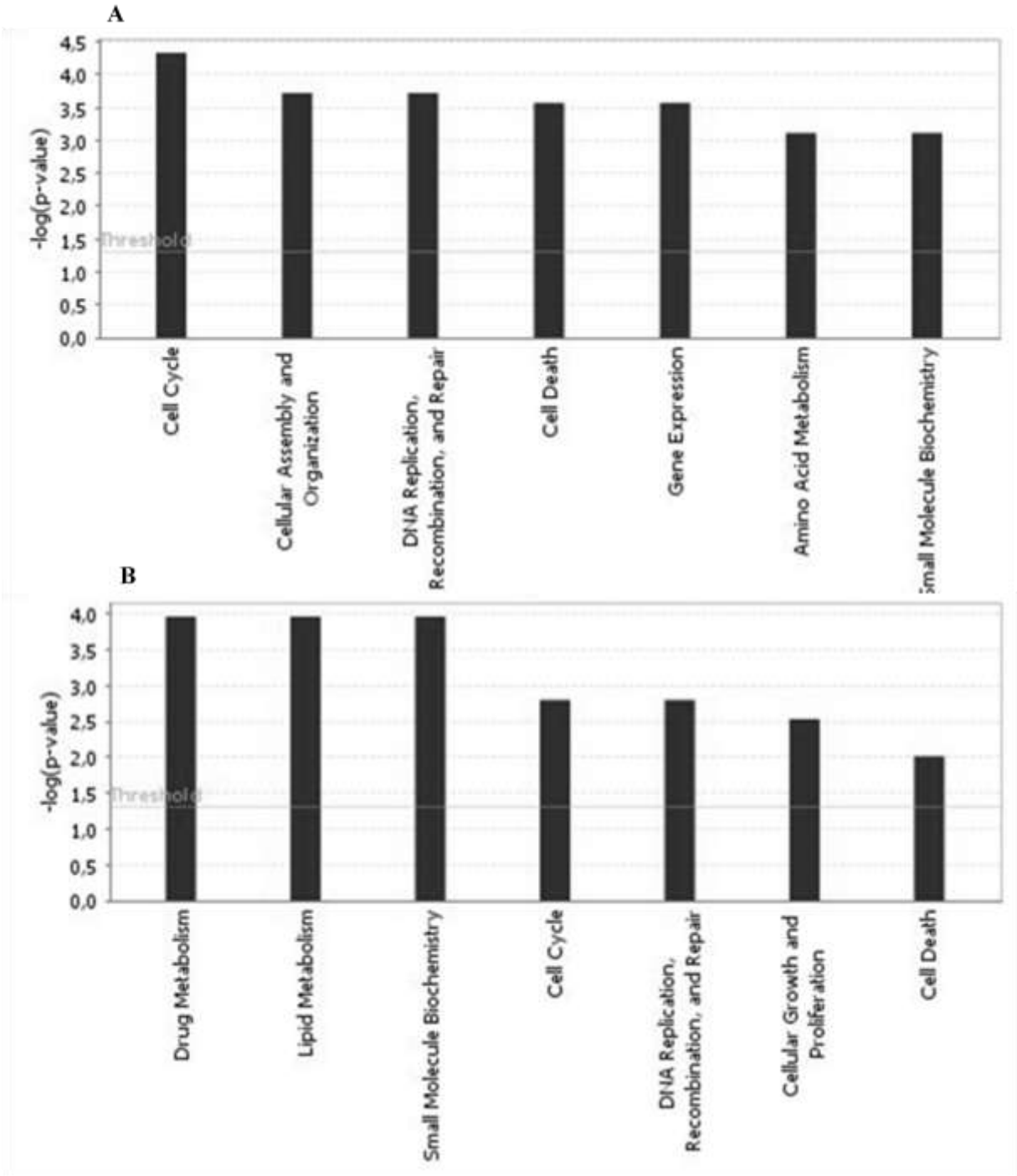

Figure 3: *mRNA-based microarray analyses of CCRF-CEM cells treated with casticin. Microarray hybridizations were performed using Illumina Sentrix BeadChip arrays (see Material and Methods). Identification of functional groups of genes regulated upon casticin treatment for 24 h* ***(A)*** *and 72 h* ***(B)*** *in CEM-CCRF cells. Gene expressions of cells treated with 50% inhibition concentration of casticin were compared to those in untreated cells. The evaluation of differentially expressed genes was performed using the Ingenuity Pathway Analysis software, version 5.5.*

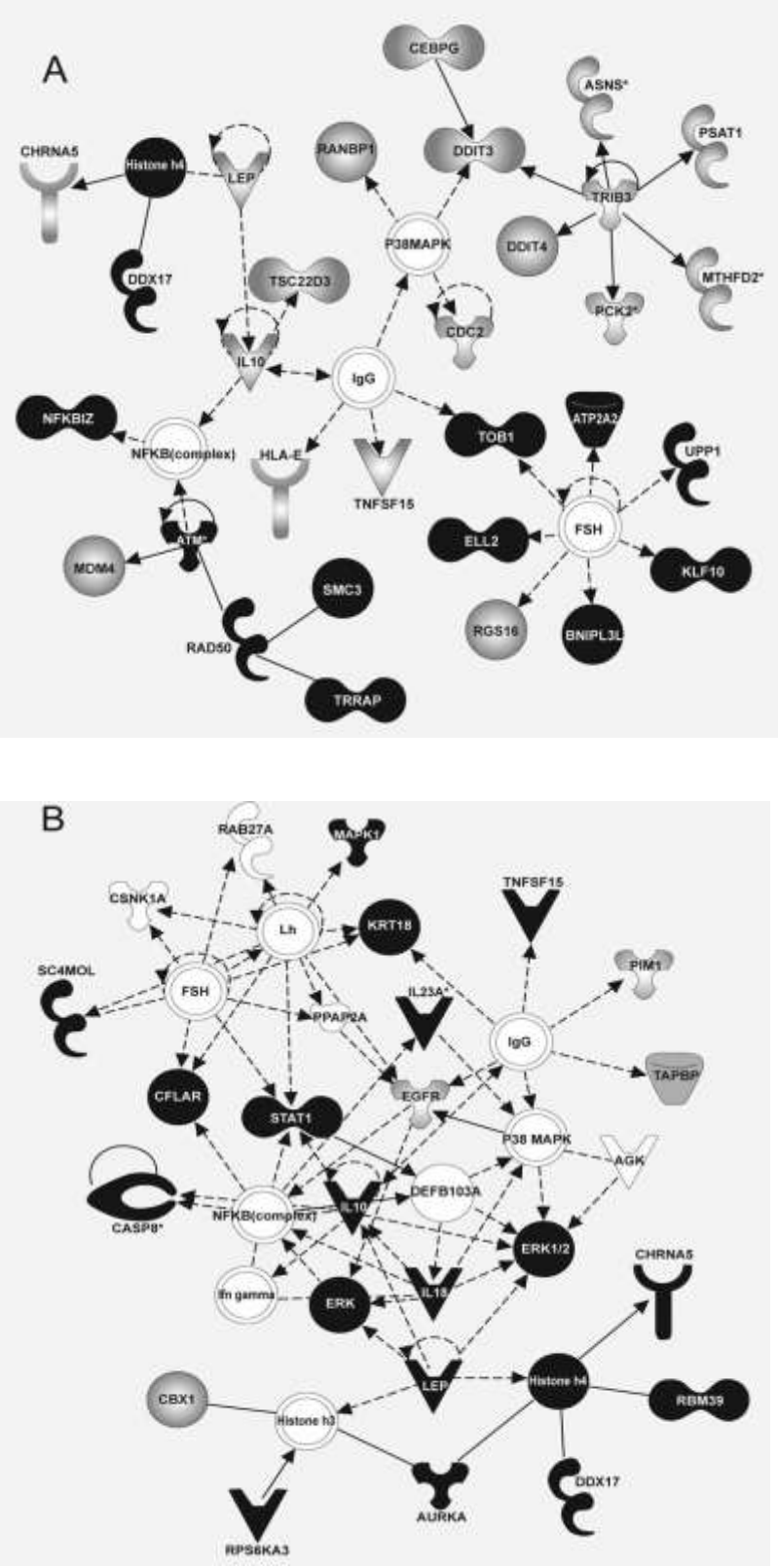

Figure 4: *Signaling network of CCRF-CEM leukemia cells treated with casticin (50% inhibition concentration) for 24 h* ***(A)*** *or 72 h* ***(B)****.*

4. DISCUSSION

In the present study, casticin was the most cytotoxic polyphenol towards CCRF-CEM leukemia cells among a group of 15 polyphenols. Casticin is an unusual polymethoxy-flavonoid bearing a methoxyl moiety at C-3 of the C-ring, which is an essential structure activity requirement of flavones for cytotoxicity (Beutler, 1998). The presence of this methoxyl group at C-3 may explain why casticin was more cytotoxic than the other polyphenols investigated by us. Polymethoxyflavones, bearing two or more methoxy groups on their basic benzo-γ-pyrone skeleton with a carbonyl group at the C4 position, are found in a limited number of plant families. Polymethoxyflavones structurally related to casticin display chemoprotective effects by inhibiting cancer cell growth, induction of apoptosis, and blocking metastasis (Li, 2009). The rate of methylation of polyphenols in chemoprevention is not fully understood. The enhanced permeability of cellular membranes to polymethoxyflavones due to their lipophilic nature may lead to enhanced cellular absorption and bioactivity. In addition, methylation may increase the oral bioavailability of these compounds. In the past, polymethoxyflavones raised only modest interest for chemoprevention because of their lack of antioxidant properties, which was suggested as a main mechanism of action. However, recent findings point to signal transduction pathways as being the main targets for flavonoids (Williams, 2004).

Polyphenols may modulate various targets either by direct interaction or by modulation of gene expression. To gain insight into the molecular networks and pathways related to the cytotoxicity of casticin towards cancer cells, we performed mRNA-based microarray analysis. Upon treatment of CCRF-CEM cells with casticin, several genes that form a network related to the transcription factor NF-κB were differentially expressed. Hence, casticin may act in part by affecting NF-κB signaling. Casticin has been described to inhibit NF-κB and many other flavonoids are also well known NF-κB inhibitors (Nam, 2006; Gillet, 2004). NFκB plays a major role in regulating immune response, cell proliferation, and apoptosis. Seven related proteins (NF-κB1 and NF-κB2, each with two alternatively spliced forms, and REL-A, REL-B and c-REL) can form dimers, which are able to bind specific DNA motifs in the promoters of target genes (Nam, 2006; Gilmore, 2006; Brasier, 2006). These heterodimers can activate the transcription of about 200 target genes (Perkins, 2007). Inactive NF-κB1 or NF-κB2 proteins are complexed with IκBα (inhibitory κB) proteins in the cytosol. Phosphorylation of IκBα by IκBα kinase (IKK) leads to IκB degradation and translocation of NF-κB1 and NF-κB2 into the nucleus. Casticin demonstrated anti-inflammatory effects *in vivo* (Kobayakawa, 2004) confirming the use of plants from the genus *Vitex* for the treatment of inflammation in European, Asian and Chinese traditional medicines. In addition, casticin inhibited leukemia and breast cancer growth *in vitro* (Wang, 2005; Haidara, 2006). The results of our microarray analysis testify to NF κB as being involved in the underlying mechanism of casticin against cancer cells.

p38MAPK is another protein in the network affected by casticin treatment of CCRF-CEM cells. MAPKs form signaling cascades regulating important cellular functions such as cell growth, differentiation and apoptosis (Vakifahmetoglu, 2008 ;Pearson, 2001). They are activated by stress

stimuli including cancer therapy (Vega, 2004). No effect on p38MAPK signaling by casticin has yet been described, but p38MAPK inhibition is known for other polyphenols (Choi, 2008; Li, 2009; Adhikary, 2010; Ho, 2010). p38MAPK is known to act upstream of NF-κB and to activate NF-κB (Itatsu, 2009) indicating that the effect of casticin on both these signaling molecules may contribute to its cytotoxic properties. Interestingly, another polyphenol, furosin, has been reported to suppress RANKL-induced osteoclast differentiation and function through inhibition of MAPK activation (Park, 2004). Together with our results concerning casticin, this may speak for a more general role of polyphenols affecting RANKL, NF-κB, and MAPK signaling pathways.

Casticin treatment led to differential expression of a network of genes with different functions, including histones. Histones are constituents of nuclear chromatin and organize DNA condensation during meiotic and mitotic chromosome formation. The histones H3 and H4, which appeared in our casticin-specific genetic network are core histones whose epigenetic modifications (*e.g.* methylation, acetylation, phosphorylation SUMOylation, and ubiquitinylation) play a role in gene regulation (Rosenfeld, 2009). While casticin is not yet known to affect histones, the role of flavonoids in chromatin remodeling during inflammatory processes is well described (Rahman, 2006; Gilbert, 2010; Rahman, 2010). Epigenetic modification by flavonoids may represent an attractive novel treatment strategy for cancer, and as such deserves further exploration.

In our microarray-based network, another set of genes centered on FSH. In both females and males, FSH regulates the maturation of germ cells, and the development, growth and pubertal maturation of the organism (Dickerson, 2008). Interestingly, endothelia of tumor blood vessels frequently reveal elevated FSH receptor levels, and FSH seems to contribute to neoangiogenesis in tumors by vascular endothelial growth factor-dependent and independent pathways (Radu, 2010). Hence, inhibition of FSH signaling may represent a strategy for antiangiogenic cancer therapy. Our finding that casticin affected FSH-associated genes in the signaling network may be taken as a hint that casticin might inhibit tumor angiogenesis. This speculation merits further analysis.

In conclusion, the cytotoxicity of casticin towards sensitive and multidrug-resistant leukemia cells was associated with multiple effects on different signal transduction pathways. A general feature of natural products is their ability to act on multiple targets and pathways rather than one single target (Efferth, 2011). This plays a major role in preventing the development of resistance, which has been an important selection advantage during the evolution of life. In the case of casticin, this feature might be explained in future therapy of cancers.

5. REFERENCES

Adhikary A,., et al., Theaflavins retard human breast cancer cell migration by inhibiting NF-κB *via* p53-ROS cross-talk. FEBS Lett. 2010, 584: 7-14.

Ahmad N., et al., Green tea constituent epigallocatechin-3-gallate, and induction of cell cycle arrest in human carcinoma cells. J Natl Cancer Inst. 1997, 89: 1881–1886.

Barnes S., et al., Nutritional genomics, polyphenols, diets, and their impact on dietetics. J Am Diet Assoc. 2008, 108: 1888-1895.

Beutler J.A., et al., Structure-activity requirements for flavone cytotoxicity and binding to tubulin. J Med Chem. 1998, 41: 2333–2338.

Brasier A.R., et al., The NF-κB regulatory network. Cardiovasc Toxicol. 2006, 6: 111-130.

Choi J.A., et al., Induction of cell cycle arrest and apoptosis in human breast cancer cells by quercetin. Int J Oncol. 2001, 19: 837–844.

Choi J.S., et al., Dietary flavonoids differentially reduce oxidized LDL-induced apoptosis in human endothelial cells: role of MAPK and JAK/STAT signaling. J Nutr. 2008, 13: 983- 990.

Clement M.V., et al., Chemopreventive agent resveratrol, a natural product derived from grapes, triggers CD95 signalling-dependent apoptosis in human tumor cells. Blood. 1998, 92: 996–1002.

Cui X., et al., Resveratrol suppresses colitis and colon cancer associated with colitis. Cancer Prev Res (Phila Pa) 2010, 3: 549–559.

Dickerson L.M., et al., Chapter 8: Pharmacotherapy: a pathophysiologic approach. Wells BG, DiPiro, JT, Talbert RL, Yee GC, and Matzke GR (eds.): McGraw-Hill Medical, New York, NY, USA. 2008. pp. 1313-1328.

Duvoix A., et al., Chemopreventive and therapeutic effects of curcumin. Cancer Lett. 2005, 223: 181–190.

Eberwine J., et al., Analysis of gene expression in single live neurons. Proc Natl Acad Sci USA, 1992, 89: 3010-3014.

Efferth T. et al., Complex interactions between phytochemicals. The multitarget therapeutic concept of phytotherapy. Curr Drug Targets, 2011, 12: 122-132.

Efferth T., et al., Activity of drugs from Traditional Chinese Medicine toward sensitive and MDR1- or MRP1-overexpressing multidrug-resistant human CCRF-CEM leukemia cells. Blood Cells Mol Di. 2002, 28: 160– 168.

Efferth T., et al., Molecular modes of action of artesunate in tumor cell lines. Mol Pharmacol. 2003, 64: 382-394.

Efferth T., et al., Prediction of broad spectrum resistance of tumors towards anticancer drugs. Clin Cancer Res. 2008, 14: 2405-2412.

Ghosh D., et al., Vascular action of polyphenols. Mol Nutr Food Res. 2009, 53: 322-331.

Gilbert E.R., et al., Flavonoids influence epigenetic modifying enzyme activity: structure - function relationships and the therapeutic potential for cancer. Curr Med Chem. 2010, 17: 1756- 1768.

Gillet J.P., et al., Microarray-based detection of multidrug resistance in human tumor cells by expression profiling of ATP-binding cassette transporter genes. Cancer Res. 2004, 64: 8987-8993.

Gilmore T.D., et al., Introduction to NF-κB: players, pathways, perspectives. Oncogene. 2006, 25: 6680-6684.

Gordaliza M., Natural products as leads to anticancer drugs. Clin Transl Oncol. 2007, 9: 767-776.

Haidara K., et al., The flavonoid casticin has multiple mechanisms of tumor cytotoxicity action. Cancer Lett. 2006, 242: 180-190.

Han X., et al., Isolation of high-purity casticin from *Artemisia annua* L. by high-speed counter-current chromatography. J Chromatogr A. 2007, 1151: 180-182.

Heber D., et al., Overview of mechanisms of action of lycopene. Exp Biol Med. 2002, 227: 920–923.

Ho H.H., et al., Anti-metastasis effects of gallic acid on gastric cancer cells involves inhibition of NF-κB activity and down-regulation of PI3K/AKT/small GTPase signals. Food Chem Toxicol. 2010, 48: 2508-2516.

Hounsome N., et al., Plant metabolites and nutritional quality of vegetables. J Food Sci. 2008, 73: R48-R65.

Itatsu K., et al., Phosphorylation of extracellular signal-regulated kinase 1/2, p38 mitogen-activated protein kinase and nuclear translocation of nuclear factor-κB are involved in up-regulation of matrix metalloproteinase-9 by tumour necrosis factor-α. Liver Int. 2009, 29: 291-298.

Karioti A., et al., Proanthocyanidin glycosides from the leaves of *Quercus ilex* L. (Fagaceae) Tetrahedron Lett. 2009, 50: 1771-1776.

Karioti A., et al., *Quercus ilex* L.: A rich source of polyacylated flavonoid glucosides. Food Chem. 2010. 123: 131-142.

Karioti A., et al., Novel Secoiridoid glucosides in *Olea europaea* leaves suffering from boron deficiency. Biosci Biotechnol Biochem. 2006, 70: 1898-1903.

Karioti A., et al., Rapid and efficient purification of naphthodianthrones from St. John's Wort extract by using liquid-liquid extraction and SEC. J Sep Sci. 2007, 32: 1374-1382.

Kimmig A., et al., Susceptibility of multidrug-resistant human leukemia cell lines to human interleukin 2-activated killer cells. Cancer Res. 1990, 50: 6793-6799.

Kobayakawa J,., et al., G2/M arrest and antimitotic activity mediated by casticin a flavonoid isolated from Viticis Fructus (*Vitex rotundifolia* Linne fil.). Cancer Lett. 2004, 208: 59-64.

Koide T., et al., Influence of flavonoids on cell cycle phase as analyzed by flow cytometry. Cancer Biother Radiopharm. 1997, 12: 111–115.

Kong A. N., et al., Induction of xenobiotic enzymes by the MAP kinase pathway and the antioxidant or electrophile response element (ARE/EpRE), Drug Metab Rev. 2001, 33: 255–271.

Konkimalla V. B., et al., Inhibition of epidermal growth factor receptor over-expressing cancer cells by the aphorphine-type isoquinoline alkaloid, dicentrine. Biochem Pharmacol. 2010, 79: 1092-1099.

Li Y., et al., Green tea polyphenols down-regulate caveolin-1 expression *via* ERK1/2 and p38MAPK in endothelial cells. J Nutr Biochem. 2009, 20: 1021-1027.

Liesveld J.L., et al., Flavonoid effects on normal and leukemic cells. Leuk Res. 2003, 27: 517–527.

Lin S., et al., *In vivo* effect of casticin on acute inflammation. Zhong Xi Yi Jie He Xue Bao. 2007, 5: 573–576.

Loo G., Redox-sensitive mechanisms of phytochemicalmediated inhibition of cancer cell proliferation. J Nutr Biochem. 2003, 14: 64–73.

Matsui J., et al., Dietary bioflavonoids induce apoptosis in human leukemia cells. Leuk Res. 2005, 29: 573–582.

McKay J.A., et al., Diet induced epigenetic changes and their implications for health. Acta Physiol (Oxf). 2011, 202:103-18.

Nam N.H., Naturally occurring NF-κB inhibitors. Mini Rev Med Chem. 2006, 6: 945-95.

Narayanan B.A., et al., p53/p21(WAF1/CIP1) expression and its possible role in G1 arrest and apoptosis in ellagic acid treated cancer cells. Cancer Lett. 1999, 136: 215–221.

Narayanan B.A., et al., IGF-II down regulation associated cell cycle arrest in colon cancer cells exposed to phenolic antioxidant ellagic acid. Anticancer Res. 2001, 21: 359–364.

Park A.M., et al., Signal transduction pathways: targets for green and black tea polyphenols. J Biochem Mol Biol. 2003, 36: 66–77.

Park E.K., et al., Furosin, an ellagitannin, suppresses RANKL-induced osteoclast differentiation and function through inhibition of MAP kinase activation and actin ring formation. Biochem Biophys Res Commun. 2004, 325: 1472-1480.

Pearson G., et al., Mitogen-activated protein (MAP) kinase pathways: Regulation and physiological functions. Endocr Rev. 2001, 22: 153-183.

Perkins N.D., et al., Integrating cell-signalling pathways with NF-κB and IKK function. Nat Rev Mol Cell Biol. 2007, 8: 49-62.

Potter J.D., Cancer prevention: epidemiology and experiment. Cancer Lett. 1997, 114: 7–9.

Radu A., et al., Expression of follicle stimulating hormone receptor in tumor blood vessels. N Engl J Med. 2010, 363: 1621-1630.

Rafter J.J., et al., Scientific basis of biomarkers and benefits of functional foods for reduction of disease risk: cancer. Br J Nutr. 2002, 88 (Suppl. 2): S219–S224.

Rahman I. et al., Dietary polyphenols, deacetylases and chromatin remodeling in inflammation. World Rev Nutr Diet. 2010, 101: 84-94.

Rahman I., et al., Regulation of inflammation and redox signaling by dietary polyphenols. Biochem Pharmacol. 2006, 72: 1439-1452.

Richter M., et al., Quercetin-induced apoptosis in colorectal tumor cells: possible role of EGF receptor signaling. Nutr Cancer. 1999, 34: 88–99.

Rosenfeld J.A., et al., Determination of enriched histone modifications in non-genic portions of the human genome. BMC Genomics. 2009, 10: 143.

Roy M., et al., Anticlastogenic, antigenotoxic and apoptotic activity of epigallocatechin gallate: a green tea polyphenol. Mutat Res. 2003, 523–524: 33–41.

Scudiero D.A., et al., Evaluation of a soluble tetrazolium/formazan assay for cell growth and drug sensitivity in culture using human and other tumor cell lines. Cancer Res. 1988, 48: 4827-4833.

Singh U.P., et al., Resveratrol (trans-3, 5, 40-trihydroxystilbene) induces SIRT1 and down-regulates NF-kappaB activation to abrogate DSS-induced colitis. J Pharmacol Exp Ther. 2009, 332:829-39.

Singh U.P., et al., Resveratrol (trans-3,5,40-trihydroxystilbene) induces silent mating type information regulation-1 and down-regulates nuclear transcription factor-kappaB activation to abrogate dextran sulfate sodium-induced colitis. J Pharmacol Exp Ther. 2010, 332: 829–839.

Sporn M.B., et al., Chemoprevention: an essential approach to controlling cancer. Nat Rev Cancer. 2002, 2: 537–543.

Strissel P.M., et al., Multiple effects of bioflavonoids on gene regulation, cell proliferation and apoptosis: natural compounds move into the lime light of cancer research. Leuk Res. 2005, 29: 859–861.

Timóteo P., et al., HPLC/DAD/ESI-MS analysis of non-volatile constituents of three Brazilian chemotypes of Lippia alba (Mill.) N.E. Brown. Natural Product Communications. 2008, 3: 2017–2020.

Vakifahmetoglu H., et al., Death through a tragedy: mitotic catastrophe. Cell Death Differ. 2008, 15: 1153-1162.

Vega M.I., et al., Rituximab inhibits p38 MAPK activity in 2F7 B NHL and decreases IL-10 transcription: pivotal role of p38 MAPK in drug resistance. Oncogene. 2004, *23*: 3530-3540.

Wang H.Y., et al., Vitexicarpin, a flavonoid from *Vitex trifolia* L., induces apoptosis in K562 cells *via* mitochondria-controlled apoptotic pathway. Yao Xue Xue Bao. 2005, 40: 27-31, 2005. [Article in Chinese]

Wang I.K., et al., Induction of apoptosis by apigenin and related flavonoids through cytochrome c release and activation of caspase-9 and caspase-3 in leukaemia HL-60 cells. Eur J Cancer. 1999, 35: 1517–1525.

Wang M., et al., Rapid Isolation of Salvianolic acid B from polar extracts of *Salvia miltiorrhiza* Bge. (Danshen). International Symposium, Traditional Chinese Medicine, Modernization of Acupuncture and Herbal Medicine Research, May 14-16, 2009, Graz, Austria.

Williams R.J., et al., Flavonoids: antioxidants and signaling molecules? Free Radic Biol Med. 2004, *36*: 838-849.

Yang C.S., et al., Inhibition of carcinogenesis by dietary polyphenolic compounds. Annu Rev Nutr. 2001, 21: 381–406.

Yoshida M., et al., Quercetin arrests human leukemic T-cells in late G1 phase of the cell cycle. Cancer Res. 1992, 52: 6676–6681.

Yoshida M., et al., The effect of quercetin on cell cycle progression and growth of human gastric cancer cells. Fed Eur Biochem Soc Lett. 1990, 260: 10–13.

Ringraziamenti

Ringrazio la Prof.ssa Bilia per avermi dato la possibilità di realizzare questo lavoro e per le opportunità di crescita personale e professionale che mi ha offerto in questi tre anni.
Un ringraziamento particolare per la collaborazione e per l'accoglienza ricevuta all'interno dei loro gruppi di ricerca alla prof.ssa Coronnello del Dipartimento di Farmacologia Clinica e Preclinica dell'Università di Firenze; alla Prof.ssa Maria J. Alonso e alla dott.ssa Noemi Csaba del Dipartimento di Farmacia dell'Università di Santiago de Compostela ed al Prof. Thomas Efferth del Dipartimento di Bilogia Farmaceutica dell'Università di Mainz.
Grazie a Camilla, Benedetta, Anastasia, Francesca e a tutte le colleghe del gruppo di ricerca del Prof. Vincieri per l'aiuto e per tutti i momenti condivisi insieme in questi anni.